Exploring the Interaction of Small Molecules Modulating Myoglobin Function

By

JESSICA SCOUT GREGORY

THESIS

Submitted in partial satisfaction of the requirements for the degree of

MASTER OF SCIENCE

in

Biophysics

in the

OFFICE OF GRADUATE STUDIES

of the

UNIVERSITY OF CALIFORNIA

DAVIS

Approved:

Thomas Jue, chair

Robert Fairclough

Tsung-Yu Chen

Committee in Charge

2023

ABSTRACT

Myoglobin is one of the longest studied proteins on earth, in part because it was the first to have its structure solved and it is a ubiquitous protein found in muscle tissue across most of the animal kingdom. Myoglobin (Mb) has also garnered attention within the wider scientific community as a classic example of 'structure dictates function' philosophy. Historically, scientists believed Mb was strictly an oxygen storage and transport protein. This however was brought into question when modified mice completely devoid of Mb showed no apparent deficit from the wild type. These revelations lead to new schools of thought about Mb function, of which the debate continues today.

New schools of thought theorize a range of ideas for Mb's potential function(s), from nitric oxide regulation to fatty acid (FA) interactions involved in the electron transport chain. Studies show that Mb interacts with FA specifically and non-specifically in its oxygenated state. Further studies show evidence of a possible chain length dependence on this interaction. A species dependence is also possible considering the variability of Mb concentration and structure discrepancies across species. Some new theories even suggest an interaction between 4-hydroxy-2-nonenal (HNE) and Mb.

The research described in this thesis explores the plausibility of new theories about the function half of the structure--function relationship of Mb using a variety of advanced modeling techniques. Chapter 1 includes an in-depth analysis of docking methodology to assert a sound scientific foundation for Mb research, including important learnings from reproducibility studies. Chapter 2 investigates structure and function theories of Mb, including studies of ligation state dependence of FA binding and the differences between oxy- and deoxy-Mb. Lastly, Chapter 3 explores the chain length dependence of FA binding, cross comparison of Mb from different

species, Mb's potential to contribute to the electron transport chain (ETC), and *in silico* simulation models that support data from both UV-Vis and NMR spectroscopy studies.

This research asserts a new framework for understanding the structure and function relationship of Mb that not only advances our understanding of this important biological molecule, but also modernizes the field of understanding for all proteins. Technological advances have shown that Mb, a protein that was believed to only transport and store oxygen, has a far more diverse array of functions. It reminds us that a healthy interrogation of commonly held scientific knowledge is beneficial to our greater understanding of the world around us and that no textbook is immune from the possibility of a revision.

CHAPTER 1. INTRODUCTION TO MYOGLOBIN RESEARCH AND DOCKING METHODOLOGY 1
I. ABSTRACT 3
II. INTRODUCTION TO MYOGLOBIN 4
A. Historical Background 4
B. Physiological Background 5
III. INTRODUCTION TO MOLECULAR DOCKING 25
A. Historical Background 25
B. Approaches 27
C. AutoDock 4 30
D. Molecular Dynamics 42
IV. USING AUTODOCK TO EXPLAIN NMR 43
A. Previous molecular docking studies of Mb and FA 43
B. Proposed Aims of Studies 45
V. REFERENCES 46

CHAPTER 2. MOLECULAR MODEL OF MYOGLOBIN, FATTY ACID INTERACTION 54
I. ABSTRACT 55
II. INTRODUCTION 55
III. MATERIALS AND METHODS 59
A. Macromolecule Preparation 59
B. Ligand Preparation 59
C. Docking Simulation 61
D. Molecular Visualization 64
IV. RESULTS 64
V. DISCUSSION 73
A. Fatty Acid Binding Sites 73
B. Contrasting Differences for Oxy v Deoxy Mb 73
VI. CONCLUSION 74
VII. REFERENCES 76

CHAPTER 3. OTHER WORK 80
I. ABSTRACT 81
II. UNPUBLISHED WORK 81
A. FA Chain Length Dependence 81
B. Whale vs Horse Mb Studies 89
III. COLLABORATIVE EFFORTS 95
A. Nonenal—Mb Studies 95
B. Cytochrome C—Mb Studies 98
C. Future: Ethanol—Mb Studies 107
IV. REFERENCES 110

LIST OF FIGURES

Figure 1: Three-dimensional structure of myoglobin. 5
Figure 2: Mb ribbon drawing 6
Figure 3: Oxygen Binding Activity 7
Figure 4: View of the oxygen binding to Mb 8
Figure 5: Stereo Pair Image of Heme Pocket with Hydrophobicity Surface 10
Figure 6: Heme 11
Figure 7: MbO_2 Desaturation Post Ischemia 13
Figure 8: Relative O_2 Flux Contribution 14
Figure 9: FABP, Mb Side-by-side Ribbon 17
Figure 10: Fatty Acid Flux Model at Low [PAM] 18
Figure 11: Nonenal line drawing 20
Figure 12: $^{13}C_1$ NMR Spectra of Mb and PAM 22
Figure 13: NMR oxy-Mb interaction with PAM 24
Figure 14: Van der Waals Lennard-Jones Potential 31
Figure 15: Hydrogen Bond Schematic 32
Figure 16: Coulomb's Law 33
Figure 17: Rotatable bonds and W Pseudo-atoms 35
Figure 18: Genotype conversion to Phenotype 36
Figure 19: Comparison of Genetic Algorithms 38
Figure 20: Grid Map 40
Figure 21: oxy-Mb with hydrophobicity surface and scale 65
Figure 22: External positively charged amino acids of oxy-Mb 68
Figure 23: Heme-pocket structural differences between oxy- and deoxy-Mb 70
Figure 24: Close up of PAM docked to oxy- and deoxy-Mb 72
Figure 25: ^{1}H-NMR Spectra of MbCN with varying chain lengths FA 82
Figure 26: ^{1}H-NMR spectra of MbCN with varying concentrations of FA 84
Figure 27: Oxy- and deoxy-Mb binding various chain lengths of FA from 8-18 87
Figure 28: Model of FA flux at high palmitate concentration 90
Figure 29: Amino Acid Sequence Comparison of Horse and Whale oxy-Mb 91
Figure 30: AutoDock 100 conformers of PAM with oxy-Mb 93
Figure 31: ^{1}H NMR spectra of MbCN with and without HNE 96
Figure 32: Hydrated Nonenal 97
Figure 33: AutoDock 100 conformers of nonenal with Mb 98
Figure 34: MbCO vs Cytochrome C ribbon drawings 99
Figure 35: Electron Transport Chain 101
Figure 36: Select spectra of the MbO_2 autoxidation and electron transfer to $Cyt^{3+}C$ 103
Figure 37: Plot of MbO_2 vs. time for autoxidation and electron transfer. 104
Figure 38: Hydrated $Cyt^{3+}C$ 106
Figure 39: Preliminary docking Mb—$Cyt^{3+}C$ results 107
Figure 40: ^{1}H NMR spectra of MbCN with and without EtOH 108
Figure 41: Stick drawing of Hydrated EtOH 109

LIST OF EQUATIONS

Equation 1: CHARMM force field....29
Equation 2: Estimated Free Energy of Binding....30
Equation 3: Hydrogen-bond energy potential....32
Equation 4: Desolvation Energy....34
Equation 2: Estimated Free Energy of Binding (repeated)....62
Equation 5: Standard Reduction Potentials and The Nernst Equation....100

LIST OF TABLES

Table 1: Palmitate Binding in Complex with Myoglobin Global Energy....66
Table 2: 7 Heme-Propionate & Histidine-97 Hydrogen Bonding....71
Table 3: AutoDock Binding Energy of oxy- and deoxy-Mb with FA C8-18 at K96....88
Table 4: AutoDock Binding Energy for PAM with Horse, Whale oxy-Mb....94

LIST OF ABBREVIATIONS AND ACRONYMS

Å	Angstrom; 10^{-10} meter	
AA	Amino acid	
BPTI	Bovine Pancreatic Trypsin Inhibitor	
CHARMM	Chemistry at HARvard Molecular Mechanics	
$Cyt^{3+}C$	Cytochrome-C Oxidase; CytC	
DEC	Decanoic acid; Capric acid; decanoate	$C_{10}H_{20}O_2$
deoxy-Mb	Deoxygenated myoglobin	
DET	detergent	
EDTA	Edetic acid; Ethylenediaminetetraacetic acid	$C_{10}H_{16}N_2O_8$
ETC	Electron Transport Chain	
EtOH	Ethanol; ethyl alcohol	CH_3CH_2OH
FA	Fatty acid	
FABP	Fatty Acid Binding Protein	
GA	Genetic Algorithm	
Hb	Hemoglobin	
-hem	-heme methyl	$-CH_3$
HNE	Nonenal; 4-hydroxynon-2-enal; 4-HNE; 4-Hydroxynonenal	$C_9H_{16}O_2$
kDa	kilodalton; 1000 daltons (Da or u)	
KO	knockout	
L-BABP	Liver-Bile Acid Binding Protein	
LAU	Lauric acid; (C12:0); Dodecanoic acid; laurate	$C_{12}H_{24}O_2$
LELC	Lowest Energy Largest Cluster	
LGA	Lamarckian Genetic Algorithm	
LS	Local search	
LVDP	Levodropropizine; Levdropropizine; Levotuss	$C_{13}H_{20}N_2O_2$
Mb	Myoglobin; reduced Mb; $Mb(Fe^{2+})$	
MD	Molecular dynamics	
met-Mb	met-myoglobin; oxidized Mb; $Mb(Fe^{3+})$	
MMFF	Merck Molecular Force Field	
MYR	Myristic acid; (C14:0); Tetradecanoic acid; myristate	$C_{14}H_{28}O_2$
NMR	Nuclear Magnetic Resonance	
OCT	Octanoic acid; (C8:0); Caprylic acid; octoate	$C_8H_{16}O_2$
OLE	Oleic acid; (C18:1); oleate	$C_{18}H_{34}O_2$
oxy-Mb	Oxygen bound Myoglobin, MbO_2 or surrogate	
PAM	Palmitic acid; (C16:0); Hexadecanoic acid; palmitate	$C_{16}H_{32}O_2$
PDB	Protein DataBank	
prop	Propionate; Propanoic acid anion	$C_{16}H_{32}O_2$
RCSB	Research Collaboratory for Structural Bioinformatics	
SDS	lauric sulfate; sodium dodecyl sulfate	LAU 1-SO_4
UV-Vis	Ultraviolet-Visible	
W atom	Water pseudo-atom	
WT	Wild type	

ACKNOWLEDGEMENTS

I am grateful to my committee chair and advisor, Dr. Thomas Jue, and members of my committee, Dr. Robert Fairclough, and Dr. Tsung-Yu Chen for their guidance throughout this research and writing process.

No research is done alone, so I have to acknowledge the enormous help I received from my fellow group members and collaborators past and present: Usman Rehman, Clayton Germolus M.S., Dr. Amjad Ramahi, Dr. Lifan Shih, Dr. Ulrike Kreutzer, and Dr. Youngran Chung. They've learned alongside me, added technical as well as conceptual contributions, and given moral support throughout my tenure as a graduate student. A special thanks goes to Dr. Katherine Dahlhausen, friend and comrade, her support and expertise in scientific writing is the reason this thesis is readable.

To the other 2 musketeers, Dr. Jan Maly and Clayton Germolus M.S. -- we're finally all finish!

DEDICATION

This thesis is dedicated to my family, friends, and their assorted pets.

Thanks for helping me see this adventure through to the end.

CHAPTER 1. INTRODUCTION TO MYOGLOBIN RESEARCH AND DOCKING METHODOLOGY

TABLE OF CONTENTS

I. ABSTRACT 3
II. INTRODUCTION TO MYOGLOBIN 4
A. Historical Background 4
B. Physiological Background 5
i. Structure 5
a. Heme Pocket 8
b. Propionate Flexibility 11
ii. Function 12
a. Textbook Myoglobin Function 12
(i) Oxygen Storage 12
(ii) Oxygen transport 13
b. New Theories on Myoglobin Function 15
(i) Life without Myoglobin 15
(ii) Nitric Oxide Regulation 16
(iii) Myoglobin with Fatty acid 16
(a) Structural Comparison to FABP 17
(b) Physiological Comparison to FABP 17
(iv) Myoglobin Oxidization 19
iii. Myoglobin NMR Studies 20
a. Oxy vs Deoxy Myoglobin 21
b. Fatty Acid Chain Length Dependence 23
c. Myoglobin—Nonenal Interaction 24
(i) HNE and Mb Autoxidation 25
(ii) HNE and Mb Oxidation by Electron Transfer 25
III. INTRODUCTION TO MOLECULAR DOCKING 25
A. Historical Background 25
B. Approaches 27
i. Matching 27
ii. Docking 27
a. Force-field Based Scoring Functions 28
b. Empirical Scoring Functions 29
c. Knowledge-based Scoring Functions 29
C. AutoDock 4 30
i. Theory and Force-fields 30
a. Free Energy Scoring Function 30
b. Discrete Water Pseudo-atoms 34
ii. Genetic Algorithm 35
a. Hybrid Search Method 37
b. Lamarckian Genetic Algorithm 37
c. Implementation 38
d. Box Size 41

D. Molecular Dynamics 42
IV. USING AUTODOCK TO EXPLAIN NMR 43
A. Previous Molecular Docking Studies of Myoglobin and Fatty Acid 43
i. Summary 43
a. Macromolecule Preparation 43
b. Ligand Preparation 44
ii. Conclusions 44
B. Proposed Aims of Studies 45
V. REFERENCES 46

CHAPTER 1 LIST OF FIGURES

Figure 1: Three-dimensional structure of myoglobin. 5
Figure 2: Mb ribbon drawing 6
Figure 3: Oxygen Binding Activity 7
Figure 4: View of the oxygen binding to Mb 8
Figure 5: Stereo Pair Image of Heme Pocket with Hydrophobicity Surface 10
Figure 6: Heme 11
Figure 7: MbO2 Desaturation Post Ischemia 13
Figure 8: Relative O2 Flux Contribution 14
Figure 9: FABP, Mb Side-by-side Ribbon 17
Figure 10: Fatty Acid Flux Model at Low [PAM] 18
Figure 11: Nonenal line drawing 20
Figure 12: 13C1 NMR Spectra of Mb and PAM 22
Figure 13: NMR oxy-Mb interaction with PAM 24
Figure 14: Van der Waals Lennard-Jones Potential 31
Figure 15: Hydrogen Bond Schematic 32
Figure 16: Coulomb's Law 32
Figure 17: Rotatable bonds and W Pseudo-atoms 34
Figure 18: Genotype conversion to Phenotype 36
Figure 19: Comparison of Genetic Algorithms 38
Figure 20: Grid Map 40

CHAPTER 1 LIST OF EQUATIONS

Equation 1: CHARMM force field 29
Equation 2: Estimated Free Energy of Binding 30
Equation 3: Hydrogen-bond energy potential 32
Equation 4: Desolvation Energy 34

CHAPTER 1. INTRODUCTION TO MYOGLOBIN RESEARCH AND DOCKING METHODOLOGY

I. ABSTRACT

Myoglobin was the first protein to have its structure solved, making it one of the longest studied proteins on Earth. Found in the muscle tissues throughout much of the animal kingdom, myoglobin (Mb) is used as a classic example for learning about the relationship between structure and function in proteins. It's well understood that Mb is strictly an oxygen storage and transport protein. Or is it?

The "structure dictates function" school of thought for Mb was brought into question most remarkably when modified mice completely devoid of Mb showed no apparent deficit from the wild type (Garry et al. 1998; Godecke et al. 1999). Now, myoglobin is debated by the scientific community when it comes to function. These revelations lead to the formation of new schools of thought about Mb's function, with theories ranging from nitric oxide regulation to fatty acid (FA) interactions involved in the electron transport chain (ETC).

Studies have shown that Mb interacts with FA specifically and non-specifically in its oxygenated state. Further studies have shown a possibility of chain length dependence on this interaction.

Some studies have suggested a possible interaction with nonenal (HNE) enhanced autoxidation or even oxidation by electron transfer of Mb. Although more recent research has found HNE not to be the causative agent they also suggest a different possible suspect for Mb enhancement.

To elucidate which theories about Mb's function hold scientific merit, molecular docking was done with AutoDock 4 using hydrated docking protocols on different physiological states of Mb with various ligands including FAs, HNE, and Cytochrome C (CytC). These docking simulations

were used to confirm corresponding NMR data and to predict and validate potential binding sites for these ligands on Mb. Multiple simulation box sizes were tested to reduce the likelihood of biasing results towards a particular binding site, starting with a global full box size that encompassed the entire Mb macromolecule and progressively narrowed in on sites of interest. AutoDock simulations were conducted for Mb from different species, namely from sperm whale (*Physeter catodon*) and horse heart (*Equus caballus*), to discern any preferential binding differences.

II. Introduction to Myoglobin

A. Historical Background

Max Perutz chose to work on solving the molecular structure of Hemoglobin (Hb), the protein that is in red blood cells that transports oxygen and carbon dioxide to and from the lungs and tissues. Difficulty arose from the complexity of the protein, which has 4 separate amino acid chains, and proved to be a time-consuming project. John Kendrew, who worked closely with Perutz, suggested a smaller, related protein with a single amino acid chain: Myoglobin (Mb). After examining 110 crystals and measuring the intensities of around 250,000 X-ray reflections using Perutz's x-ray crystallography method, the structure of myoglobin was solved; its handmade clay 3D model is shown in Figure 1. Being the first people to ever do so earned them both the Nobel Prize for Chemistry in 1962. It also makes myoglobin, and specifically its structure, the first and therefore longest studied protein, of which we are still learning new things about its function today.

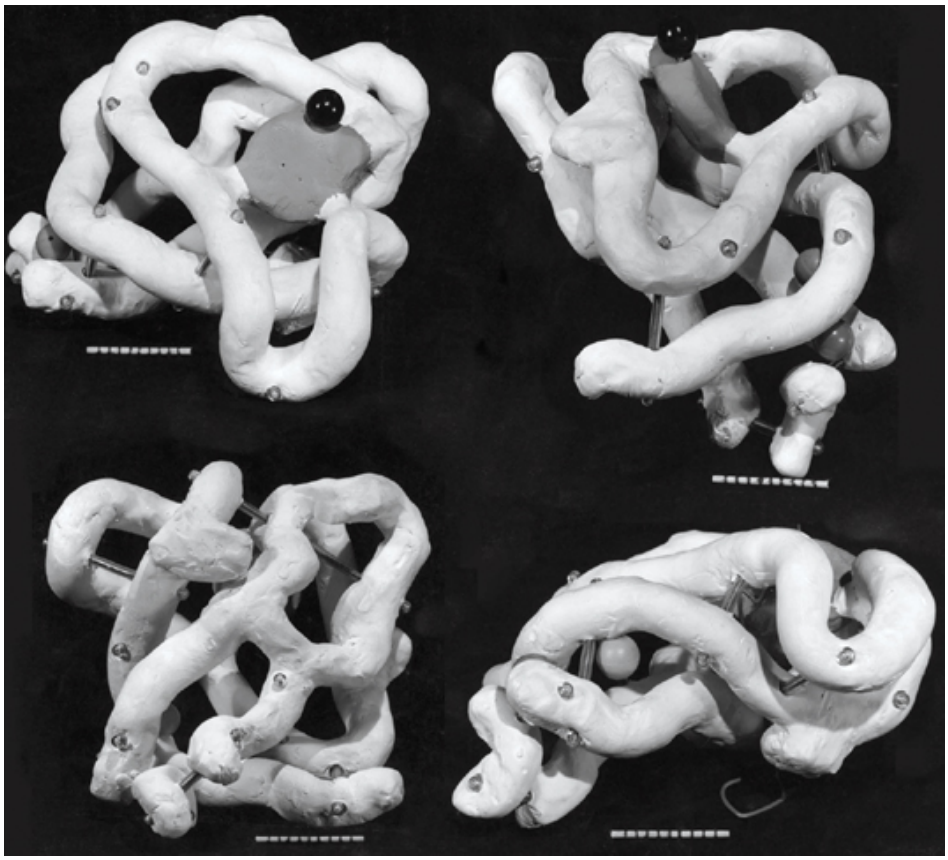

Figure 1: Three-dimensional structure of myoglobin.
The low-resolution structure of myoglobin that was published by John Kendrew and colleagues in 1958. Polypeptide chains are in white, and the grey disc represents the haem group. The three spheres show positions at which heavy atoms were attached to the molecule (black, Hg of p-chloro-mercuri-benzene-sulphonate; dark grey, Hg of mercury diammine; light grey, Au of auri-chloride). The marks on the scale are 1 Å apart. This figure in the Nature paper was reconstructed using the original figures in the archives of the Medical Research Council Laboratory of Molecular Biology, Cambridge, UK (Kendrew, Bodo et al. 1958).

B. Physiological Background

i. Structure

With better technology and computer graphics, we can now visualize Mb even more accurately. Figure 2 shows the ribbon drawing of Mb from modern high resolution x-ray crystallography.

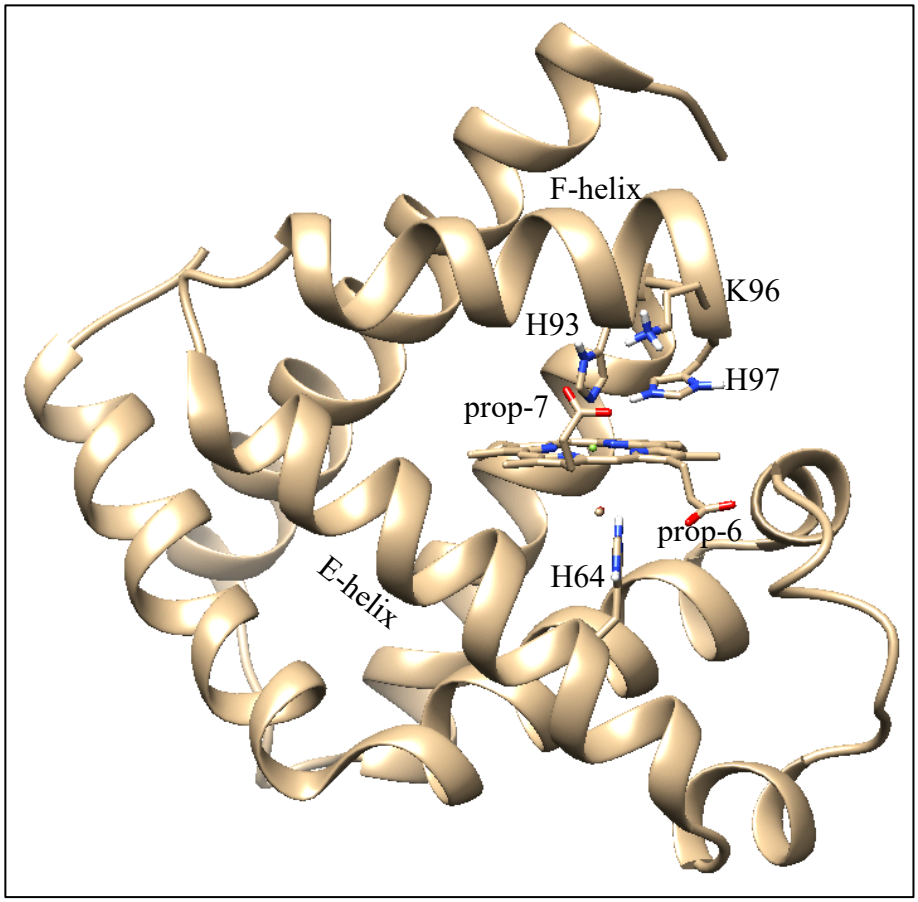

Figure 2: Mb ribbon drawing
α-helical segments (residues): A (3-18), B (20-35), C (36-42), D (51-57), E (58-76), F (83-95), G (100-118), & H (124-149).

A newer higher resolution crystallographic representation of Mb can be seen in Figure 2. With its primary structure of a single polypeptide chain of 153 amino acids building a secondary structure of 8 right-handed α-helices, and its heme group, Mb weighs in at ~17kDa and ranks as one of the most copious proteins in muscles and cardiomyocytes. So copious and ubiquitous in fact, that Mb and Mb-like proteins are found in many taxa including bacteria, plants, fungi, and animals (Wilson and Reeder 2006). The single heme group binds O_2 just like the similar α and β subunits of its heterotetrameric 'blood relative', Hemoglobin (Hb). Considering the quaternary structure of Hb having 4 subunits similar to Mb, you'd be forgiven for thinking Hb would bind O_2 better than Mb. But as shown in Figure 3, the P50 (the pressure at which the

concentration of oxygenated protein is equal to the concentration of non-oxygenated protein) for Mb is ~1.5 mmHg whereas the P50 of Hb is ~26 mmHg. This suggests Mb is substantially better than Hb at binding O_2.

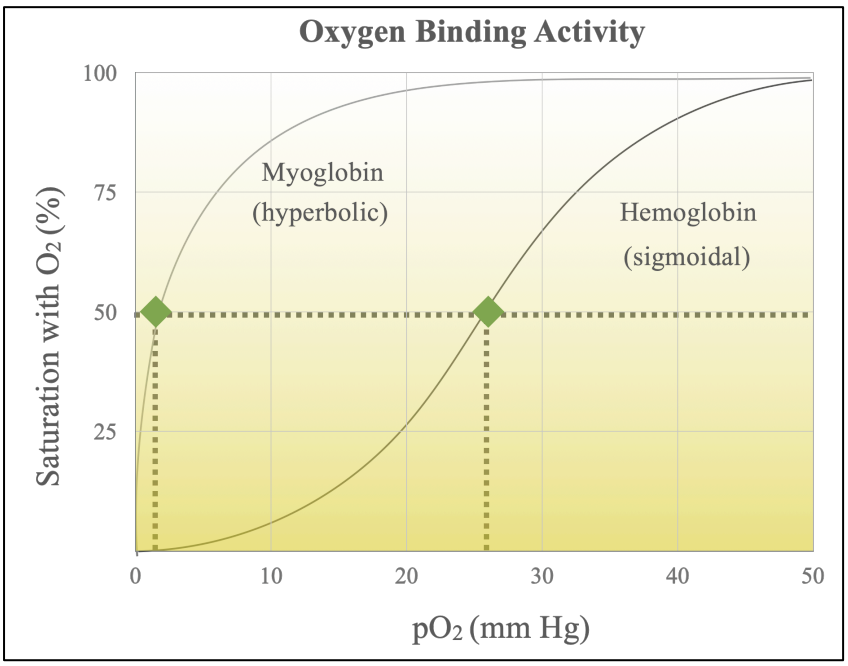

Figure 3: Oxygen Binding Activity
Showing the hyperbolic curve of Mb and the sigmoidal curve of Hb suggesting Mb is the superior O_2 binder.

We know Mb can reversibly bind O_2, but it has also demonstrated binding of other ligands including carbon monoxide (CO), cyanide (CN), and water depending on the valence state of the Iron in the center of the heme group's porphyrin ring, as seen in Figure 6. The porphyrin ring of the heme is held by the proximal Histidine (H93) and on the opposite side of the heme plane the distal Histidine (H64), while not directly bonded to the iron, is involved in ligand binding. As shown in Figure 4, when Mb is non-ligated the proximal histidine is pulling the iron out of plane in a "puckered" state. Then, when O_2 binds between the iron and the distal Histidine, the Iron is tugged down into the heme plane, pulling along with it the proximal histidine and its secondary structure α-helix F towards α-helix E.

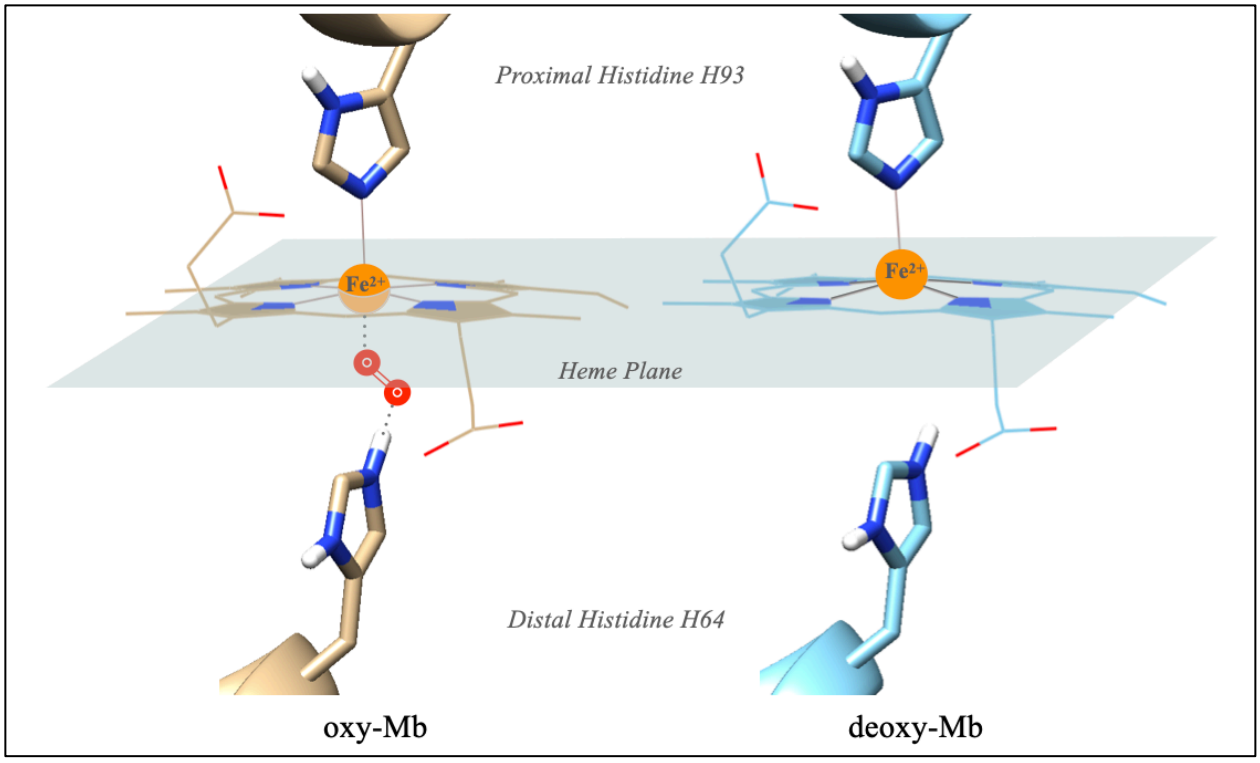

Figure 4: View of the oxygen binding to Mb
Where the Heme Plane is in grey, the Iron is in orange, proximal Histidine 93 above and distal Histidine 64 below. If it were shown, H97 would be on the next loop of the F- helix (top, right of H93) pointing towards the 7-propionate (above plane).

a. Heme Pocket

On the surface of Mb between the α-helices F and E there is a hydrophobic region that acts as a pocket that holds the Heme group, seen in stereo pair in Figure 5. Although the crystal structures from the *Research Collaboratory for Structural Bioinformatics* (RCSB) Protein DataBank (PDB) of various states of Mb appear to show a closely packed structure, they do exhibit transient fluctuations. These fluctuations create distinct openings for ligands to reach the heme from solution (Elber and Karplus 1987). Researchers have postulated that the 6- and 7-heme-propionates play a major role in regulating the ligand's access to the heme-pocket (La Mar, Viscio et al. 1978, Lecomte and La Mar 1985, Carver, Olson et al. 1991). In this study the

interaction between the 7 heme-propionate and the Histidine-97 side chain is studied more in depth to see its relevance in stabilizing the heme-pocket in different ligation states of myoglobin.

Crystallographic structures also do not show effector binding. In the process of crystallization, effectors often do not remain bound. Yet these effectors can rapidly modulate protein function.

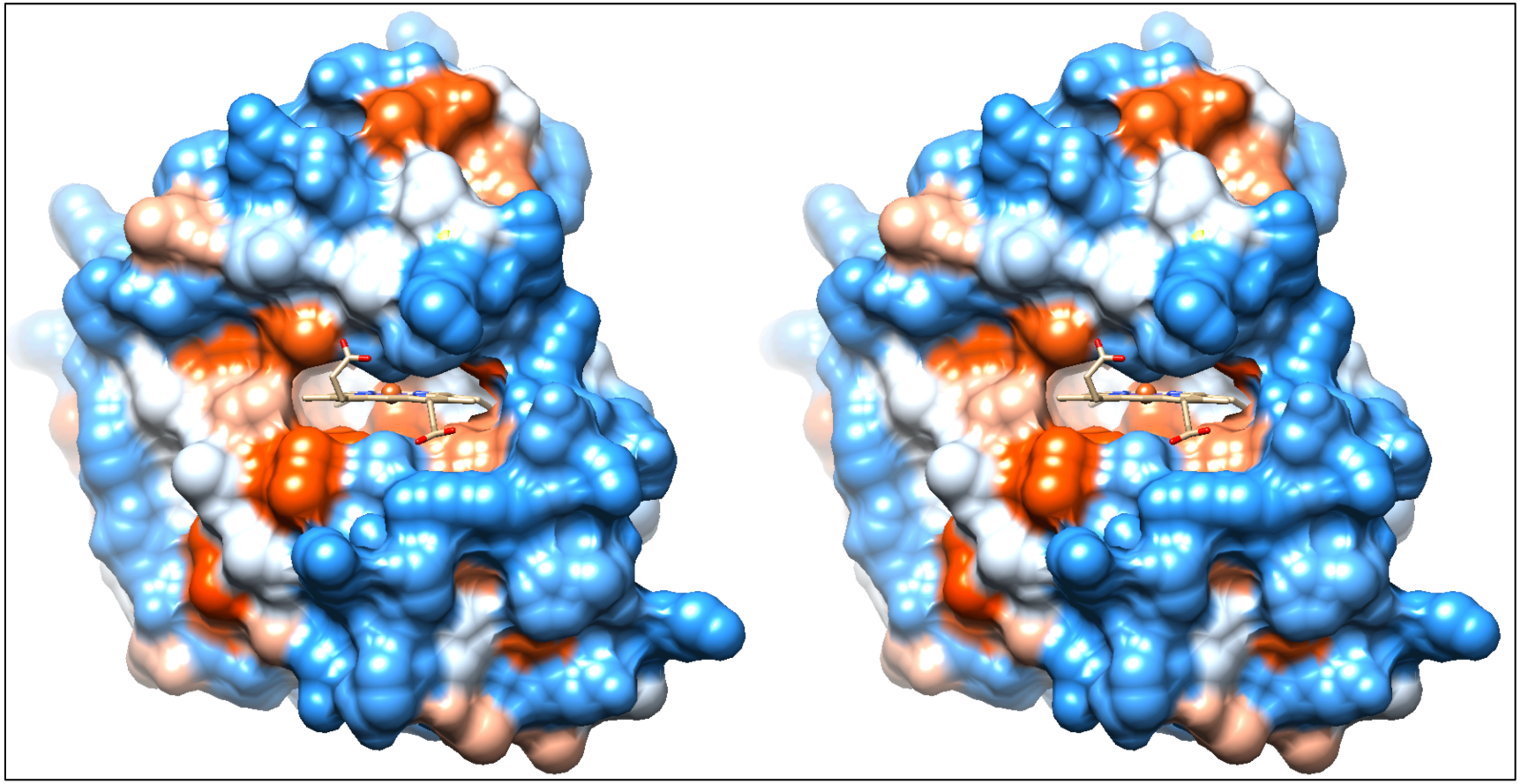

Figure 5: Stereo Pair Image of Heme Pocket with Hydrophobicity Surface
Oxy-Mb (PDB ID: 5CN5) with hydrophobicity surface, heme in tan

b. Propionate Flexibility

2D NMR measurements have previously detected that the 7-heme-propionate exhibits a greater level of mobility than the 6-heme-propionate group in deoxy-Mb, as reflected by the Nuclear Overhauser Enhancements (NOEs) from the heme-propionates to their respective 5 and 8-heme-methyls (Busse and Jue 1994). The mobility of the heme-propionates in different ligation states of Mb not only influences ligand migration, but may also modulate the selective binding of ligands, such as fatty acids (FAs) (La Mar, Viscio et al. 1978, Ramaprasad, Johnson et al. 1984, Lecomte and La Mar 1985). The interaction between the 7-heme-propionate and the Histidine-97 side chain needs to be studied more in depth to explore its potential relevance in stabilizing the heme-pocket in different ligation states of Mb.

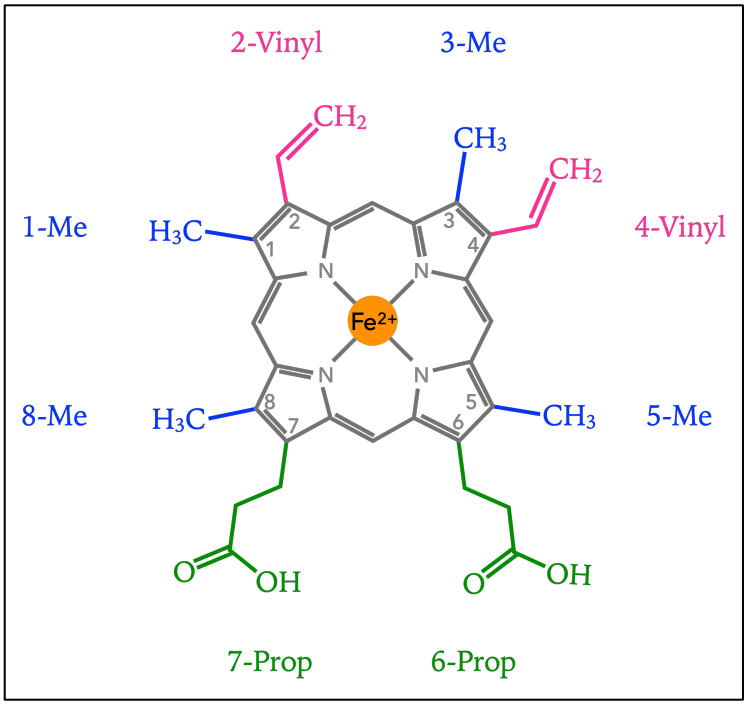

Figure 6: Heme
Heme group with porphyrin ring in grey, methyl groups in blue, Vinyl groups in pink, propionate groups in green and Iron in orange.

ii. Function

a. Textbook Myoglobin Function

Orthodox biochemistry and physiology typecast Mb as an oxygen-centric protein, its principal roles of being both oxygen storage and transport depot are dogma.

(i) Oxygen Storage

As far as oxygen storage capabilities are concerned, certainly, studies have shown Mb supplying O_2 in plants, in mammalian tissues, and during seal apnea (Wittenberg and Wittenberg 1989, Ponganis, Kreutzer et al. 2002, Chung, Molé et al. 2005, Gros, Wittenberg et al. 2010). The high concentration of Mb in marine mammals could certainly supply oxygen during a dive or apnea (Dolar, Suarez et al. 1999, Guyton, Stanek et al. 1995, Kooyman and Ponganis 1998, Ponganis, Kreutzer et al. 2002). Resembling that of the depths of the oceans, an adaptation to high altitude in certain avian species enhances Mb expression and increases O_2 supply (Gimenez, Sanderson et al. 1977, Terrados, Jansson et al. 1990). These observations correlate well the Mb concentration (O_2 supply) with the animal's respiratory/oxidative capacity (Wittenberg and Wittenberg 2003).

Whereas in terrestrial mammals like rats, Mb does not appear to be a very effective O_2 storage system. Dropping to 50% desaturation, as seen in Figure 7 marked in orange, in under 1 minute post ischemia (Chung and Jue 1996).

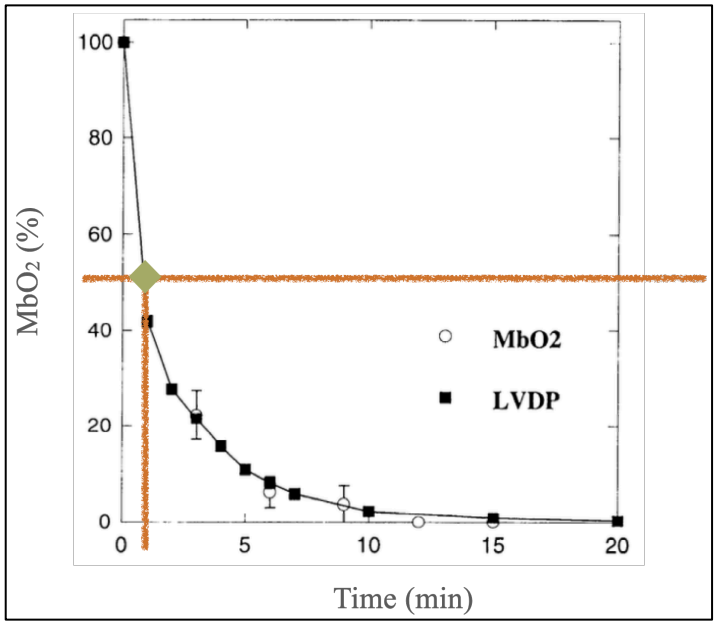

Figure 7: MbO_2 Desaturation Post Ischemia
Oxygenated Mb (MbO_2) saturation and left ventricle developed pressure (LVDP) decrease after ischemia onset. The 0 time-point corresponds to the beginning of global ischemia. Within 12 minutes of ischemia both intracellular O_2 level and LVDP have approached zero. The t20% is ~3.5 min. Adapted from Chung and Jue 1996.

(ii) Oxygen transport

As for its other canonical role of facilitating the diffusion of O_2, the low solubility of O_2 contrasts the high O_2 carrying capacity of Mb, which can confer an advantage in transporting O_2 from the sarcolemma to the mitochondria (Wittenberg, 1970; Wittenberg & Wittenberg, 1989). Studies confirm that O_2 diffuses faster in a solution containing Mb than in an Mb-free solution *in vitro*. Mb exhibits sufficient mobility and O_2 carrying capacity to compete effectively with free O_2 (Johnson *et al.* 1996). However, *in vivo* studies have produced differing results, at best, depleting the entire Mb store of O_2 , prolongs terrestrial mammal cardiac function for only a few seconds (Chung and Jue 1996). Researchers were also able to establish an equipoise diffusion (P_{O2}) in the cell, where Mb and O_2 equally contribute to O_2 transport.

For terrestrial mammals, the equipoise P_{O2} (the PO_2 where Mb begins to have a prominent transport role) is too low to support life and therefore Mb cannot play a significant role in O_2 transport in the cell, as shown in Figure 8 where the vertical dashed line marks the physiological minimum for life.

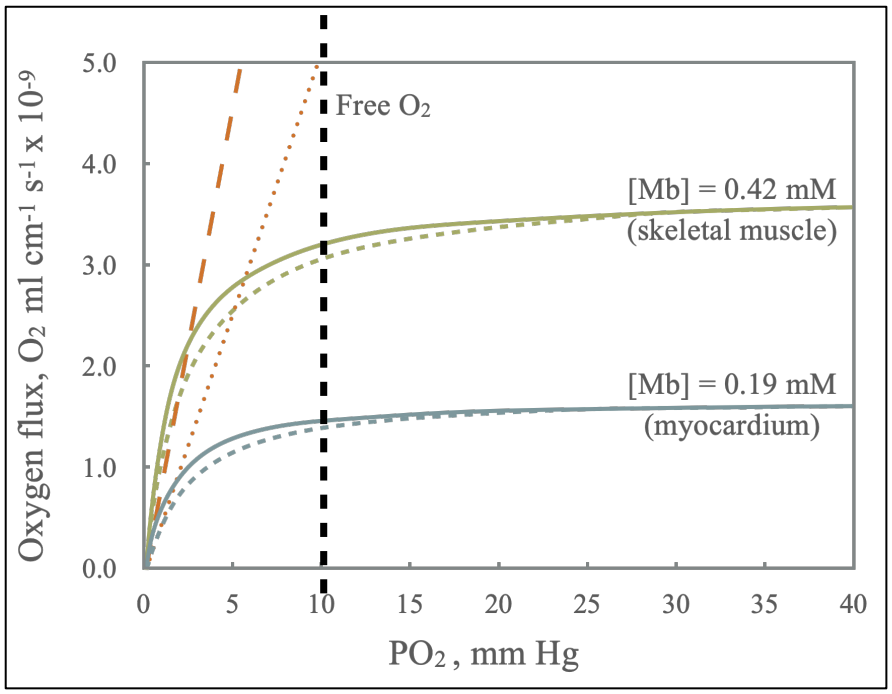

Figure 8: Relative O_2 Flux Contribution
Plot of free O_2 flux vs. Mb facilitated O_2 diffusion as a function of PO_2 at 22°C: the free O_2 flux increases linearly with PO_2. Two lines depict the rate of change given a cellular free O_2 diffusion constant of K_0 = 4.28 x 10^{-5} (_ _) ml O_2 cm^{-2} min^{-1} atm^{-1} and K_0 = 2.52 x 10^{-5} (.....) ml O_2 cm^{-2} min^{-1} atm^{-1}. The two non-linear curves show the O_2 flux contribution from Mb facilitated diffusion increases as the cellular Mb concentration raises from 0.19 mM to 0.42 mM. With a P50 of 2.3 (dashed) and 1.5 mmHg (solid). With a P50 of 1.5 mmHg, the equipoise PO_2 values are 1.77 (0.19 mM Mb, K_0 = 2.52 x 10^{-5} ml O_2 cm^{-1} min^{-1} atm^{-1}) and 5.72 (0.42 mM Mb, K_0 = 2.52 x 10^{-5} ml O_2 cm^{-1} min^{-1} atm^{-1}). With a P50 of 2.3 mmHg, the equipoise PO_2 falls to 0.97 and 4.92 mmHG respectively. *Adapted from Lin, Kreutzer et al. 2007.*

In contrast, marine mammal muscle, which has a higher concentration of Mb, can utilize Mb-facilitated O_2 diffusion under all physiological conditions (Lin, Kreutzer et al. 2007). This concurs with studies that blocked the binding of oxygen to Mb with CO wherein cardiac performance and respiration in rat myocardium were not impaired (Glabe, Chung et al.

1998, Chung, Huang et al. 2006). Indeed, previous studies have even shown that Mb *in situ* or in a muscle fiber model may diffuse too slowly to compete effectively with free O_2 in the cell (Papadopoulos, Jürgens et al. 1995, Papadopoulos, Endeward et al. 2001, Lin, Kreutzer et al. 2007, Lin, Kreutzer et al. 2007).

b. New Theories on Myoglobin Function

With mounting evidence conflicting with the textbook function of Mb, scientists search for different "outside the box" functionality.

(i) Life without Myoglobin

If the doctrine of oxygen storage and transport are to be believed, how then can a Mb total knockout (Mb KO) mouse (*Mus musculus*), show no signs of respiration deficits, contractile function deterioration, or any other physiological impairments (Garry et al. 1998; Godecke et al. 1999)? Biochemists fall back on the dogmatic Mb functions to explain this anomaly, specifically when it comes to the metabolic profile of the Mb KO mouse. The Mb KO mouse displays a slight decrease in myocardial FA metabolism relative to the wild type (WT) mouse, while the FA to Glucose utilization ratio drops drastically from 3/1 to 0.7/1 (Flögel, Laussmann et al. 2005). Since the β-oxidation of FA during metabolism requires O_2, most researchers have attributed this decrease to the missing contribution of O_2 that would have been from Mb facilitated transport. Or they might point broadly to the impact of multiple different compensation pathways in the Mb KO model, which raises legitimate questions about using the Mb KO model in the first place. If the dwindling FA metabolism does not arise from Mb's missing contribution to the intracellular O_2 flux, and Mb does not appear to play a significant role in normoxic myocardium or skeletal muscle, then it is plausible that the missing Mb itself reduces intracellular FA transport.

(ii) Nitric Oxide Regulation

Varied and perplexing experimental observations have steered scientists to investigate a new and controversial nitric oxide (NO) bio-scavenger and reductase role for Mb (Flögel, Merx et al. 2001, Kreutzer and Jue 2004, Kreutzer and Jue 2006, Rassaf, Flögel et al. 2007). Some studies have refuted Mb's role in NO regulation (Li, Jue et al. 2004, Kreutzer and Jue 2006). Despite the reassurance by biochemistry and physiology zealots of the canon, the cellular function of Mb remains uncertain (Wittenberg and Wittenberg 2003, Gros, Wittenberg et al. 2010).

(iii) Myoglobin with Fatty acid

Previous studies that investigated Mb and FA interactions have presented conflicting findings (Gloster 1977, Gloster and Harris 1977, Götz, Hertel et al. 1994). Only some studies find Mb binding to FA. The presence of a similar molecular weight Fatty Acid Binding Protein (FABP) has clouded the interpretation. However, recent ^{1}H-NMR experiments from the Jue Lab have established convincing evidence for MbO_2, MbCO, and MbCN's specific and non-specific interactions with the FAs palmitate (PAM) and oleate (OLE) (Sriram, Kreutzer et al. 2008, Shih, Chung et al. 2014). Furthermore, FA does not appear to bind to Deoxy-Mb. The FA flux model from Shih et al. 2014, shows that Mb-PAM (K_d = 48 μM) has a lower FA binding affinity than the Fatty Acid Binding Protein (FABP-PAM K_d = 0.014 μM). However, the high cellular concentration and diffusion coefficient of Mb can compensate for its lower binding affinity, thus allowing Mb to compete effectively with FABP above a FA concentration threshold. Additionally, it allows for a convenient FA loading–unloading mechanism that conveniently follows the O_2 gradient from the sarcolemma and delivers FA to the mitochondria (Sriram, Kreutzer et al. 2008, Shih, Chung et al. 2014).

(a) Structural Comparison to FABP

Structurally speaking, Mb and FABP are very different proteins. Mb is composed of eight α-helices, whereas FABP is ten anti-parallel β-strands organized into two nearly orthogonal β-sheets that form a β-barrel as seen in Figure 9 (Banaszak, Winter et al. 1994, Zhang, Lücke et al. 2003). As far as molecular weight is concerned, Mb varies slightly by species ranging from 16-17kD and FABP comes in around 17kD (Zaia, Annan et al. 1992, Siegenthaler, Hotz et al. 1994).

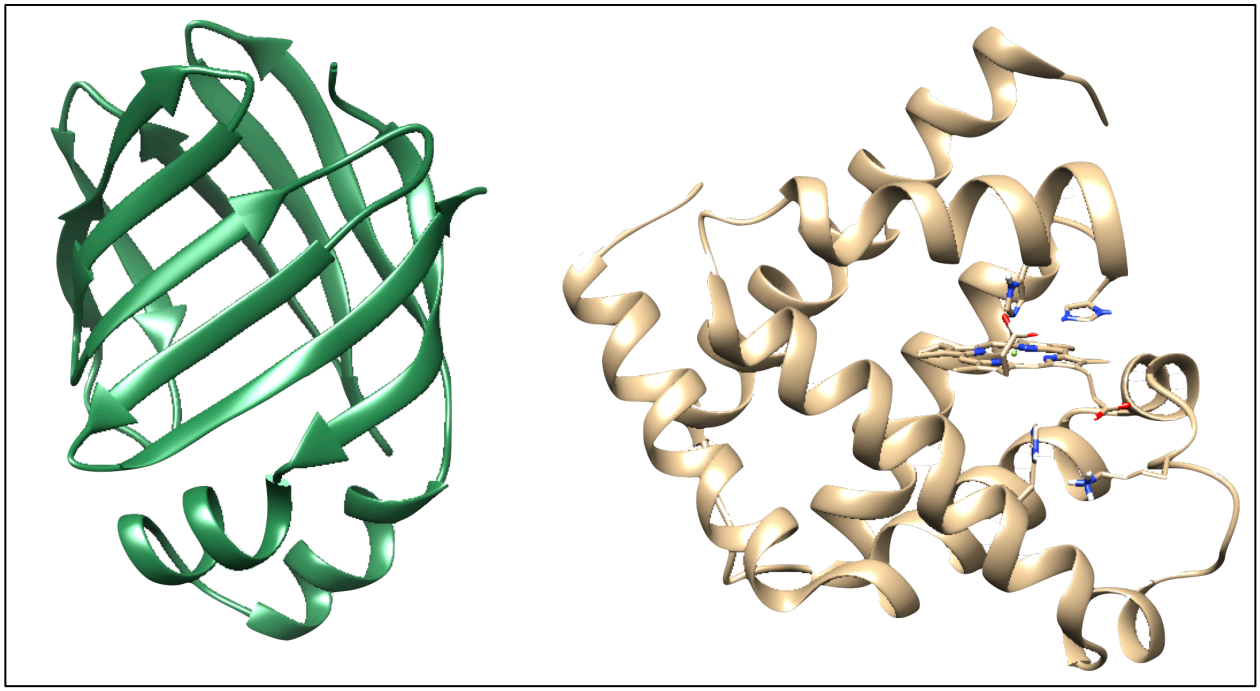

Figure 9: FABP, Mb Side-by-side Ribbon
FABP (PDB ID: 2LKK) Shown in green beta strands shown with arrows, Mb (PDB ID: 5CN5) shown in tan.

(b) Physiological Comparison to FABP

FABP has a high affinity for FA, which is good for uptake at the sarcolemma, but when it travels to the mitochondria this high affinity makes it difficult to deliver the FA for beta oxidation (Glatz and Veerkamp 1983, Corsico, Liou et al. 2004). Mb has ~3000x lower binding affinity than FABP, but its considerably higher cellular concentration and the

ligation state effect on affinity could be a convenient mechanism for FA transport. The model of FA flux in the cell shows in Figure 10 that Mb can out-compete FABP in transporting FA at FA concentrations greater than 0.02 μM (Shih et al., 2014).

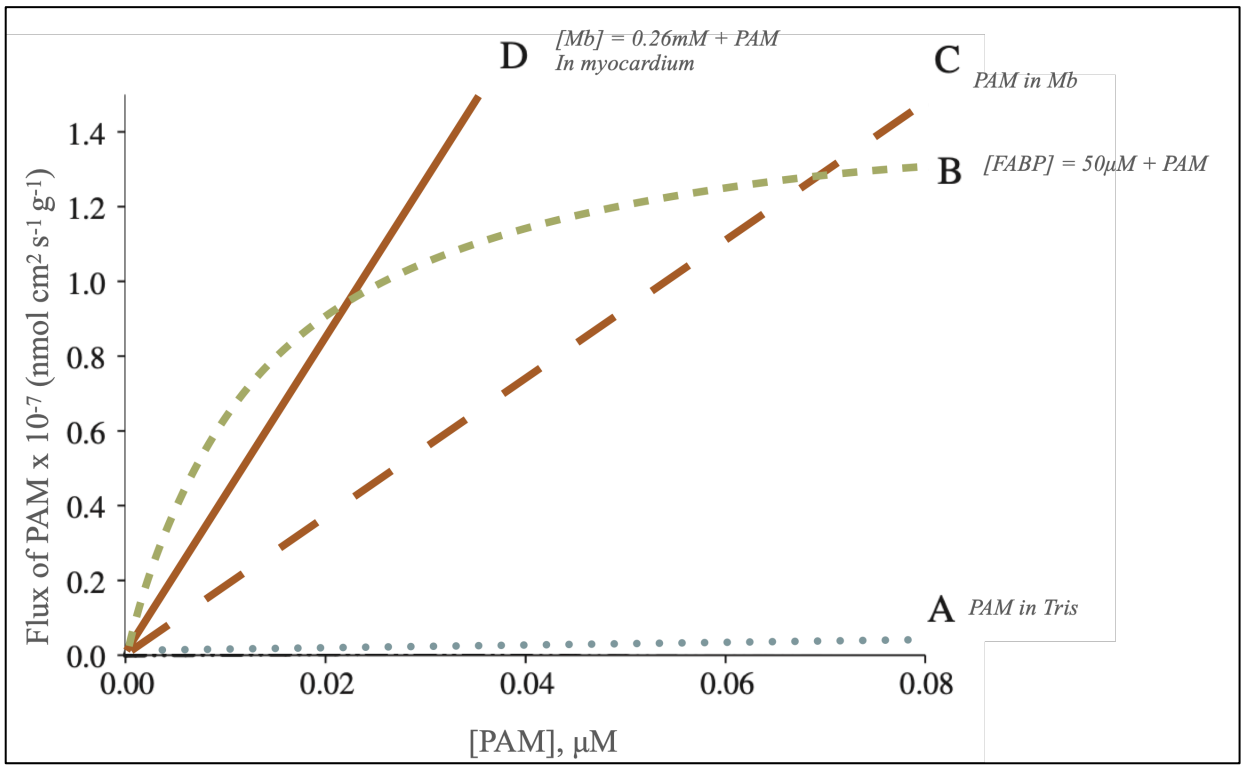

Figure 10: Fatty Acid Flux Model at Low [PAM]
*Model of palmitate flux at low palmitate concentration: **A** PAM in Tris (0.8% solubility). **B** FABP facilitated transport of FA (50 μM FABP, K_d = 14 nM). **C** PAM in the presence of Mb (PAM increased 41% solubility). **D** Mb facilitated transport of PAM (Mb = 0.26 mM, K_d = 48 μM). PAM flux in the presence of Mb exceeds FABP facilitated PAM flux above 0.07 μM PAM. Mb mediated transport of PAM exceeds FABP–PAM flux at PAM concentration above 0.02 μM PAM. The V_{max} values per g tissue for FABP = 1.5×10^{-7} nmol cm^2 s^{-1} g^{-1} and for Mb = 2.0×10^{-4} nmol cm^2 s^{-1} g^{-1}. The corresponding 1/2 V_{max} for FABP = 7.5×10^{-4} nmol cm^2 s^{-1} g^{-1} and for Mb = 1.0×10^{-4} nmol cm^2 s^{-1} g^{-1}.* *Adapted from Shih, Chung et al. 2014.*

Oxy-Mb has a larger dissociation constant than FABP and displays both specific and non-specific binding, so it does have lower affinity for FA than FABP in the sarcolemma during uptake. Deoxy-Mb has a much lower FA binding affinity than oxy-Mb (Shih et al, 2014). However, when Mb gets to the mitochondria, where there is a lower oxygen

concentration, it releases its O_2 becoming deoxy-Mb. Since deoxy Mb has an even lower affinity for FA than oxy-Mb, FA can be released easily.

(iv) Myoglobin Oxidization

One of the ways the average person observes Mb in their day-to-day life is at the deli counter. The bright red color of fresh meat is due to oxy-Mb being in the Fe^{2+} state; over time this oxidizes to the brown colored Fe^{3+} of met-myoglobin (met-Mb) (Mancini and Hunt 2005, Faustman, Sun et al. 2010, Suman and Joseph 2013, Ramanathan, Hunt et al. 2021). In live tissue, the met-Mb levels are kept extremely low by a Mb reductase that rapidly converts met-Mb back to MbO_2 (Hagler, Coppes et al. 1979, Chung, Xu et al. 1996, Kreutzer and Jue 2006).

Post-mortem, the redox chemistry is less clear once the Mb reductase activity diminishes, as it can no longer convert the met-Mb back to MbO_2. Food science has been looking for ways to slow down the tissue oxidization to keep meat looking fresher for longer since Mb's role in this process was discovered. Typically, in food science, studies have focused on the standard Mb autoxidation mechanism that involves the release of a reactive superoxide that allows hydrogen peroxide (H_2O_2) to readily react with met-Mb producing reactive species of Mb, which promotes lipid oxidization that degrades food quality (Baron and Andersen 2002, Wallace, Houtchens et al. 1982, Gorelik and Kanner 2001). However, this focus ignores the superoxide-free oxidization reaction that occurs when MbO_2 transfers an electron to an acceptor, such as Cytochrome C Oxidase ($Cyt^{3+}C$), but nevertheless produces met-Mb (Wu, Duffy et al. 1972, Frankel 1980).

Reports that a normal lipid oxidation product, nonenal: 4-hydroxynon-2-enal (HNE), seen in Figure 11, could create a positive feedback loop to accelerate Mb autoxidation seemed too good to be true, because controlling HNE production could break that feedback loop,

reducing Mb oxidization, and in turn, decreasing meat discoloration (Alderton, Faustman et al. 2003, Faustman, Sun et al. 2010, Grunwald, Tatiyaborworntham et al. 2017). Any HNE-induced autoxidation would require a significant interaction between the 9 carbon HNE and Mb, contradicting recent NMR observations that FA interaction with Mb requires a minimum carbon chain length of more than 10. Shorter chains do not bind specifically or nonspecifically to Mb (Shih, Chung et al. 2014, Shih, Chung et al. 2015, Jue, Shih et al. 2017). After recent optical and NMR spectroscopy studies found no evidence of a Mb—HNE interaction, nor the formation of a histidine adduct, it doesn't seem that HNE can alter the rate of Mb autoxidation. Furthermore, HNE also does not increase Mb oxidation via electron transfer to Cytochrome C (Wu, Duffy et al. 1972, Foucat, Renerre et al. 1994, Shih, Chung et al. 2015).

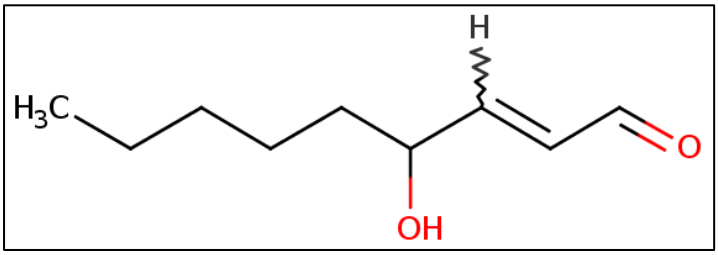

Figure 11: Nonenal line drawing
4-hydroxynon-2-enal

iii. Myoglobin NMR Studies

Many NMR studies have been conducted on a variety of Mb states and ligands in order to gain insight on interactions. The three topics of study I focus on can be boiled down to: oxy- vs deoxy-Mb, FA chain length dependent interactions with Mb, and oxidization rate of Mb.

a. Oxy vs Deoxy Myoglobin

Previous studies found that PAM does not appear to interact with deoxy-Mb. In the presence of PAM, deoxy-Mb exhibits no significant change in signal intensity or chemical shift. Contrastingly, PAM interacts specifically with oxy-Mb. Past $^{13}C_1$-NMR experiments with PAM in oxy-Mb and deoxy-Mb also confirmed contrasting interactions shown in Figure 12. When PAM was added to oxy-Mb, the spectra showed the PAM carboxyl group signal. Whereas with deoxy-Mb, no PAM signal appeared (Shih, Chung et al. 2014).

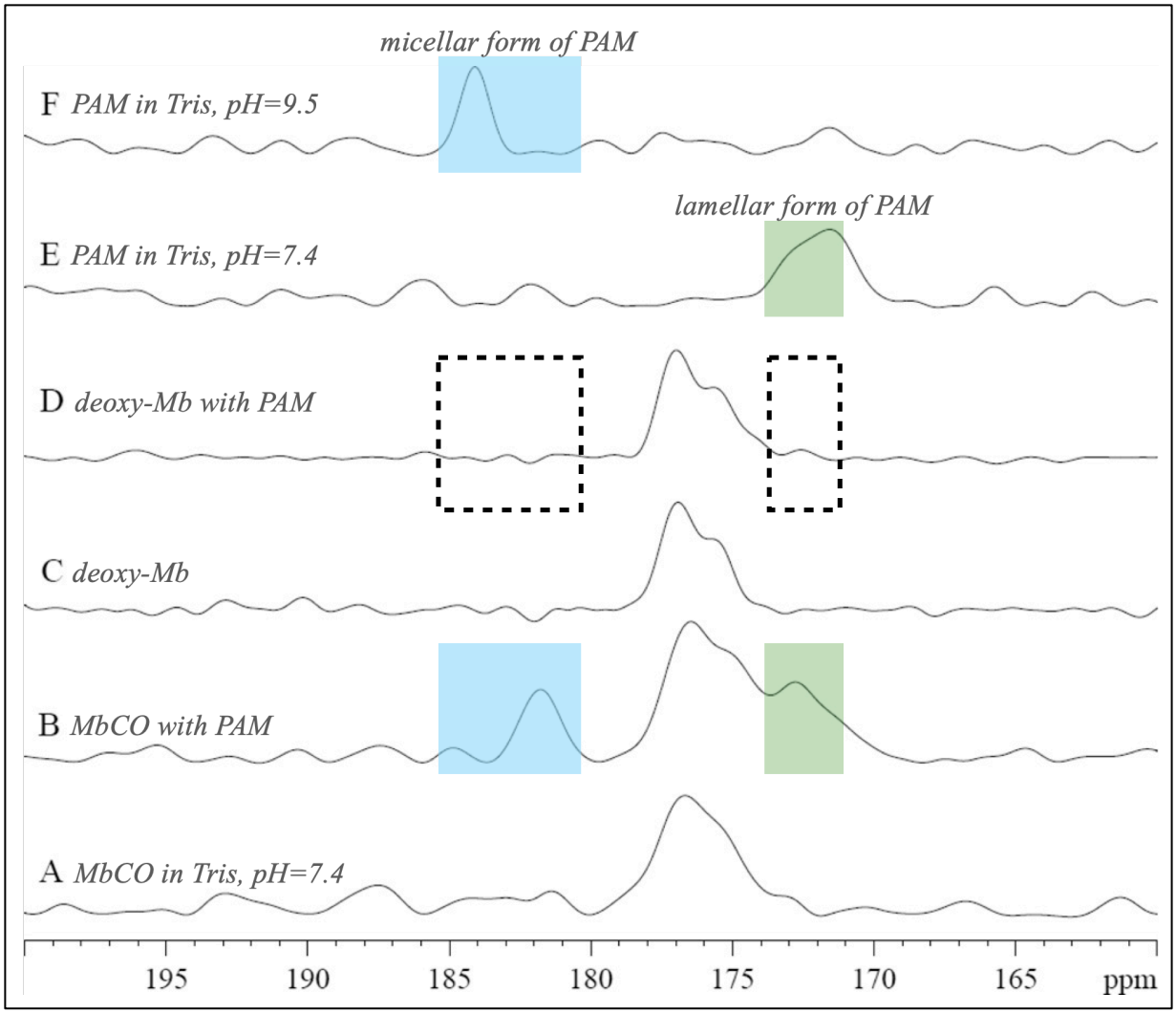

Figure 12: $^{13}C_1$ NMR Spectra of Mb and PAM

PAM in MbCO, deoxy Mb, and Tris exhibit contrasting spectra:

A *0.8 mM MbCO in 30 mM Tris buffer at pH 7.4 at 35°C.*

B *0.8 mM MbCO with 0.8 mM PAM. PAM peaks appear at 173 (green, lamellar) and 182 ppm (blue, micellar).*

C *0.8 mM deoxy Mb.*

D *0.8 mM deoxy-Mb with 0.8 mM PAM. The dashed boxes represent where we would expect to see PAM if it interacted with deoxy-Mb.*

E *3.2 mM PAM in Tris buffer, pH 7.4. $^{13}C_1$ PAM appears at 172 ppm.*

F *3.2 mM PAM in Tris buffer, pH 9.5. $^{13}C_1$ PAM appears at 184ppm.*

Adapted from Shih, Chung et al. 2014.

In contrast previous studies have noted a specific PAM—oxy-Mb interaction is indicated by selective ^{1}H-NMR signal intensity loss upon the addition of PAM (Shih, Chung et al. 2014). PAM induces intensity changes in several ring current shifted peaks; reported literature assignments suggest these are Valine-17 and Leucine-2 (Mabbutt and Wright 1985).

b. Fatty Acid Chain Length Dependence

Previous studies have found that FA-Mb interaction is dependent on the FA carbon chain length seen in Figure 13 (Jue, Shih et al. 2017). Short chain FAs (octanoic, OCT C8:0 and decanoic, DEC C10:0) do not appear to interact with Mb. Whereas medium and long chain FAs (lauric acid, LAU C12:0; myristic acid, MYR C14:0; and palmitic acid, PAM C16:0) do show an interaction with Mb. Pronounced effect can be seen in LAU and its 'relative' lauric sulfate, LAU 1-SO_4, (commonly known as sodium dodecyl sulfate or SDS) even at lower ratios than previously reported (Tofani, Feis et al. 2004). One thought would be that the detergent (DET) property of FA would explain the interaction with myoglobin, but we can refute this hypothesis since cationic, anionic, and neutral DETs at a DET:Mb ratio of 1:1 do not perturb any Mb signal. They show no binding to Mb, neither specifically nor non-specifically.

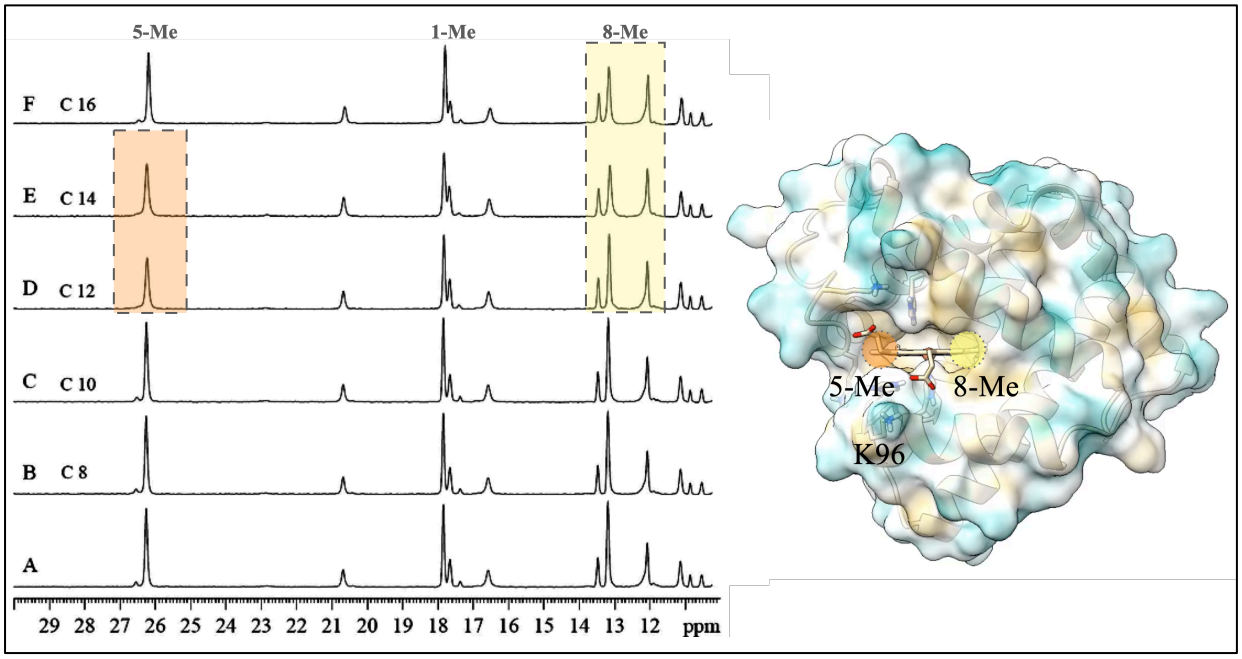

Figure 13: NMR oxy-Mb interaction with PAM
^{1}H-NMR spectra (30– 10 ppm) of 0.8 mM MbCN in 30 mM Tris at 35°C with FA of different chain lengths at added FA to reach FA:Mb of 1:1 ***A*** *ratio control,* ***B*** *octanoic acid (C8:0, OCT).* ***C*** *decanoic (C10:0, DEC),* ***D*** *lauric acid (C12:0, LAU),* ***E*** *myristic acid (C14:0, MYR),* ***F*** *palmitic acid (C16:0, PAM). C8:0 and C10:0 FA do not significantly perturb the spectra. C12:0 and C14:0 FA perturb both the 5(orange)- and 8(yellow)-heme-methyl groups. C16:0 perturbs only the 8-heme-methyl group. Adapted from Jue, Shih et al. 2017.*

Adding palmitic acid, PAM C16:0, or oleic acid, OLE C18:0, to Fe (III) MbCN perturbs the hyperfine shifted 8-heme-methyl signal selectively and increases the apparent solubility of the FA (Shih et al 2014, Sriram et al 2008). Neither PAM nor OLE appear to interact specifically or non-specifically with the unligated form, deoxy-Mb (DMb). This again supports the convenient mechanism in loading and unloading FA described above in I.B.ii.b.*(iii)*.

c. Myoglobin—Nonenal Interaction

Other studies suggested an interaction between Mb and nonenal (HNE), that could increase the oxidization by electron transfer and the autoxidation rate of Mb. Jue lab further investigations suggest another possible explanation.

(i) HNE and Mb Autoxidation

Recent studies report an equine Mb autoxidation rate constant of 1.64×10^{-3} min^{-1} (Germolus, Rehman et al. 2022). Experiments claiming HNE-enhanced Mb autoxidation used an HNE:Mb ratio of 6:1 and 1.5% ethanol (EtOH) for solubilization, which can obscure the NMR results either with non-specific interactions or with the formation of hemichrome, respectively (Akhrem, Andreyuk et al. 1989). More recent studies at more appropriate ratios, similar to those of FA:Mb, conclude HNE does not impact Mb autoxidation (Shih, Chung et al. 2014, Shih, Chung et al. 2015, Germolus, Rehman et al. 2022). In fact, the same NMR data suggests it's more likely EtOH is doing the heavy lifting in increasing Mb autoxidation. HNE has no observed effect (Germolus, Rehman et al. 2022).

(ii) HNE and Mb Oxidation by Electron Transfer

As opposed to the autoxidation of Mb, an appropriate electron acceptor can also oxidize Mb. Indeed, recent studies observed Mb transferring an electron to $Cyt^{3+}C$ 2.3 times faster than Mb autoxidation. Even at a ratio of 4:1 HNE:Mb researchers did not observe any change to the rate of Mb oxidation via electron transfer. Again, it seems the EtOH used in the experiments is the causative factor in Mb redox reaction, increasing the Mb electron transfer rate to $Cyt^{3+}C$ by more than 15%.

III. Introduction to Molecular Docking

In order to investigate the NMR results from previous studies, and possibly confirm them *in silico*, molecular docking is a far more cost-effective method of research.

A. Historical Background

While we may consider molecular docking a newer field beginning as this thesis did, with Kendrew and Perutz, truth be told its beginnings are more than those 60 years past. General

consensus among scientific historians is that the first theory describing binding dates back to 1894, with Emil Fischer's "lock-and-key" model (Fischer 1894). It's one of the first models we learn when studying enzyme specificity. The model entails both a rigid ligand and macromolecule that are naturally complementary shapes that fit together like lock and key. However, when scientists were observing new enzyme behavior, such as non-competitive inhibition and allosteric modulation in the 1950s, the lock-and-key model needed to be augmented to describe these new phenomena.

In 1958, Koshland introduced a new model called the "induced fit" theory where, according to his observations, a ligand can induce conformational changes in the macromolecule, thus allowing for optimized ligand-active site interactions (Koshland 1958). Later scientists would suggest that proteins naturally exist as an ensemble of conformations on an energy landscape, where ligands preferentially bind to one of the conformations (Monod, Wyman et al. 1965, Austin, Beeson et al. 1975, Frauenfelder, Sligar et al. 1991, Foote and Milstein 1994). This "conformational selection" model interprets binding as the ligand stabilizing one of the protein conformations, resulting in a shift in the protein population equilibrium on the energy landscape (Kumar, Ma et al. 2000).

The two newer models: "induced fit" and "conformational selection" conflict in the timeline of events that the binding process can be broken down into (Kobilka and Deupi 2007, Okazaki and Takada 2008, Zhou 2010). Newer theories like the "extended conformational selection" model combine these different models where a conformational selection is made and then is followed by a conformational adjustment based on the induced fit theory (Csermely, Palotai et al. 2010). This evolution of binding models describing ligand-target binding is at the root of rational drug design.

B. Approaches

There are two broad categories in molecular docking methodology: matching and docking simulations (Rosenfeld, Vajda et al. 1995).

i. Matching

The matching approach focuses on the spatial and geometrical fit of a ligand into a static active site. This method approximates hydrogen bonding and steric accessibility constraints. An example of a matching simulation program is DOCK, which can rapidly screen chemical databases for potential compounds. This is especially useful in drug discovery (Kuntz, Blaney et al. 1982, Shoichet and Kuntz 1993). However, this method is not as effective in cases of induced fit, structural water active site interaction, or more energetically dependent binding.

ii. Docking

In contrast, the docking approach is more in depth, with flexible active site residues and ligand torsional degrees of freedom to explore the ligands translation, orientation, and conformation trajectory. Of course, this level of detail in molecular mechanics and approximation of binding energy comes at a cost, making it more computationally expensive as well as time intensive. An example of a docking simulation program is AutoDock, which has effectively modeled a range of complexes including: enzyme-inhibitor, peptide-antibody, and even protein-protein for over 30 years (Stoddard and Koshland 1992, Friedman, Roberts et al. 1994, Lunney, Hagen et al. 1994, Goodsell, Morris et al. 1996, Morris, Goodsell et al. 1996, Goodsell, Sanner et al. 2021). AutoDock also has a method of hydrated docking, where W-pseudo atoms are used instead of a 3-point water molecule discussed later.

Scoring functions are used to discern relevant binding conformations from non-binders in the resulting pool of conformations generated. It can help by 'scoring' the quality of a conformation. There are three main types of scoring functions:

a. Force-field Based Scoring Functions

A force-field approximates the potential energy of a system using molecular mechanics by combining intramolecular and intermolecular components. A well-known and widely utilized force-field is called CHARMM (Chemistry at HARvard Molecular Mechanics) whose governing equations can be seen in Equation 1 where V is the potential energy (Brooks, Brooks III et al. 2009). Molecular mechanics is used to reduce computational cost by applying the laws of classical mechanics onto molecules to approximate the quantum mechanical calculations typically required on the molecular scale (Vanommeslaeghe, Guvench et al. 2014). In this method atoms are charged spheres connected by springs whose electrons are ignored in accordance with the Born-Oppenheimer approximation (Born and Oppenheimer 1927). The bonded portion of the force-field is approximated by trigonometric functions that describe torsional potentials, whereas the nonbonded portion is made up of various terms, like van der Waals and Coulomb electrostatic interactions between atom pairs. The parameters of the force-field are obtained by fitting quantum mechanical or experimental values.

Equation 1: CHARMM force field

$$V = V_{bonded} + V_{nonbonded} \quad \text{Eqn. 1}$$

$$V_{bonded} = \sum_{bonds} K_b(b - b_0)^2 + \sum_{angles} K_\theta(\theta - \theta_0)^2 + \sum_{dihedrals} K_x\left(1 + \cos\left(n_\chi - \delta\right)\right)$$

$$V_{nonbonded} = \sum_{\substack{nonbonded \\ pairs\ ij}} \frac{q_i q_j}{\varepsilon r_{ij}} + \sum_{\substack{nonbonded \\ pairs\ ij}} \varepsilon_{ij}\left[\left(\frac{R_{min,ij}}{r_{ij}}\right)^{12} - 2\left(\frac{R_{min,ij}}{r_{ij}}\right)^{6}\right]$$

Where: K_b , K_θ , and K_χ are the bond, angle, and torsional force constants; b, θ, and χ are bond length, bond angle, and dihedral angle (those with the 0 - subscript are the equilibrium values); n is multiplicity and δ the phase of the torsional periodic function; r_{ij} is the distance between atoms i and j; q_i and q_j are the partial charges of atoms i and j; ε is the effective dielectric constant; ε_{ij} is the Lennard-Jones well depth and $R_{min,ij}$ is the distance between atoms at Lennard-Jones minimum. These terms may appear slightly different in different force-fields, and anharmonicity and cross-terms are generally added (Brooks, Brooks III et al. 2009).

b. Empirical Scoring Functions

The first empirical scoring function was named LUDI, after an impossibly sophisticated game whose rules are so complex they were only ever alluded to, in Herman Hesse's futuristic novel, "Das Glasperienspiel" translated as "The Glass Bead Game" (Hesse 1969, Böhm 1992). While highly sophisticated like its namesake, the rules of this program are known. This type of scoring function is the sum of various empirical energy terms, including van der Waals, electrostatic, hydrogen bond, desolvation, entropy, hydrophobicity, and weighted by coefficients optimized to reproduce binding affinity data of a training set by least squares fitting (Huang and Zou 2010).

c. Knowledge-based Scoring Functions

This method works off the idea that if a ligand-protein contact is more statistically explored, it correlates to a favorable interaction. The score in this method starts with a database of structures where the frequencies of the ligand-protein atom pairwise contacts are

calculated and converted to an energy term. Then when evaluating a conformation, the energy terms of all ligand-protein atom pairs are summed resulting in that conformation's score.

There are also strategies that combine multiple scoring functions to get a "consensus scoring' method (Charifson, Corkery et al. 1999). Machine learning is also a technology being used to calculate quantum mechanical scores (Yuriev, Holien et al. 2015).

C. AutoDock 4

A force-field based scoring function is augmented as a semi-empirical scoring function in the fourth version of AutoDock.

i. Theory and Force-fields

When developing a force-field, certain sacrifices and assumptions must be made in the interest of efficiency and efficacy. Approximations must be made based on previous experimental data, where applicable, and finding a balance that results in relevant and useful data is a real feat. In this fourth iteration, AutoDock's creators refine their scoring function.

a. Free Energy Scoring Function

Equation 2: Estimated Free Energy of Binding

$$\Delta G_{total} = \Delta H_{vdW} + \Delta H_{hb} + \Delta H_{elec} + \Delta S_{tor} + \Delta G_{desolv} \quad \text{Eqn. 2}$$

		Ligand Portion	+ Water Portion	
where,	ΔH_{vdW}	$=\sum_{i,\ j}\left(\frac{A_{ij}}{{r_{ij}}^{12}}-\frac{B_{ij}}{{r_{ij}}^{6}}\right)$	$+W_{wat}\sum_{w,\ j}\left(\frac{A_{wj}}{{r_{wj}}^{12}}-\frac{B_{wj}}{{r_{wj}}^{6}}\right)$	a.
	ΔH_{hb}	$=\sum_{i,\ j}E(t)\left(\frac{C_{ij}}{{r_{ij}}^{12}}-\frac{D_{ij}}{{r_{ij}}^{10}}\right)$	$+W_{wat}\sum_{w,\ j}E(t)\left(\frac{C_{wj}}{{r_{wj}}^{12}}-\frac{D_{wj}}{{r_{wj}}^{10}}\right)$	b.
	ΔH_{elec}	$=\sum_{i,\ j}\left(\frac{q_i q_j}{\varepsilon(r_{ij})\, r_{ij}}\right)$	$+0$	c.
	ΔS_{tor}	$=N_{tor}$	$+0$	d.
	ΔG_{desolv}	$=\sum_{i,\ j}(S_i V_j + S_j V_i)\, exp\left(-\frac{{r_{ij}}^2}{2\sigma^2}\right)$	$+(K_{wat})$	e.

The potentials include:

Equation 2a. a Lennard−Jones (Lennard-Jones 1929) 12−6 dispersion/ repulsion term (ΔH_{vdW}); where A_{ij} and B_{ij} are coefficients and functions of the well depth and the van der Waals radii, depicted in Figure 14.

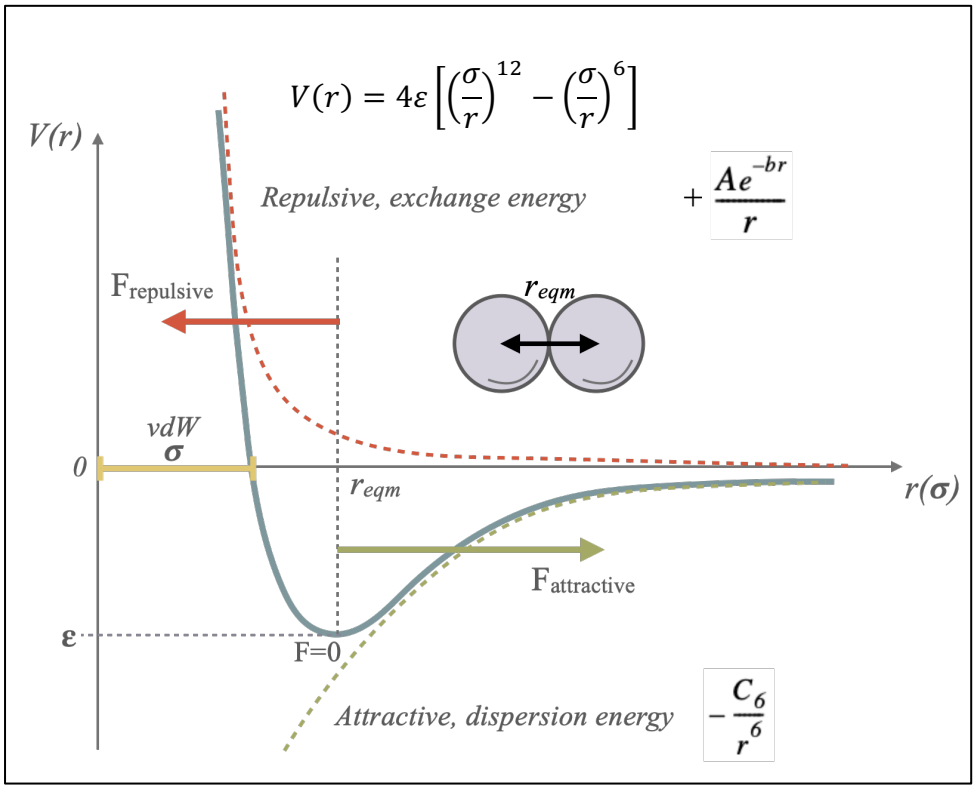

Figure 14: Van der Waals Lennard-Jones Potential
Graphical representation of the model describing the interaction between two non-bonded and uncharged atoms where, V is the intermolecular potential between the two atoms or molecules, ε is the well depth and a measure of how strongly the two particles attract each other, σ is the distance at which the intermolecular potential between the two particles is zero, r is the distance of separation between the centers of both particles.

Equation 2b. a directional 12−10 hydrogen-bonding term (ΔH_{hb}), where E(t) is the directional weight as a function of the angle, t, between the probe and the target atom, described in Equation 3, and shown in Figure 15 (Thorpe, Lei et al. 2001).

Equation 3: Hydrogen-bond energy potential

$$E_{hb} = V_0\left\{5\left(\frac{r_0}{r}\right)^{12} - 6\left(\frac{r_0}{r}\right)^{10}\right\}F(\theta,\phi,\gamma) \qquad \text{Eqn. 3}$$

where,

$$F(\theta,\phi,\gamma) = \begin{cases} \cos^2\theta\exp(-[\pi-\theta]^6)\cos^2(\phi-109.5) & , \quad sp^3 \cdots sp^3 \\ \cos^2\theta\exp(-[\pi-\theta]^6)\cos^2\phi & , \quad sp^3 \cdots sp^2 \\ \{\cos^2\theta\exp(-[\pi-\theta]^6)\}^2 & , \quad sp^2 \cdots sp^3 \\ \cos^2\theta\exp(-[\pi-\theta]^6)\cos^2(\max[\phi,\gamma]) & , \quad sp^2 \cdots sp^2 \end{cases}$$

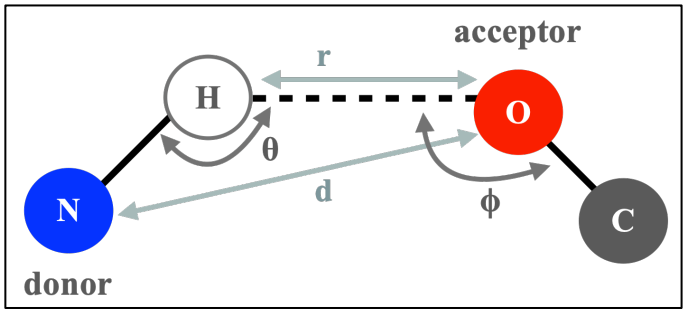

Figure 15: Hydrogen Bond Schematic
The geometry used in the hydrogen-bond energy potential E_{hb}, given in Equation 3. Here θ is the donor—hydrogen—acceptor angle, ϕ is the hydrogen – acceptor—base angle, d is the donor acceptor distance, r is the hydrogen—acceptor distance, and γ (not Shown) is the angle between the normal to the planes defined by the bonds from the donor and acceptor.

Equation 2c. a Coulombic electrostatic potential (ΔH_{elec}) with a distance-dependent dielectric screening (ε) described in Figure 16. The potentials have been parameterized and optimized in earlier versions of AutoDock (Morris, Goodsell et al. 1996).

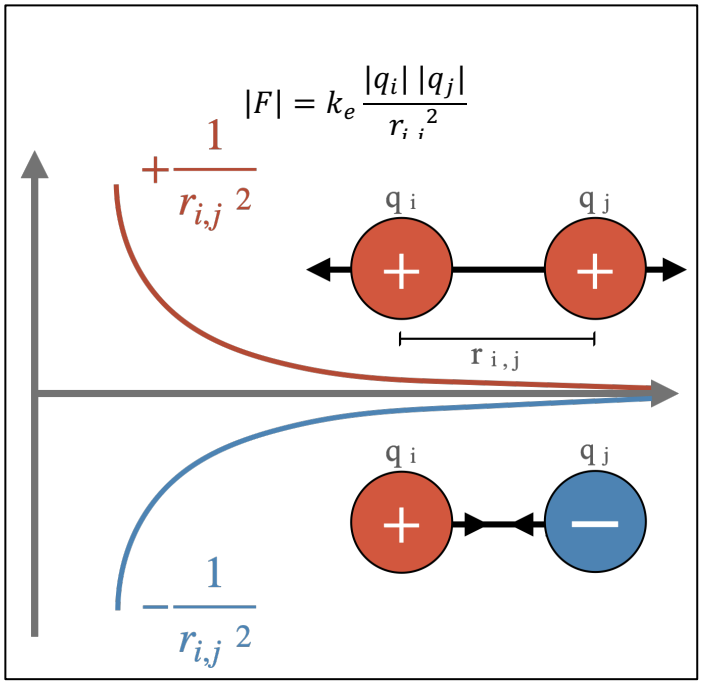

Figure 16: Coulomb's Law
Depiction of the magnitude of the electrostatic force of attraction or repulsion between two point charges as directly proportional to the product of the magnitudes of charges and inversely proportional to the square of the distance between them (Coulomb 1789).

Equation 2d. The entropy of ligand binding (ΔS_{tor}) is included to account for the loss of degrees of freedom upon binding, which is proportional to the number of sp^3 bonds in the ligand (N_{tor}).

Equation 2e. The desolvation term (ΔG_{desolv}) is a function of the solvent-accessible surfaces of ligand (S_i) and protein (S_j) (Mehler and Solmajer 1991) and accounts for the implicit bulk waters present in the docking volume. See Equation 4.

Equation 4: Desolvation Energy

$$\Delta G_{desolv} = W_{desolv} \sum_{i,\ j} (S_i V_j + S_j V_i)\, e^{\left(-\frac{r_{ij}^{\ 2}}{2\sigma^2}\right)} \qquad \text{Eqn. 4}$$

where, $S_i = a_i + k\,|q_i|$

and $a_i = ASP, for\ atom\ i, where$:

Type	ASP		std. error	
C	-0.001	43	0.000	19
A	-0.000	52	0.000	12
N	-0.001	62	0.001	82
O	-0.002	51	0.001	89
H	0.000	51	0.000	52
S	-0.002	14	0.001	18
$k = QASP$	0.010	97	0.002	63

b. Discrete Water Pseudo-atoms

A long known and hotly debated issue with simulations involving proteins could be summed up in the question: "what about the water?" Water, and therefore the hydrophobic effect, is a difficult phenomenon to simulate efficiently or even realistically. There are programs that dry dock, focusing on steric hindrances and geometric basis for binding, but these have limited usefulness *in situ* experimental predictions. There are 3-point water molecules some softwares use to approximate bulk water and then use shells on ordered water enveloping the protein. This method may be more accurate but is certainly more time consuming, not to mention computationally expensive.

To mitigate the disparity between the dry docking and the 3-point water model, AutoDock created a hydrated docking technique using a discrete spherical pseudo-atom, 'W', that has characteristics of both hydrogen and oxygen atoms without the computational cost of 3 atoms per water molecule, and of which an example is shown in Figure 17. This neutrally charged W atom ignores the molecular dipole of a real water molecule while combining the van der Waals and hydrogen bond potentials of hydrogen and oxygen atoms, including acceptor and donor

interactions. The electrostatic component is ignored, and the W atoms do not interact with each other or with the other atoms of the ligand; this prevents water from limiting the ligand flexibility (Forli and Olson 2012).

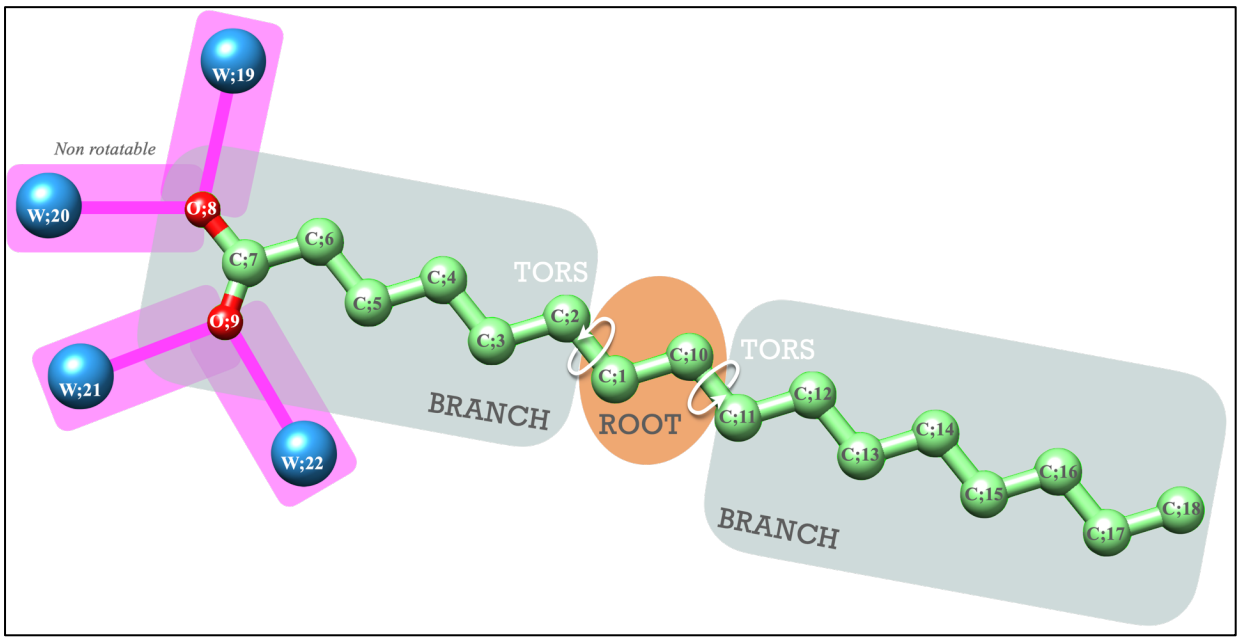

Figure 17: Rotatable bonds and W Pseudo-atoms
Example of W-pseudo-atoms(blue) attached to PAM by non-rotatable bonds (pink), and the Root (orange) from which the rotatable "branches" (grey) sprout. Numbering may look strange but AutoDock numbers each atom starting at the root and branching out, so this example of hydrated PAM has a total of 22 atoms.

ii. Genetic Algorithm

Genetic algorithms (GA) rely on the use of an evolutionary allegory based on the language of natural genetics and biology (Chetverikov, Barker et al. 1926). In molecular docking, the particular state of the ligand in complex with the protein can be represented by the ligand's state variables. That is, a set of values describing the translation, orientation, and conformation of the ligand with respect to the protein, where each of these state variables corresponds to a gene. That would make the ligand's state its genotype and its atomic coordinates represent its phenotype, depicted in Figure 18. The fitness of an individual in molecular docking is evaluated using the

energy function and represents the total interaction energy of the ligand in complex with the protein. Parents, i.e., random pairs of individuals, 'mate' using a crossover operator where offspring inherit genes from either parent. There is also a random mutation operator where some offspring have one gene changed by a random amount. The parental selection process of the current generation is based on the individual's fitness. This corresponds to the "survival of the fittest" concept where the better adapted individuals reproduce and the weaker of the population die without progeny (Spencer 1864).

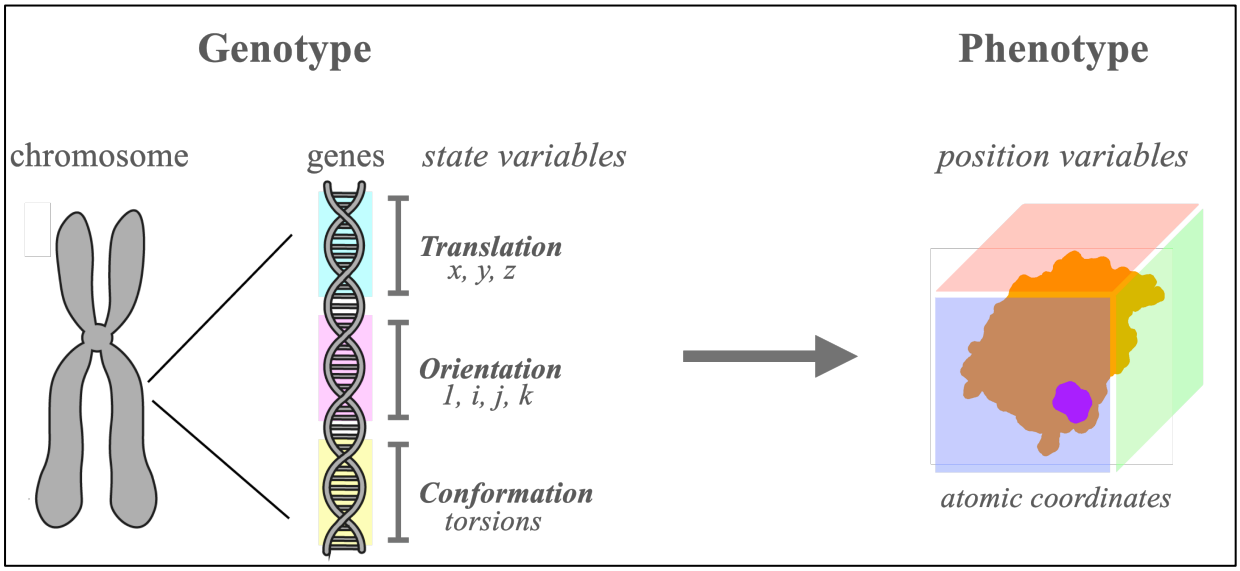

Figure 18: Genotype conversion to Phenotype
Visual representation of the Genotype: 3 state variables of the ligand as genes on a chromosome relating to the Phenotype: position variables, atomic coordinates. Further depicted in the algorithm in Figure 19.

Classical GAs use fixed-length bit 'string' genomes that engage in binary crossover and binary mutation on parents to spawn the next generation of individuals in the population. However, these binary operators can cause the search to be inefficient by producing values outside the domain of interest, i.e., illegal individuals (Morris, Goodsell et al. 1998). Search performance in GAs can be enhanced with the addition of a local search (LS) method (Hart 1994, Hart, Kammeyer et al. 1995).

a. Hybrid Search Method

AutoDock 3.0 implements this GA-LS hybrid by applying a user selected GA for global searching and utilizing a LS method for energy minimization or some combination of both methods, building on previous method refinements (Hart, Kammeyer et al. 1995, Belew and Mitchell 2018). The LS is based on the Solis and Wets method which facilitates torsional space searching (Solis and Wets 1981). This adaptive LS method adjusts the step size based on the recent energies. If there are a {user-defined} number of consecutive failures, i.e., increases of energy, the step-size is doubled to escape local maxima. Conversely a {user-defined} number of consecutive successes, i.e., decreases in energy, results in a halved step size to better explore local minima (Morris, Goodsell et al. 1998). This hybridization of the GA and adaptive LS methods is referred to as the Lamarckian Genetic Algorithm (LGA) (Hart 1994, Rosin, Halliday et al. 1997).

b. Lamarckian Genetic Algorithm

Most GAs utilize Mendelian genetics and follow the major characteristics of Darwinian evolution shown in Figure 19 (Mendel 1865, Darwin 1909). The right side of Figure 19 illustrates the one-way transfer of information from genotype to the phenotype, the Darwinian evolutionary path (shaded in yellow), which utilizes a developmental mapping function. Whereas the left side of Figure 19 shows those cases in which an inverse mapping function can be used to yield a genotype from a given phenotype. This inverse mapping allows the algorithm to finish a LS by replacing the individual with the result of the LS, imitating the Lamarckian evolutionary path (shaded blue). This Lamarckian Genetic Algorithm (LGA) is constructed on Jean Batiste de Lamarck's assertion *(sic)* that phenotypic traits acquired during a lifetime can be inherited by offspring (Lamarck 1914).

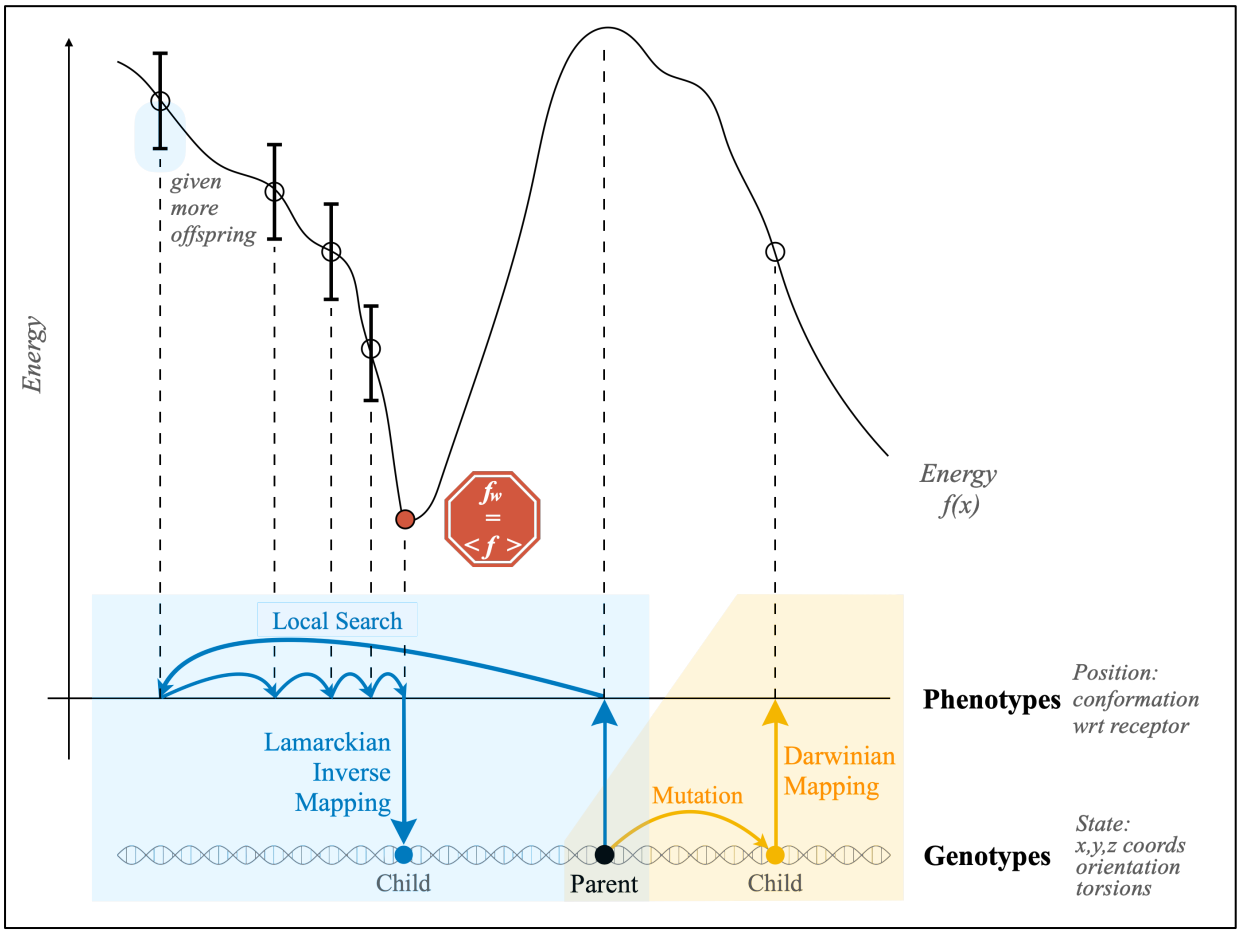

Figure 19: Comparison of Genetic Algorithms
This figure illustrates genotypic and phenotypic search, and contrasts Darwinian and Lamarckian search. The genotypic space is represented by the lower horizontal strand, and the phenotypic space is represented by the upper horizontal line. The fitness function is f(x) which can also be thought of as the energy landscape, the lower the energy the more 'fit' the individual.
Adapted from Morris, Goodsell et al. 1998.

c. Implementation

In AutoDock's implementation, the chromosome is composed of a string of real-valued genes in order: Translation (three Cartesian coordinates of the ligand), Orientation (four-variable quaternion (Maillot 1990)), and Conformation (one real-value for each {user selected} ligand torsion) resulting in a one-to-one mapping of the ligands state variables to the genes of the individual's chromosome (Morris, Goodsell et al. 1998).

From the start, the user defines the number of individuals created in the random population. Each random individual in the starting population is randomized with respect to each gene: the Translation genes are given random x, y, and z values, the Orientation genes are a randomly generated quaternion with a random unit vector and a random rotation angle between +180° and –180°, and the Confirmation genes are given random torsion angles between +180° and –180°. The creation of the random initial population is followed by a loop over generations, repeating until either the maximum number of generations or energy evaluations is reached (Morris, Goodsell et al. 1998). A generation is formally comprised of five ordered stages: 1) mapping and fitness evaluation, 2) selection, 3) crossover, 4) mutation, and 5) elitist selection. Each generation is then followed by LS on a {user defined} portion of the population.

1) **Mapping** roughly mimics the process of translation. Over the entire population, going from an individual's genotype to its analogous phenotype where its fitness can be evaluated, a depiction of the grid files used in mapping can be seen in Figure 20. Fitness is appraised by an energy evaluation function, the sum of the intermolecular interaction energy between the ligand and protein, and the intramolecular interaction energy of the ligand.

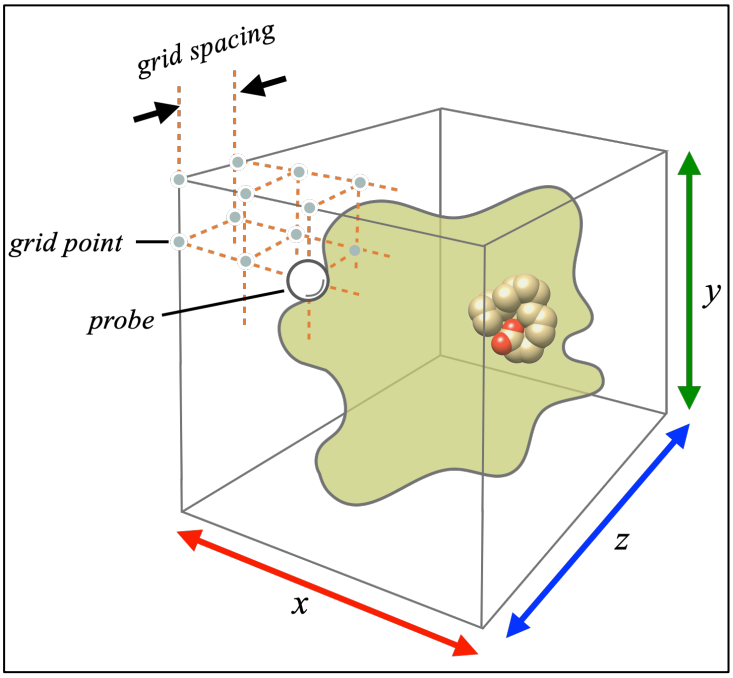

Figure 20: Grid Map
The main features of a grid map. The ligand can be seen 'buried' inside the active site of the globular macromolecule. In this case the grid map encompasses the entire protein. The grid spacing is the same in all 3 dimensions. Adapted from (Olson 2001)

2) **Selection** decides which individuals and to what extent they will mate and reproduce. Thus, the fittest individuals (lower, more favorable energy) produce proportionally more offspring. If the worst fitness in the generation is equal to the mean fitness, the population has converged and docking is terminated.

3) **Crossover** is then performed on random members of the population at {user defined} rates. Each parent's chromosome is broken into the three genes and two-point crossover, where breaks only occur between genes not inside the gene, is implemented. The two resulting offspring then replace their parents in the next generation of the population, keeping a constant population size. (e.g., Parents: ABC and abc, produce offspring: AbC and aBc)

4) **Mutation** is then performed by adding a random real number that has a Cauchy Distribution to one of the genes.

5) **Elitism** (optional) {user defined} integer parameter then determines the number of top individuals that automatically survive to the next generation.

Until one of the termination criteria is met, the LGA will continue to iterate over generations. At termination, AutoDock reports the docked energy, the state variables, the coordinates, and the estimated free energy of binding of the docked conformer. After AutoDock has performed the {user defined} number of GA docking 'runs', clustering analysis is performed on all resulting conformers, and these clusters are ranked from low to high energy (Morris, Goodsell et al. 1998).

d. Box Size

Choosing a box size can be an important, but sometimes overlooked, step in AutoDock. The standard maximum box size is 126pts x 126pts x 126pts (~ 47.25 $Å^3$) however you can directly edit the box size to encompass the entire protein. In the case of Mb, a box of $150pts^3$ (~ 56.25 $Å^3$) was used to contain the entire protein, in all the forms tested. This ensures that the LGA—LS algorithm can search the entire protein for possible binding sites. This all-encompassing method helps prevent biasing the data to a certain binding site from the start. After viewing the results from the full-sized box, you will note the lowest energy cluster will most likely be the N-terminus in our docking runs. This is due to the negative charge on the carboxy head group of the FA being drawn to the positive charge of the N-terminus. Since this is the lowest energy conformation we cannot discount it, but since it is on the opposite side of the protein from the heme-pocket we can set it aside for now, as probably a non-specific interaction.

Now we can continue our docking with a new, more informed box, choosing the heme-facing side of the protein to exclude the N-terminus, so that our algorithm can better investigate the subset of binding sites we saw in the full box results that may have only had a few conformers in their respective clusters. Removing the N-terminus removes the global minimum that absorbed nearly half of our docking runs in the full box. This half-sized box should reveal a more complete picture of possible binding sites, or local minima, that were previously obscured, namely K96, K45, K98, K42. These Lysine residues have the positively charged side chains to bind the FA head but are also lining the heme-pocket and therefore warrant further investigation. With progressively smaller box sizes narrowing in on the heme pocket, your algorithm can focus on the local minima and iterate over it to find lower energy states and possible conformations.

Using this incremental box-sizing method ensures you get all possible binding sites. Then allows for more deep examination of these different sites. Instead of making a box that only contains the region you are interested in from the . Which could lead you down a biased path towards your preferred solution. This way safeguards against the "garbage-in-garbage-out" pitfall of in silico scientific research.

D. Molecular Dynamics

AutoDock has a flexible residues option that basically makes the selected residues flexible with torsional degrees of freedom and grouped with the ligand during docking to find the most stable state. From this, the next step up would be making everything flexible. Called Molecular Dynamics (MD), this 'next step' in protein-ligand interaction modeling treats everything inside the box: the protein, ligand, and water, as flexible (Salmaso, Sturlese et al. 2016). It simulates dynamic interactions over time. The time scales of these simulations vary, but are usually on the order of picoseconds. Originally developed to simulate simple systems, its first

application was in 1957: collisions among hard spheres by Alder and Wainwright (Alder and Wainwright 1957). Biomolecular simulations would take another 20 years to be accomplished. In 1977 Bovine Pancreatic Trypsin Inhibitor (BPTI), a protein with 58 amino acid residues consisting of 454 united atoms, without waters, was used as a test case using a crude by today's standards, molecular mechanics potential, the simulations lasted only 9.2 ps (van Gunsteren and Berendsen 1977).

Although modern MD can span longer time scales, the steps must be short (femtosecond scale) as the events of interest for much of biological research typically occur in nano- to microsecond time scales.

IV. Using AutoDock to Explain NMR

A. Previous Molecular Docking Studies of Myoglobin and Fatty Acid

i. Summary

Studies using AutoDock on Mb and FA have previously been published and I initially intended to reproduce the results and work from there. However, there were a few issues I needed to investigate before I started my work. The use of patchwork PDB models and mixing of organisms' structures were the first to be scrutinized.

a. Macromolecule Preparation

The unavailability of horse (*Equus caballus*) oxy-Mb crystal structure in the *RCSB* Protein DataBank presented the first issue. Chintapalli et al. used horse deoxy-Mb (PDB ID: 2VIK) crystal structure as a base, then clipped the O_2 out of the crystal structure of sperm whale (*Physeter catodon*) oxy-Mb (PDB ID: 1MBO). Its coordinates were transferred into the horse deoxy-Mb crystal structure (Phillips 1980, Hersleth, Uchida et al. 2007). As mentioned in previous sections, the crystal structure and especially the heme positioning is very different in

deoxy-Mb than in oxy-Mb, so this cut and paste technique creates a biologically inaccurate model with questionable practical applicability. However, in order to ameliorate this pitfall, MD simulations were performed on the horse Mb-- whale O_2 complex for 10ns to attain equilibrium and stability before using the model in AutoDock. In later studies, Chintapalli built a mouse (*Mus musculus*) Mb structure using pairwise sequence alignment to their horse model, moving even further away from biological accuracy, because once again the PDB was unavailable.

b. Ligand Preparation

The AutoDock studies that Chintapalli et al. performed used palmitate (PAM) clipped from the human muscle FABP crystal structure (PDB ID: 2HMB) (Zanotti, Scapin et al. 1992). This FA was already in a "characteristic U shape", then was randomized, but the results are still found to have the 'U' shape. Oleic Acid (OLE) taken from axolotl (*Ambystoma mexicanum*) Liver-Bile Acid Binding Protein (L-BABP) crystal structure (PDB ID: 2FTB) was also used (Capaldi, Guariento et al. 2006).

ii. Conclusions

This reproducibility study highlights the need for open access databases, consensus and precedent in the field for modeling practices, and standards for cross-species Mb modeling. Given these issues when following the materials and methods from Chintapalli et al. it was decided the assumptions lacked downstream biological accuracy. For example, the differences in FA binding to Whale Mb vs Horse Mb are presented in Chapter 3, making this callus cut and paste macromolecule construction seem illogical.

B. Proposed Aims of Studies

With an established AutoDock framework for accurate and effective simulations, the structure and function of Mb can be better elucidated. The processes and evidence-based assumption outlined in this chapter lay the groundwork for confirming the ligation dependence of FA binding to Mb seen in NMR data (Chapter 2) and confirming the chain length dependence of FA binding to Mb seen in NMR data (Chapter 3). It creates a baseline to explore the differences in binding FA between species, and a comparison of physiological levels and rates (Chapter 3). The framework allows for AutoDock simulations to investigate bindings of Mb—Cytochrome C Oxidase, Mb—nonenal, and Mb—Ethanol that complement spectrometry data (Chapter 3).

V. REFERENCES

Akhrem, A. A., G. M. Andreyuk, M. A. Kisel and P. A. Kiselev (1989). "Hemoglobin conversion to hemichrome under the influence of fatty acids." Biochimica et Biophysica Acta (BBA) - General Subjects 992(2): 191-194.

Alder, B. J. and T. E. Wainwright (1957). "Phase Transition for a Hard Sphere System." The Journal of Chemical Physics **27**(5): 1208-1209.

Alderton, A. L., C. Faustman, D. C. Liebler and D. W. Hill (2003). "Induction of redox instability of bovine myoglobin by adduction with 4-hydroxy-2-nonenal." Biochemistry **42**(15): 4398-4405.

Austin, R. H., K. W. Beeson, L. Eisenstein, H. Frauenfelder and I. C. Gunsalus (1975). "Dynamics of ligand binding to myoglobin." Biochemistry **14**(24): 5355-5373.

Banaszak, L., N. Winter, Z. Xu, D. A. Bernlohr, S. Cowan and T. A. Jones (1994). "Lipid-binding proteins: a family of fatty acid and retinoid transport proteins." Adv Protein Chem **45**: 89-151.

Baron, C. P. and H. J. Andersen (2002). "Myoglobin-induced lipid oxidation. A review." J Agric Food Chem **50**(14): 3887-3897.

Belew, R. K. and M. Mitchell (2018). Adaptive Individuals In Evolving Populations: Models And Algorithms.

Böhm, H.-J. (1992). "The computer program LUDI: A new method for the de novo design of enzyme inhibitors." Journal of Computer-Aided Molecular Design **6**(1): 61-78.

Born, M. and R. Oppenheimer (1927). "Zur Quantentheorie der Molekeln." Annalen der Physik **389**(20): 457-484.

Brooks, B. R., C. L. Brooks III, A. D. Mackerell Jr., L. Nilsson, R. J. Petrella, B. Roux, Y. Won, G. Archontis, C. Bartels, S. Boresch, A. Caflisch, L. Caves, Q. Cui, A. R. Dinner, M. Feig, S. Fischer, J. Gao, M. Hodoscek, W. Im, K. Kuczera, T. Lazaridis, J. Ma, V. Ovchinnikov, E. Paci, R. W. Pastor, C. B. Post, J. Z. Pu, M. Schaefer, B. Tidor, R. M. Venable, H. L. Woodcock, X. Wu, W. Yang, D. M. York and M. Karplus (2009). "CHARMM: The biomolecular simulation program." Journal of Computational Chemistry **30**(10): 1545-1614.

Busse, S. C. and T. Jue (1994). "Two-dimensional NMR characterization of the deoxymyoglobin heme pocket." Biochemistry **33**(36): 10934-10943.

Capaldi, S., M. Guariento, M. Perduca, S. M. Di Pietro, J. A. Santomé and H. L. Monaco (2006). "Crystal structure of axolotl (Ambystoma mexicanum) liver bile acid-binding protein bound to cholic and oleic acid." Proteins **64**(1): 79-88.

Carver, T. E., J. S. Olson, S. J. Smerdon, S. Krzywda, A. J. Wilkinson, Q. H. Gibson, R. S. Blackmore, J. D. Ropp and S. G. Sligar (1991). "Contributions of residue 45(CD3) and heme-6-propionate to the biomolecular and geminate recombination reactions of myoglobin." Biochemistry **30**(19): 4697-4705.

Charifson, P. S., J. J. Corkery, M. A. Murcko and W. P. Walters (1999). "Consensus Scoring: A Method for Obtaining Improved Hit Rates from Docking Databases of Three-Dimensional Structures into Proteins." Journal of Medicinal Chemistry **42**(25): 5100-5109.

Chetverikov, S. S., M. Barker and I. M. Lerner (1926). "On Certain Aspects of the Evolutionary Process from the Standpoint of Modern Genetics." Proceedings of the American Philosophical Society **105**(2): 167-195.

Chung, Y., S. J. Huang, A. Glabe and T. Jue (2006). "Implication of CO inactivation on myoglobin function." Am J Physiol Cell Physiol **290**(6): C1616-1624.

Chung, Y. and T. Jue (1996). "Cellular response to reperfused oxygen in the postischemic myocardium." Am J Physiol **271**(2 Pt 2): H687-695.

Chung, Y., P. A. Molé, N. Sailasuta, T. K. Tran, R. Hurd and T. Jue (2005). "Control of respiration and bioenergetics during muscle contraction." Am J Physiol Cell Physiol **288**(3): C730-738.

Chung, Y., D. Xu and T. Jue (1996). "Nitrite oxidation of myoglobin in perfused myocardium: implications for energy coupling in respiration." American Journal of Physiology-Heart and Circulatory Physiology **271**(3): H1166-H1173.

Corsico, B., H. L. Liou and J. Storch (2004). "The alpha-helical domain of liver fatty acid binding protein is responsible for the diffusion-mediated transfer of fatty acids to phospholipid membranes." Biochemistry **43**(12): 3600-3607.

Coulomb, C. A. (1789). Mémoires sur l'électricité et la magnétisme. Académie royale des sciences (France), Chez Bachelier, libraire**:** 569-577.

Csermely, P., R. Palotai and R. Nussinov (2010). "Induced fit, conformational selection and independent dynamic segments: an extended view of binding events." Trends in Biochemical Sciences **35**(10): 539-546.

Darwin, C. (1909). The Origin of Species, P. F. Collier.

Dolar, M. L., P. Suarez, P. J. Ponganis and G. L. Kooyman (1999). "Myoglobin in pelagic small cetaceans." J Exp Biol **202**(Pt 3): 227-236.

Elber, R. and M. Karplus (1987). "Multiple conformational states of proteins: a molecular dynamics analysis of myoglobin." Science **235**(4786): 318-321.

Faustman, C., Q. Sun, R. Mancini and S. P. Suman (2010). "Myoglobin and lipid oxidation interactions: mechanistic bases and control." Meat Sci **86**(1): 86-94.

Fischer, E. (1894). "Einfluss der Configuration auf die Wirkung der Enzyme." Berichte der deutschen chemischen Gesellschaft **27**(3): 2985-2993.

Flögel, U., T. Laussmann, A. Gödecke, N. Abanador, M. Schäfers, C. D. Fingas, S. Metzger, B. Levkau, C. Jacoby and J. Schrader (2005). "Lack of myoglobin causes a switch in cardiac substrate selection." Circ Res **96**(8): e68-75.

Flögel, U., M. W. Merx, A. Gödecke, U. K. M. Decking and J. Schrader (2001). "Myoglobin: A scavenger of bioactive NO." Proceedings of the National Academy of Sciences **98**(2): 735-740.

Foote, J. and C. Milstein (1994). "Conformational isomerism and the diversity of antibodies." Proceedings of the National Academy of Sciences **91**(22): 10370-10374.

Forli, S. and A. J. Olson (2012). "A Force Field with Discrete Displaceable Waters and Desolvation Entropy for Hydrated Ligand Docking." Journal of Medicinal Chemistry **55**(2): 623-638.

Foucat, L., M. Renerre and M. Anton (1994). "1H-NMR study of bovine myoglobin autoxidation. Influence of muscle type and time post mortem." International journal of food science & technology **29**(1): 8.

Frankel, E. N. (1980). "Lipid oxidation." Progress in Lipid Research **19**(1): 1-22.

Frauenfelder, H., S. G. Sligar and P. G. Wolynes (1991). "The Energy Landscapes and Motions of Proteins." Science **254**(5038): 1598-1603.

Friedman, A. R., V. A. Roberts and J. A. Tainer (1994). "Predicting molecular interactions and inducible complementarity: fragment docking of Fab-peptide complexes." Proteins **20**(1): 15-24.

Germolus, C. B., U. N. Rehman, A. A. Ramahi and T. Jue (2022). "Lipid oxidation product nonenal and myoglobin oxidation." International Journal of Food Science & Technology **57**(10): 6602-6612.

Gimenez, M., R. J. Sanderson, O. K. Reiss and N. Banchero (1977). "Effects of altitude on myoglobin and mitochondrial protein in canine skeletal muscle." Respiration **34**(3): 171-176.

Glabe, A., Y. Chung, D. Xu and T. Jue (1998). "Carbon monoxide inhibition of regulatory pathways in myocardium." American Journal of Physiology-Heart and Circulatory Physiology **274**(6): H2143-H2151.

Glatz, J. F. C. and J. H. Veerkamp (1983). "A Radiochemical Procedure for the Assay of Fatty-Acid Binding by Proteins." Analytical Biochemistry **132**(1): 89-95.

Gloster, J. (1977). "Studies on fatty acid binding characteristics of myoglobin and Z protein." Journal of Molecular and Cellular Cardiology **9**(9, Supplement): 15.

Gloster, J. and P. Harris (1977). "Fatty acid binding to cytoplasmic proteins of myocardium and red and white skeletal muscle in the rat. A possible new role for myoglobin." Biochem Biophys Res Commun **74**(2): 506-513.

Goodsell, D. S., G. M. Morris and A. J. Olson (1996). "Automated docking of flexible ligands: applications of AutoDock." J Mol Recognit **9**(1): 1-5.

Goodsell, D. S., M. F. Sanner, A. J. Olson and S. Forli (2021). "The AutoDock suite at 30." Protein Science **30**(1): 31-43.

Gorelik, S. and J. Kanner (2001). "Oxymyoglobin Oxidation and Membrane Lipid Peroxidation Initiated by Iron Redox Cycle: Prevention of Oxidation by Enzymic and Nonenzymic Antioxidants." Journal of Agricultural and Food Chemistry **49**(12): 5945-5950.

Götz, F. M., M. Hertel and U. Gröschel-Stewart (1994). "Fatty acid binding of myoglobin depends on its oxygenation." Biol Chem Hoppe Seyler **375**(6): 387-392.

Gros, G., B. A. Wittenberg and T. Jue (2010). "Myoglobin's old and new clothes: from molecular structure to function in living cells." The Journal of Experimental Biology **213**(16): 2713-2725.

Grunwald, E. W., N. Tatiyaborworntham, C. Faustman and M. P. Richards (2017). "Effect of 4-hydroxy-2-nonenal on myoglobin-mediated lipid oxidation when varying histidine content and hemin affinity." Food Chemistry **227**: 289-297.

Guyton, G. P., K. S. Stanek, R. C. Schneider, P. W. Hochachka, W. E. Hurford, D. G. Zapol, G. C. Liggins and W. M. Zapol (1995). "Myoglobin saturation in free-diving Weddell seals." J Appl Physiol (1985) **79**(4): 1148-1155.

Hagler, L., R. I. Coppes and R. H. Herman (1979). "Metmyoglobin reductase. Identification and purification of a reduced nicotinamide adenine dinucleotide-dependent enzyme from bovine heart which reduces metmyoglobin." Journal of Biological Chemistry **254**(14): 6505-6514.

Hart, W. E. (1994). Adaptive global optimization with local search. Doctor of Philosophy Thesis, University of California, San Diego.

Hart, W. E., T. E. Kammeyer and R. K. Belew (1995). The Role of Development in Genetic Algorithms. Foundations of Genetic Algorithms. L. D. Whitley and M. D. Vose, Elsevier. **3:** 315-332.

Hersleth, H. P., T. Uchida, A. K. Røhr, T. Teschner, V. Schünemann, T. Kitagawa, A. X. Trautwein, C. H. Görbitz and K. K. Andersson (2007). "Crystallographic and spectroscopic studies of peroxide-derived myoglobin compound II and occurrence of protonated FeIV O." J Biol Chem **282**(32): 23372-23386.

Hesse, H. (1969). The glass bead game (Magister Ludi) / Hermann Hesse ; translated from the German by Richard and Clara Winston ; with a foreword by Theodore Ziolkowski. New York, Holt, Rinehart and Winston.

Holland, J. H. (1992). Adaptation in Natural and Artificial Systems: An Introductory Analysis with Applications to Biology, Control, and Artificial Intelligence, The MIT Press.

Huang, S.-Y. and X. Zou (2010). "Advances and Challenges in Protein-Ligand Docking." International Journal of Molecular Sciences **11**(8): 3016-3034.

Jue, T., L. Shih and Y. Chung (2017). "Differential Interaction of Myoglobin with Select Fatty Acids of Carbon Chain Lengths C8 to C16." Lipids **52**(8): 711-727.

Kendrew, J. C., G. Bodo, H. M. Dintzis, R. G. Parrish, H. Wyckoff and D. C. Phillips (1958). "A three-dimensional model of the myoglobin molecule obtained by x-ray analysis." Nature **181**(4610): 662-666.

Kobilka, B. K. and X. Deupi (2007). "Conformational complexity of G-protein-coupled receptors." Trends in Pharmacological Sciences **28**(8): 397-406.

Kooyman, G. L. and P. J. Ponganis (1998). "The physiological basis of diving to depth: birds and mammals." Annu Rev Physiol **60**: 19-32.

Koshland, D. E. (1958). "Application of a Theory of Enzyme Specificity to Protein Synthesis[*]." Proceedings of the National Academy of Sciences **44**(2): 98-104.

Kreutzer, U. and T. Jue (2004). "Role of myoglobin as a scavenger of cellular NO in myocardium." American Journal of Physiology-Heart and Circulatory Physiology **286**(3): H985-H991.

Kreutzer, U. and T. Jue (2006). "Investigation of bioactive NO-scavenging role of myoglobin in myocardium." Pflügers Archiv **452**(1): 36-42.

Kumar, S., B. Ma, C.-J. Tsai, N. Sinha and R. Nussinov (2000). "Folding and binding cascades: Dynamic landscapes and population shifts." Protein Science **9**(1): 10-19.

Kuntz, I. D., J. M. Blaney, S. J. Oatley, R. Langridge and T. E. Ferrin (1982). "A geometric approach to macromolecule-ligand interactions." J Mol Biol **161**(2): 269-288.

La Mar, G. N., D. B. Viscio, K. Gersonde and H. Sick (1978). "Proton nuclear magnetic resonance study of the rotational position and oscillatory mobility of vinyl groups in allosteric monomeric insect hemoglobins." Biochemistry **17**(2): 361-367.

Lamarck, J. B. (1914). Zoological Philosophy. London, Macmillan & co.

Lecomte, J. T. and G. N. La Mar (1985). "1H NMR study of labile proton exchange in the heme cavity as a probe for the potential ligand entry channel in myoglobin." Biochemistry **24**(25): 7388-7395.

Lennard-Jones, J. E. (1929). "The electronic structure of some diatomic molecules." Transactions of the Faraday Society **25**(0): 668-686.

Li, W., T. Jue, J. Edwards, X. Wang and T. H. Hintze (2004). "Changes in NO bioavailability regulate cardiac O2 consumption: control by intramitochondrial SOD2 and intracellular myoglobin." Am J Physiol Heart Circ Physiol **286**(1): H47-54.

Lin, P. C., U. Kreutzer and T. Jue (2007). "Anisotropy and temperature dependence of myoglobin translational diffusion in myocardium: implication for oxygen transport and cellular architecture." Biophys J **92**(7): 2608-2620.

Lin, P. C., U. Kreutzer and T. Jue (2007). "Myoglobin translational diffusion in rat myocardium and its implication on intracellular oxygen transport." J Physiol **578**(Pt 2): 595-603.

Lunney, E. A., S. E. Hagen, J. M. Domagala, C. Humblet, J. Kosinski, B. D. Tait, J. S. Warmus, M. Wilson and D. Ferguson (1994). "A Novel Nonpeptide HIV-1 Protease Inhibitor: Elucidation of the Binding Mode and Its Application in the Design of Related Analogs." Journal of Medicinal Chemistry **37**(17): 2664-2677.

Mabbutt, B. C. and P. E. Wright (1985). "Assignment of heme and distal amino acid resonances in the 1H-NMR spectra of the carbon monoxide and oxygen complexes of sperm whale myoglobin." Biochim Biophys Acta **832**(2): 175-185.

Maillot, P.-G. (1990). Using Quaternions for Coding 3D Transformations. Graphics Gems. A. S. Glassner, Academic Press Professional, Inc.**:** 498-515.

Mancini, R. A. and M. C. Hunt (2005). "Current research in meat color." Meat Sci **71**(1): 100-121.

Mehler, E. L. and T. Solmajer (1991). "Electrostatic effects in proteins: comparison of dielectric and charge models." Protein Engineering, Design and Selection **4**(8): 903-910.

Mendel, G. J. (1865). Experiments on Plant Hybridization. Proceedings of the Natural History Society of Brünn. Brünn, Bohemia (Czech Republic), Natural History Society of Brünn.

Monod, J., J. Wyman and J.-P. Changeux (1965). "On the nature of allosteric transitions: A plausible model." Journal of Molecular Biology **12**(1): 88-118.

Morris, G. M., D. S. Goodsell, R. S. Halliday, R. Huey, W. E. Hart, R. K. Belew and A. J. Olson (1998). "Automated docking using a Lamarckian genetic algorithm and an empirical binding free energy function." Journal of Computational Chemistry **19**(14): 1639-1662.

Morris, G. M., D. S. Goodsell, R. Huey and A. J. Olson (1996). "Distributed automated docking of flexible ligands to proteins: Parallel applications of AutoDock 2.4." Journal of Computer-Aided Molecular Design **10**(4): 293-304.

Okazaki, K.-i. and S. Takada (2008). "Dynamic energy landscape view of coupled binding and protein conformational change: Induced-fit versus population-shift mechanisms." Proceedings of the National Academy of Sciences **105**(32): 11182-11187.

Olson, G. M. M. D. S. G. R. H. W. E. H. S. H. R. B. A. J. (2001). "User's Guide AutoDock Automated Docking of Flexible Ligands to Receptors." **3.0.5**.

Papadopoulos, S., V. Endeward, B. Revesz-Walker, K. D. Jurgens and G. Gros (2001). "Radial and longitudinal diffusion of myoglobin in single living heart and skeletal muscle cells." Proc Natl Acad Sci U S A **98**(10): 5904-5909.

Papadopoulos, S., K. D. Jürgens and G. Gros (1995). "Diffusion of myoglobin in skeletal muscle cells--dependence on fibre type, contraction and temperature." Pflugers Arch **430**(4): 519-525.

Phillips, S. E. (1980). "Structure and refinement of oxymyoglobin at 1.6 A resolution." J Mol Biol **142**(4): 531-554.

Ponganis, P. J., U. Kreutzer, N. Sailasuta, T. Knower, R. Hurd and T. Jue (2002). "Detection of myoglobin desaturation in Mirounga angustirostris during apnea." Am J Physiol Regul Integr Comp Physiol **282**(1): R267-272.

Ramanathan, R., M. C. Hunt, T. Price and G. G. Mafi (2021). "Strategies to limit meat wastage: Focus on meat discoloration." Adv Food Nutr Res **95**: 183-205.

Ramaprasad, S., R. D. Johnson and G. N. La Mar (1984). "Vinyl mobility in myoglobin as studied by time-dependent nuclear Overhauser effect measurements." Journal of the American Chemical Society **106**(12): 3632-3635.

Rassaf, T., U. Flögel, C. Drexhage, U. Hendgen-Cotta, M. Kelm and J. Schrader (2007). "Nitrite reductase function of deoxymyoglobin: oxygen sensor and regulator of cardiac energetics and function." Circ Res **100**(12): 1749-1754.

Rosenfeld, R., S. Vajda and C. DeLisi (1995). "Flexible docking and design." Annu Rev Biophys Biomol Struct **24**: 677-700.

Rosin, C. D., R. S. Halliday, W. E. Hart and R. K. Belew (1997). Proceedings of the Seventh International Conference on Genetic Algorithms. Seventh International Conference on Genetic Algorithms, Michigan State University, East Lansing, MI, Morgan Kaufmann Publishers Inc.

Salmaso, V., M. Sturlese, A. Cuzzolin and S. Moro (2016). "DockBench as docking selector tool: the lesson learned from D3R Grand Challenge 2015." Journal of Computer-Aided Molecular Design **30**(9): 773-789.

Shih, L., Y. Chung, R. Sriram and T. Jue (2014). "Palmitate interaction with physiological states of myoglobin." Biochim Biophys Acta **1840**(1): 656-666.

Shih, L., Y. Chung, R. Sriram and T. Jue (2015). "Interaction of myoglobin with oleic acid." Chem Phys Lipids **191**: 115-122.

Shoichet, B. K. and I. D. Kuntz (1993). "Matching chemistry and shape in molecular docking." Protein Eng **6**(7): 723-732.

Siegenthaler, G., R. Hotz, D. Chatellard-Gruaz, L. Didierjean, U. Hellman and J. H. Saurat (1994). "Purification and characterization of the human epidermal fatty acid-binding protein: localization during epidermal cell differentiation in vivo and in vitro." Biochem J **302 (Pt 2)**(Pt 2): 363-371.

Solis, F. J. and R. J.-B. Wets (1981). "Minimization by Random Search Techniques." Mathematics of Operations Research **6**(1): 19-30.

Spencer, H. (1864). The Principles of Biology, Williams and Norgate.

Sriram, R., U. Kreutzer, L. Shih and T. Jue (2008). "Interaction of fatty acid with myoglobin." FEBS Lett **582**(25-26): 3643-3649.

Stoddard, B. L. and D. E. Koshland, Jr. (1992). "Prediction of the structure of a receptor-protein complex using a binary docking method." Nature **358**(6389): 774-776.

Suman, S. P. and P. Joseph (2013). "Myoglobin Chemistry and Meat Color." Annual Review of Food Science and Technology **4**(1): 79-99.

Terrados, N., E. Jansson, C. Sylvén and L. Kaijser (1990). "Is hypoxia a stimulus for synthesis of oxidative enzymes and myoglobin?" J Appl Physiol (1985) **68**(6): 2369-2372.

Thorpe, M. F., M. Lei, A. J. Rader, D. J. Jacobs and L. A. Kuhn (2001). "Protein flexibility and dynamics using constraint theory." J Mol Graph Model **19**(1): 60-69.

Tofani, L., A. Feis, R. E. Snoke, D. Berti, P. Baglioni and G. Smulevich (2004). "Spectroscopic and interfacial properties of myoglobin/surfactant complexes." Biophys J **87**(2): 1186-1195.

van Gunsteren, W. F. and H. J. C. Berendsen (1977). "Algorithms for macromolecular dynamics and constraint dynamics." Molecular Physics **34**(5): 1311-1327.

Vanommeslaeghe, K., O. Guvench and D. M. A. Jr (2014). "Molecular Mechanics." Current Pharmaceutical Design **20**(20): 3281-3292.

Wallace, W. J., R. A. Houtchens, J. C. Maxwell and W. S. Caughey (1982). "Mechanism of autooxidation for hemoglobins and myoglobins. Promotion of superoxide production by protons and anions." Journal of Biological Chemistry **257**(9): 4966-4977.

Wilson, M. T. and B. J. Reeder (2006). MYOGLOBIN. Encyclopedia of Respiratory Medicine. G. J. Laurent and S. D. Shapiro. Oxford, Academic Press**:** 73-76.

Wittenberg, B. A. and J. B. Wittenberg (1989). "Transport of oxygen in muscle." Annu Rev Physiol **51**: 857-878.

Wittenberg, J. B. and B. A. Wittenberg (2003). "Myoglobin function reassessed." J Exp Biol **206**(Pt 12): 2011-2020.

Wu, C.-S. C., P. Duffy and W. D. Brown (1972). "Interaction of Myoglobin and Cytochrome c." Journal of Biological Chemistry **247**(6): 1899-1903.

Yuriev, E., J. Holien and P. A. Ramsland (2015). "Improvements, trends, and new ideas in molecular docking: 2012–2013 in review." Journal of Molecular Recognition **28**(10): 581-604.

Zaia, J., R. S. Annan and K. Biemann (1992). "The correct molecular weight of myoglobin, a common calibrant for mass spectrometry." Rapid Commun Mass Spectrom **6**(1): 32-36.

Zanotti, G., G. Scapin, P. Spadon, J. H. Veerkamp and J. C. Sacchettini (1992). "Three-dimensional structure of recombinant human muscle fatty acid-binding protein." J Biol Chem **267**(26): 18541-18550.

Zhang, F., C. Lücke, L. J. Baier, J. C. Sacchettini and J. A. Hamilton (2003). "Solution structure of human intestinal fatty acid binding protein with a naturally-occurring single amino acid substitution (A54T) that is associated with altered lipid metabolism." Biochemistry **42**(24): 7339-7347.

Zhou, H.-X. (2010). "From Induced Fit to Conformational Selection: A Continuum of Binding Mechanism Controlled by the Timescale of Conformational Transitions." Biophysical Journal **98**(6): L15-L17.

CHAPTER 2. MOLECULAR MODEL OF MYOGLOBIN, FATTY ACID INTERACTION

TABLE OF CONTENTS

I. ABSTRACT 55
II. INTRODUCTION 55
III. MATERIALS AND METHODS 59
A. Macromolecule Preparation 59
B. Ligand Preparation 59
C. Docking Simulation 61
i. Free Energy of Fatty Acid Binding to Mb 61
ii. Docking Algorithm 63
D. Molecular Visualization 64
IV. RESULTS 64
V. DISCUSSION 73
A. Fatty Acid Binding Sites 73
B. Contrasting Differences for Oxy v Deoxy Mb 73
VI. CONCLUSION 74
VII. REFERENCES 76

CHAPTER 2 LIST OF FIGURES

Figure 21: oxy-Mb with hydrophobicity surface and scale 65
Figure 22: External positively charged amino acids of oxy-Mb 68
Figure 23: Heme-pocket structural differences between oxy- and deoxy-Mb 70
Figure 24: Close up of PAM docked to oxy- and deoxy-Mb 72

CHAPTER 2 LIST OF EQUATIONS

Equation 2: Estimated Free Energy of Binding (repeated) 62

CHAPTER 2 LIST OF TABLES

Table 1: Palmitate Binding in Complex with Myoglobin Global Energy 66
Table 2: 7 Heme-Propionate & Histidine-97 Hydrogen Bonding 71

CHAPTER 2. MOLECULAR MODEL OF MYOGLOBIN, FATTY ACID INTERACTION

I. ABSTRACT

Background— Previous studies have shown that palmitate (PAM) can bind specifically and non- specifically to oxy-Myoglobin (oxy-Mb). The current study presents molecular docking simulations on PAM binding with physiological states of Mb, and the resulting conformations suggest that PAM binds more efficiently with the hydrophobic groove of myoglobin in oxy-Mb than in deoxy-Myoglobin (deoxy-Mb).

Methods— AutoDock 4 Hydrated Docking models show multiple potential binding sites with different energy approximations on varying states of Mb consistent with both selective and non-selective binding sites.

Results— The propagated structural change between oxy and deoxy-Mb affects its potential for binding fatty acid (FA). Lysine 96 (K96) is the focus of this study's FA head group binding site, but its side-chain position relative to the hydrophobic groove determines whether PAM can effectively bind.

Conclusions— These results support previous studies' optical spectroscopy and Nuclear Magnetic Resonance spectroscopy (NMR) with in silico simulations and provide insight into where and how PAM binds to different states of Mb

II. INTRODUCTION

Orthodox biochemistry and physiology typecast myoglobin (Mb) as an oxygen-centric protein, its principal roles of being both oxygen storage and transport depot are dogma.

As far as storage capabilities are concerned, certainly, studies have shown Mb supplying O_2 in plants, in mammalian tissues, and during seal apnea (Wittenberg and Wittenberg 1989,

Ponganis, Kreutzer et al. 2002, Chung, Molé et al. 2005, Gros, Wittenberg et al. 2010). The high concentration of Mb in marine mammals could certainly supply oxygen during a dive or apnea (Dolar *et al.* 1999; Guyton *et al.* 1995; Kooyman, 1998; Ponganis *et al.* 2002). Resembling that of the depths of the oceans, an adaptation to high altitude enhances Mb expression and increases O_2 supply (Gimenez *et al.* 1977; Terrados *et al.* 1990). These observations in seemingly diametrically opposed systems agree with the correlation between Mb concentration (O_2 supply) and oxidative capacity in different species (Wittenberg & Wittenberg, 2003).

As for its other canonical role: facilitating the diffusion of O_2, the low solubility of O_2 contrasts the high O_2 carrying capacity of Mb which can confer an advantage in transporting O_2 from the sarcolemma to the mitochondria (Wittenberg, 1970; Wittenberg & Wittenberg, 1989). Studies confirm that O_2 diffuses faster in solution containing Mb than in Mb-free solution *in vitro*. Mb exhibits sufficient mobility and O_2 carrying capacity to compete effectively with free O_2 (Johnson *et al.* 1996). However *in vivo* studies have produced differing results, at best, depleting the entire Mb store of O_2, prolongs terrestrial mammal cardiac function for only a few seconds (Chung and Jue 1996). Researchers were also able to establish an equipoise diffusion (P_{O2}) in the cell, where Mb and O_2 equally contribute to O_2 transport. For terrestrial mammals, the P_{O2} is too low to support life and therefore Mb cannot play a significant role in O_2 diffusion. In contrast marine mammal muscle with its higher concentration of Mb can utilize Mb-facilitated O_2 diffusion under all physiological conditions. (Lin 2007) This concurs with studies that blocked the binding of oxygen to Mb with CO wherein cardiac performance and respiration in rat myocardium were not impaired (Glabe, Chung et al. 1998, Chung, Huang et al. 2006). Indeed, previous studies have even shown that Mb *in situ* or in a muscle fiber model may diffuse too slowly to compete

effectively with free O_2 in the cell (Papadopoulos, Jürgens et al. 1995, Papadopoulos, Endeward et al. 2001, Lin, Kreutzer et al. 2007, Lin, Kreutzer et al. 2007).

If the doctrine of storage and transport are to be believed, how then can a Mb total knockout (Mb KO) mouse show no signs of respiration deficits, contractile function deterioration, or any other physiological impairments (Garry *et al.* 1998; Godecke *et al.* 1999)? Biochemists fall back on the dogmatic Mb functions to explain this anomaly, specifically when it comes to the metabolic profile of the Mb KO mouse. The Mb KO mouse displays a slight decrease in myocardial fatty acid metabolism relative to the wild type (WT) mouse, while the FA to Glucose utilization ratio drops drastically from 3/1 to 0.7/1 (Flögel, Laussmann et al. 2005). Since the β-oxidation of FA during metabolism requires O_2, most researchers have attributed this decrease to the missing contribution of O_2 that would have been from Mb facilitated transport. Or they might point broadly to the impact of multiple different compensation pathways in the Mb KO model, which raises legitimate questions about using the Mb KO model in the first place. If the dwindling FA metabolism does not arise from Mb's missing contribution to the intracellular O_2 flux and Mb does not appear to play a significant role in normoxic myocardium or skeletal muscle, then it is plausible that the missing Mb itself reduces intracellular FA transport.

These varied and perplexing experimental observations have steered scientists to look into a new and controversial NO bio-scavenger and reductase role for Mb (Flögel, Merx et al. 2001, Kreutzer and Jue 2004, Kreutzer and Jue 2006, Rassaf, Flögel et al. 2007). Although some studies refute Mb's role in NO regulation (Li, Jue et al. 2004, Kreutzer and Jue 2006). Despite the reassurance by biochemistry and physiology zealots of the canon, the cellular function of Mb remains uncertain (Wittenberg and Wittenberg 2003, Gros, Wittenberg et al. 2010).

Previous studies that investigated Mb and FA interactions have had conflicting findings (Gloster 1977, Gloster and Harris 1977, Götz, Hertel et al. 1994). However, recent ^{1}H NMR experiments from the Jue Lab have established convincing evidence for MbO_2, MbCO, and MbCN's specific and non-specific interactions with the fatty acids palmitate (PAM) and oleate (OLE) (Sriram, Kreutzer et al. 2008, Shih, Chung et al. 2014). Furthermore, no such evidence was found for Deoxy-Mb in these studies. The FA flux model from Shih *et al* 2014, shows that Mb-PAM (K_d = 48 μM) has a lower FA binding affinity than the Fatty Acid Binding Protein (FABP-PAM K_d = 0.014 μM). However, the high cellular concentration and diffusion coefficient of Mb can compensate for its lower binding affinity, thus allowing Mb to compete effectively with FABP above a FA concentration threshold. Additionally, it can allow for the utilization of a potential loading–unloading mechanism that conveniently follows the O_2 gradient from the sarcolemma to the mitochondria (Sriram, Kreutzer et al. 2008, Shih, Chung et al. 2014).

In order to investigate the potential loading–unloading mechanism above, a general understanding of the active site of Mb is required. Although the crystal structures from the Protein Data Bank (PDB) of various states of Mb appear to show a closely packed structure, they do exhibit transient fluctuations. These fluctuations create distinct openings for ligands to reach the heme from solution (Elber and Karplus 1987). Researchers have postulated that the 6 and 7-heme-propionates play a major role in regulating the ligand's access to the heme-pocket (La Mar, Viscio et al. 1978, Lecomte and La Mar 1985, Carver, Olson et al. 1991). 2D NMR measurements have previously detected that the 7-heme-propionate exhibits a greater level of mobility than the 6-heme-propionate group in deoxy-Mb, as reflected by the Nuclear Overhauser Enhancements (NOEs) from the heme-propionates to their respective 5 and 8-heme-methyls (Busse and Jue 1994). The mobility of the heme-propionates in different ligation states of Mb not only influences

ligand migration, but may also modulate the selective binding of FA (La Mar, Viscio et al. 1978, Ramaprasad, Johnson et al. 1984, Lecomte and La Mar 1985).The interaction between the 7-heme-propionate and the Histidine-97 side chain needs to be studied more in depth to explore its potential relevance in stabilizing the heme-pocket in different ligation states of Mb.

III. Materials And Methods

A. Macromolecule Preparation

The experiments used the x-ray diffraction crystallographic coordinates from the *Research Collaboratory for Structural Bioinformatics* (RCSB) Protein DataBank (PDB) (Berman, Westbrook et al. 2000). Namely, an ultrafast dynamics study on different states of horse heart myoglobin MbCO (PDB ID: 5CN5) at 1.8 Å resolution and deoxy-Mb (PDB ID: 5D5R) at 1.6 Å resolution (Barends, Foucar et al. 2015). *Equus caballus* myoglobin is more economical and more readily available than human myoglobin. MbCO was used as an approximation of oxygenated myoglobin, and will be referred to as oxy-Mb, which is not readily available from horse heart. Sulphate ions used in the crystallization process were removed from both PDB files before any calculations in AutoDock in accordance with the AutoDock 4 User Guide (Morris 2012).

B. Ligand Preparation

No PDB file of unbound PAM is currently available. Instead, the drawing tool from the *University of Pittsburgh's* free software, Avogadro, was used to sketch the line schematic for palmitic acid (Hanwell, Curtis et al. 2012). The Open Babel based built in geometry optimization along with the Merck Molecular Force Field (MMFF94) energy minimization tool were used to refine the drawn fatty acid (Halgren 1996, O'Boyle, Banck et al. 2011). The PAM was then saved in its lowest energy state and exported into PDB format, as our best approximation of PAM structure within current limits and lack of x-ray crystallography data on this small molecule.

Moving into AutoDock, in order to include potentially relevant explicit waters in docking, the method for Hydrated Docking was used, wherein all of the ligand's hydrogen bond donors and acceptor groups are saturated with special W (water pseudo-atom) atoms placed along hydrogen bond vectors 3 Å from the heavy atoms in accordance with the most representative of interactions found in crystallographic complexes (Forli and Olson 2012). Bond angles were assigned by AutoDock according to experimentally determined values (Taylor, Kennard et al. 1983, Wiberg, Marquez et al. 1994, Lommerse, Price et al. 1997, Nobeli, Price et al. 1997). A special grid map describing water-protein interactions is calculated where the W pseudo-atom represents a discrete spherical water molecule, that combines properties of hydrogen and oxygen and has neutral charge. W atoms remain fixed with respect to their heavy ligand atom throughout the entire calculation, this simplification effectively models water without extra degrees of freedom. All other available ligand torsions were set to rotatable resulting in a total of 14 torsional degrees of freedom.

Hydrated ligands can be docked as regular ligands with a modification of the Estimated Free Energy of Binding equation, where the W pseudo-atom is accounted for. In this method, W atoms do not limit ligand flexibility because they neither interact with each other, nor with other ligand atoms. However, if multiple W atoms overlap in a bound conformation position, their respective contributions to binding are additive (Forli and Olson 2012).

C. Docking Simulation

AutoDock 4 (*The Scripps Research Institute)* was used with progressively smaller and smaller box sizes as potential binding sites were first found all over the protein surface (Morris, Huey et al. 2009). The first box size encompassed the entire protein, which resulted in several potential binding sites including myoglobin's N-terminus. To exclude this site, the box was halved in size disregarding the backward face (opposite the heme-pocket), which allowed the genetic algorithm to refine potential binding sites on the front face of the protein. The next box size was approximately a quarter of the original full-size box, enclosing the heme-pocket and edge residues thereof both the hydrophobic and hydrophilic grooves. The final round of box sized further narrowed the scope based on the clear preference of oxy-Mb (PDB ID: 5CN5) to bind PAM in the hydrophobic groove and deoxy-Mb (PDB ID: 5D5R) to bind PAM in the hydrophilic groove. AutoDock default 0.375 Å spacing was used in all instances.

i. Free Energy of Fatty Acid Binding to Mb

The total Estimated Free Energy of Binding, ΔG_{total}, is made up of 5 potentials (Equation 2). Each of these potentials (Equation 2a.-e.) are composed of two terms: a ligand component and water component. The first terms are calculated by summations over all pairs of ligand atoms, *i*, and protein atoms, *j*, as a function of their distances, *r*, which can be thought of as the ligand contribution. Similarly, the second terms of each Equation 2a-e. are calculated by summations over all pairs of W atoms, *w*, and protein atoms, *j*, as a function of their distances, r. These second terms are augmented by an entropy penalty, in the form of the optimized weight coefficient W_{wat} parameter, which scales W atom interactions with respect to regular atoms to account for the lost degrees of freedom of a ligand-bound water molecule. These augmented second terms can be thought of as the water contribution to each of the Equation 2a.-e.

Equation 2: Estimated Free Energy of Binding (repeated)

$$\Delta G_{total} = \Delta H_{vdW} + \Delta H_{hb} + \Delta H_{elec} + \Delta S_{tor} + \Delta G_{desolv} \quad \text{Eqn. 2}$$

		Ligand Portion	+ Water Portion	
where,	ΔH_{vdW}	$=\sum_{i,\ j}\left(\frac{A_{ij}}{r_{ij}^{12}}-\frac{B_{ij}}{r_{ij}^{6}}\right)$	$+W_{wat}\sum_{w,\ j}\left(\frac{A_{wj}}{r_{wj}^{12}}-\frac{B_{wj}}{r_{wj}^{6}}\right)$	a.
	ΔH_{hb}	$=\sum_{i,\ j}E(t)\left(\frac{C_{ij}}{r_{ij}^{12}}-\frac{D_{ij}}{r_{ij}^{10}}\right)$	$+W_{wat}\sum_{w,\ j}E(t)\left(\frac{C_{wj}}{r_{wj}^{12}}-\frac{D_{wj}}{r_{wj}^{10}}\right)$	b.
	ΔH_{elec}	$=\sum_{i,\ j}\left(\frac{q_i q_j}{\varepsilon(r_{ij})\, r_{ij}}\right)$	$+0$	c.
	ΔS_{tor}	$=N_{tor}$	$+0$	d.
	ΔG_{desolv}	$=\sum_{i,\ j}(S_i V_j + S_j V_i)\, exp\left(-\frac{r_{ij}^{2}}{2\sigma^{2}}\right)$	$+(K_{wat})$	e.

Specifically, these 5 potentials are: (Equation 2a.) The enthalpic van der Waals potential, ΔH_{vdW}, composed of: first a Lennard−Jones 12−6 dispersion/ repulsion term, where A_{ij} and B_{ij} are coefficients and functions of the well depth and the van der Waals radii and second a weighted L−J 12−6 d/r term, where A_{wj} and B_{wj} are coefficients and functions of the well depth and the van der Waals radii. (Equation 2b.) The enthalpic hydrogen bonding potential, ΔH_{hb}, composed of: first a directional 12−10 hydrogen-bonding term, where $E(t)$ is the directional weight as a function of the angle, *t*, between the probe and the target atom (Thorpe, Lei et al. 2001) and second a weighted directional 12−10 hydrogen-bonding term that includes both acceptor and donor interactions for the hydrogen and oxygen of the W atoms. (Equation 2c.) The enthalpic electrostatic potential, ΔH_{elec}, composed of: first a Coulombic electrostatic term with a distance-dependent dielectric screening (ε) and second a term assumed to be zero since the spherical, neutrally charged W atom model ignores the molecular dipole. (Equation 2d.) The entropic torsional potential, ΔS_{tor}, which includes: a first term to account for the loss of degrees of freedom

of the ligand upon binding, which is proportional to the number of sp^3 bonds in the ligand (N_{tor}) and a second term that can be considered zero since the waters do not have torsional degrees of freedom. (Equation 2e.) The desolvation potential, ΔG_{desolv}, includes: a first term which is a function of the solvent-accessible surfaces of ligand (S_i) and protein (S_j) (Mehler and Solmajer 1991) and accounts for the implicit bulk waters present in the docking volume and a second term which is the entropic contribution of displaced waters to desolvation, ΔS_{desolv}, approximated as a desolvation entropy constant, K_{wat}, water's enthalpic contribution to desolvation is null. The potentials have been parameterized and optimized in earlier versions of AutoDock (Morris, Goodsell et al. 1996).

ii. Docking Algorithm

The Lamarckian Genetic Algorithm (LGA) with "long" parameters (a maximum of 25,000,000 energy evaluations; maximum of 27,000 generations, and a starting population size of 150 individuals) was used with 100 LGA runs per docking parameter file for a total of 100 resulting conformers per simulation experiment. Statistical analysis of the docking log files clustered conformers on 5.0 Å RMS basis, as seen for each box size in Table 1.

The full-sized box encompassed the entire protein, 126 × 126 × 150 points (pts) 47.25 x 47.25 x 56.25 Å) which resulted in several potential binding sites including myoglobin's N-terminus. To exclude the N-terminus binding site, the box was halved in size and this half-sized box of 126 × 58 × 150 pts (47.25 x 21.75 x 56.25 Å) disregarded the backward face, opposite the heme-pocket, which allowed the genetic algorithm to refine potential binding sites on the front (aka heme) face of the protein. The next box size was approximately a quarter of the original full-size box, the quarter-sized box of 54 × 56 × 100 pts (20.25 x 21 x 37.5 Å) enclosed the heme-pocket and edge residues thereof and both the hydrophobic and hydrophilic grooves. The final round of box size further narrowed the scope this small-sized box of 74 × 44 × 44 pts (27.75 x 16.5 x 16.5 Å) was chosen based on the clear preference of oxy-Mb (PDB ID: 5CN5) to bind PAM in the hydrophobic groove and deoxy-Mb (PDB ID: 5D5R) to bind PAM in the hydrophilic groove while bound to K96 so only the lower half of the heme pocket was included in this final box. AutoDock default spacing of one point representing 0.375 Å was used in all instances.

D. Molecular Visualization

Visualizing PDB files of X-ray crystallography, Avogadro output of palmitic acid, and docking complexes from AutoDock was done with *University of California San Francisco*'s Chimera program. The surface for both states were calculated and modeled using the Kyte-Doolittle Hydrophobicity scale shown in Figure 23b, which allowed for interactions with the carbon chain tail to be seen (Kyte and Doolittle 1982). Chimera was also used to calculate distances and angles of hydrogen bonds and side chain interactions.

IV. Results

Molecular visualization of the Kyte-Doolittle hydrophobicity color coding scale of the surface of oxy-Mb (PDB ID: 5CN5), is the equine MbCO PDB file that was chosen as surrogate for MbO_2

because equine MbO_2 PDB file was unavailable, reveals two main areas of interest surrounding the heme pocket, shown in Figure 21. Namely the hydrophobic patch, shown with a solid box outline near the 8-heme-methyl, with approximately 400 $Å^2$ surface area and the hydrophilic patch, on the opposite side of the heme pocket, with an approximate surface area of 1200 $Å^2$.

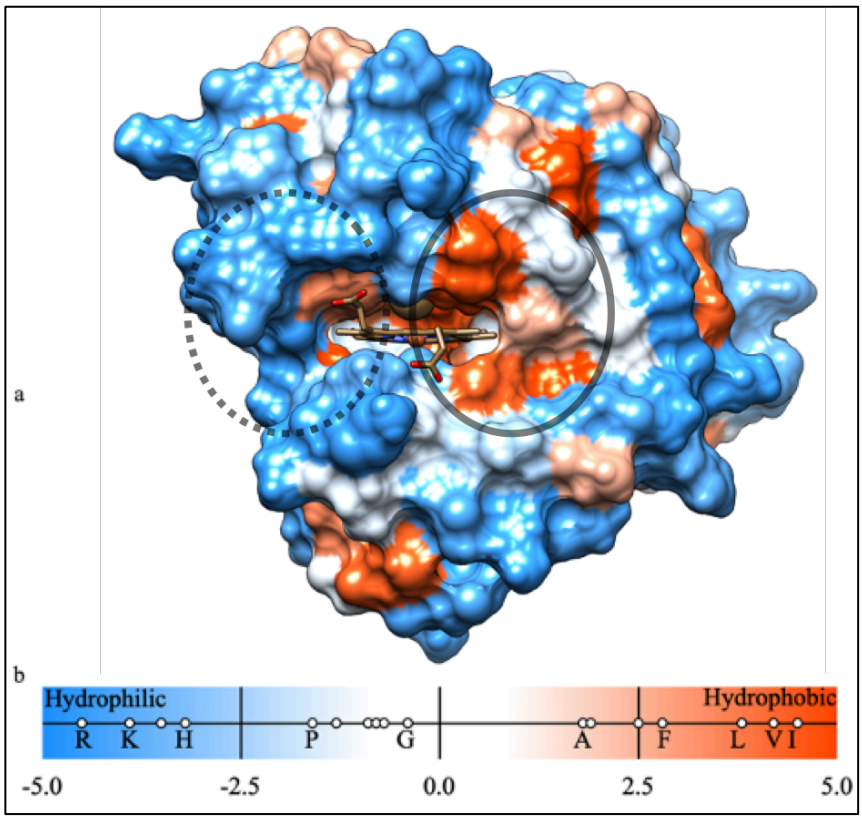

Figure 21: oxy-Mb with hydrophobicity surface and scale
Global view of oxy-Mb (PDB ID: 5CN5) with ***a)*** *its hydrophobicity surface, where the solid oval outline shows the hydrophobic patch (~400 Å²) near the 8-heme methyl and the dotted oval outline shows the hydrophilic patch on other side of the heme with an approximate surface area of 1200 Å². **b)** The color key denotes the Kyte-Doolittle hydrophobicity scale with select amino acids labeled for reference.*

AutoDock result clustering show that the lowest energy largest cluster (LELC) of oxy-Mb is far more energetically favorable than that of deoxy-Mb, as seen in Table 1. This suggests that PAM prefers to bind to the oxygenated state of myoglobin, in accordance with previous Ultraviolet-Visible (UV-Vis) and NMR spectroscopy studies (Shih, Chung et al. 2014). Table 1 shows the

total Estimated Free Energy of Binding resulting from the 4 different AutoDock box sizes. Each compares oxy-Mb (PDB ID: 5CN5 solid line) and deoxy-Mb (PDB ID: 5D5R dashed line) in binding with PAM between -6 and -3 kcal/mol energy domain. The select major PAM binding sites in each box size experiment are labeled with the amino acid residue the FA head binds to. The select major PAM binding sites in each box size experiment are labeled with the amino acid residue the FA head binds to.

Palm16		**oxy-Mb (5CN5)**				**deoxy-Mb (5D5R)**			
		Energy (kcal/mol)				**Energy** (kcal/mol)			
	Binding Site	Final Intermolecular Energy		Torsional Energy	Total Binding Energy	Final Intermolecular Energy		Torsional Energy	Total Binding Energy
		$\boldsymbol{IE_1}$	$\boldsymbol{\Delta H_{elec}}$	$\boldsymbol{\Delta S_{tor}}$	$\boldsymbol{\Delta G_{total}}$	$\boldsymbol{IE_1}$	$\boldsymbol{\Delta H_{elec}}$	$\boldsymbol{\Delta S_{tor}}$	$\boldsymbol{\Delta G_{total}}$
Small Box	K96	-7.04	-1.8	3.84	-4.99	-6.3	-1.77	3.84	-4.23
Half Box	K96	-7.15	-1.57	3.84	-4.87	-7.08	-1.68	3.84	-4.92
	K42	-7.27	-1.34	3.84	-4.77	-7.23	-1.26	3.84	-4.65
	K45	-6.72	-1.72	3.84	-4.60				ND
	K98	-6.66	-1.66	3.84	-4.47	-6.46	-1.84	3.84	-4.45
Full Box	G1	-7.65	-2.03	3.84	-5.84	-7.63	-2.06	3.84	-5.85
	K96	-7.62	-1.52	3.84	-5.3	-6.88	-1.78	3.84	-4.81
	K42	-6.9	-1.59	3.84	-4.65	-7.11	-1.75	3.84	-5.02
	K98	-6.2	-1.66	3.84	-4.02				ND

Table 1: Palmitate Binding in Complex with Myoglobin Global Energy
AutoDock Energy break-down and approximations of the Total Free Energy of Binding (ΔG_{total}) in oxy-Mb (PDB ID: 5CN5) and deoxy-Mb (PDB ID: 5D5R).
Where:
$IE_1 = \Delta H_{vdW} + \Delta H_{hb} + \Delta G_{desolv}$
Small Box: 27.75 × 16.5 × 16.5 Å
Quarter Box: 20.25 × 21 × 37.5 Å
Half Box: 47.25 × 21.75 × 56.25 Å
Full Box: 47.25 × 47.25 × 56.25 Å

Out of thirty-two total positively charged amino acid residues (11 H, 2 R, 19 K), twenty-nine are susceptible to FA binding on the exterior of the protein (8 H, 2 R, 19 K). The AutoDock experiments further narrowed this to a list of thirteen PAM binding sites. Figure 22 shows oxy-Mb (PDB ID: 5CN5) with the a) Front (aka heme-facing) view and b) back view with its hydrophobicity surface. All of the PAM binding site amino acid residues indicated by the full-sized box in AutoDock are highlighted in royal (dark) blue.

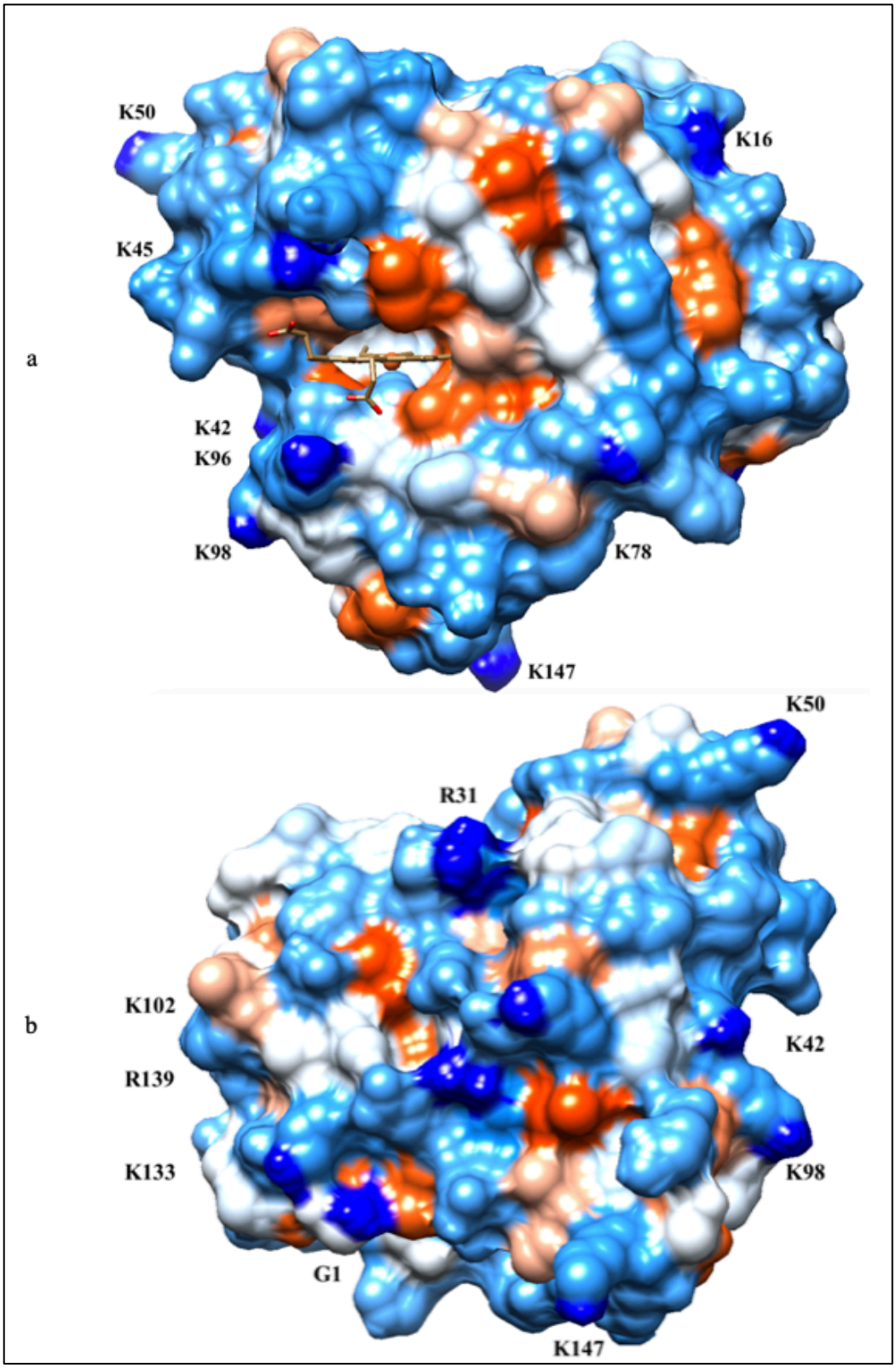

Figure 22: External positively charged amino acids of oxy-Mb
a) *Front and* ***b)*** *back view of oxy-Mb (PDB ID: 5CN5) with its hydrophobicity surface and PAM binding site amino acid residues indicated by AutoDock highlighted in royal (dark) blue.*

Figure 23 shows the detailed line and ribbon view of the heme-pocket where oxy-Mb (PDB ID: 5CN5) is in gold and the F helix is pulled towards the iron that is now in-plane with the heme. deoxy-Mb (PDB ID: 5D5R) is shown in purple and its iron is puckered out of the heme plane. In the transition from deoxy- to oxy-Mb the hydrogen bond length and angle between Prop-7 and H97, denoted by the dashed orange lines, change, Table 2. The K96 is also changed after oxygen binds a) in deoxy-Mb K96 points away from the hydrophobic groove. b) In oxy-Mb K96 points towards the hydrophobic groove.

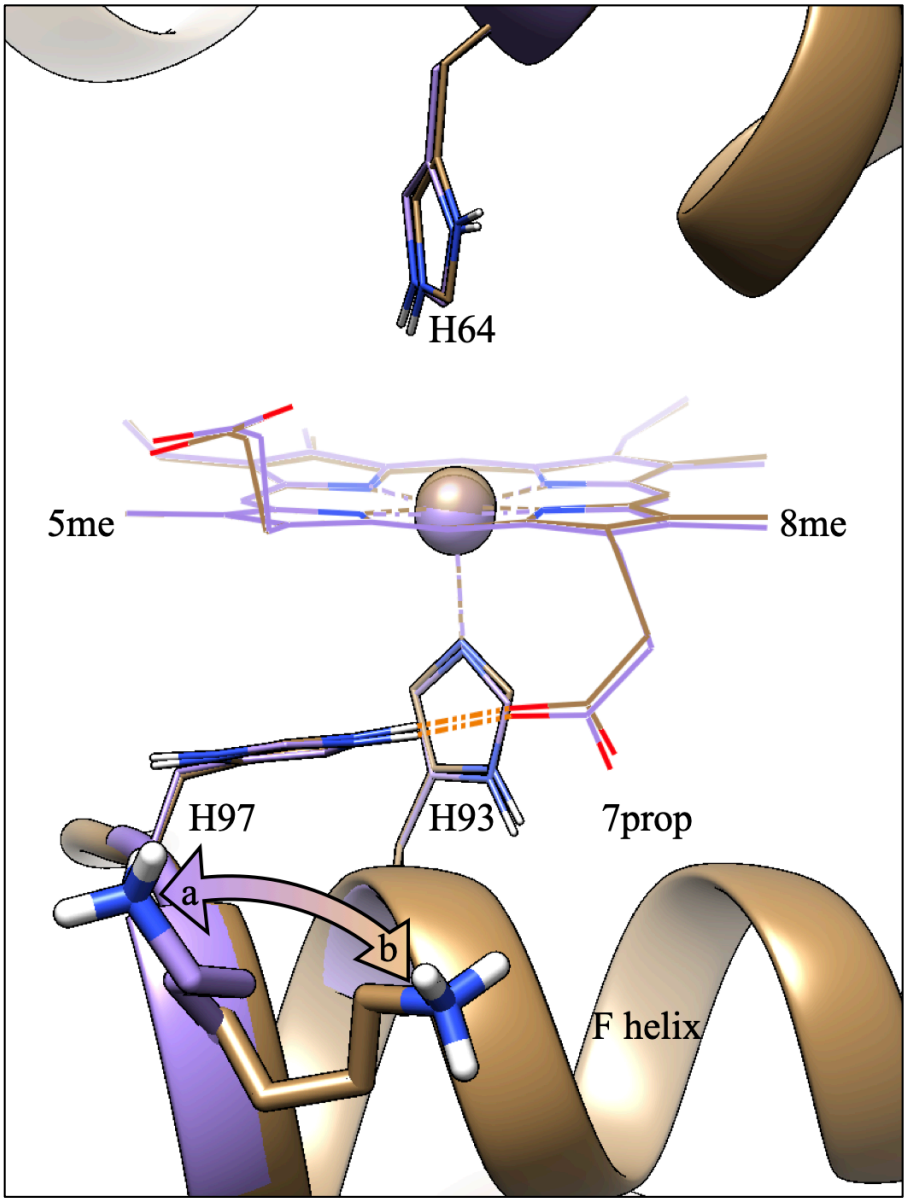

Figure 23: Heme-pocket structural differences between oxy- and deoxy-Mb
oxy-Mb (PDB ID: 5CN5) is in gold, the iron is in plane. deoxy-Mb (PDB ID: 5D5R) is shown in purple, the iron is puckered out of plane. ***a)*** *In deoxy-Mb K96 points away from the hydrophobic groove.* ***b)*** *In oxy-Mb K96 points towards the hydrophobic groove. In the transition from deoxy- to oxy-Mb the hydrogen bond length and angle between Prop-7 and H97, denoted by the dashed orange lines, change, Table 2.*

UCSF Chimera was used to visualize the hydrophobic groove on the 8 heme-methyl side and the hydrophilic groove on the 5 heme-methyl side of myoglobin. The PDB files of oxy-Mb and deoxy-Mb show a conformational difference at Lysine-96. Depending on whether oxygen is

bound, the K96 side chain is either swung towards the hydrophobic groove Figure 23b, or away, towards the hydrophilic groove Figure 23a. This structural change is thought to be triggered by the binding of oxygen (in this case, carbon monoxide) to the deoxy state. This binding locally propagates conformational changes through the heme Iron, proximal histidine, its respective F α-helix, and the residues thereof, namely Lysine-96 and Histidine-97. The positional change of Histidine-97 increases the strength of its hydrogen bond with the 7 heme-propionate (detailed in Table 2). During this time the Lysine-96 sidechain is swung towards the new stronger 7prop--H97 hydrogen bond (Figure 23, shown as orange dashed line) and the hydrophobic groove.

		Length (Å)		$\sphericalangle\boldsymbol{\theta}$ (°)	$\sphericalangle\boldsymbol{\phi}$ (°)	$\Delta\boldsymbol{G_{hb}}$ (kcal/mol)
		C ↔ N	O ↔ H	N-H ••• O	H ••• O-C	
oxy-Mb	**No PA**	3.76	1.82	161.03	125.88	-7.07
	with PA	3.81	1.83	153.61	120.40	-6.07
deoxy-Mb	**No PA**	3.72	1.83	160.18	121.79	-6.26
	with PA	3.61	1.99	138.16	105.52	-2.11

Table 2: 7 Heme-Propionate & Histidine-97 Hydrogen Bonding
Measurements and approximations of the H bond between the 7 heme-propionate of the heme and Histidine-97 of oxy-Mb (PDB ID: 5CN5) and deoxy-Mb (PDB ID: 5D5R) with and without PAM binding at K96 as seen in Figure 23.

Figure 24 shows an enlarged view of the heme-pocket with a sheer hydrophobicity surface showing the underlying ribbon structure of a) deoxy-Mb (PDB ID: 5D5R, purple) with PAM docked to K96 in the hydrophilic groove. b) oxy-Mb (PDB ID: 5CN5, gold) showing PAM docked to K96 in the hydrophobic groove created by the F α-helix. These conformers are representative of the energy breakdowns of the clusters in Table 1. The AutoDock LELC conformer clusters of the oxy-Mb and deoxy-Mb in complex with PAM show the carboxyl head group binding to Lysine-96 and, depending on the ligation state, either having the fatty acid carbon tail in the hydrophobic or hydrophilic groove. Considering that the carbon chain tail of the fatty acid is hydrophobic, one

can assume it would prefer the hydrophobic patch and therefore the oxygen ligated state of myoglobin.

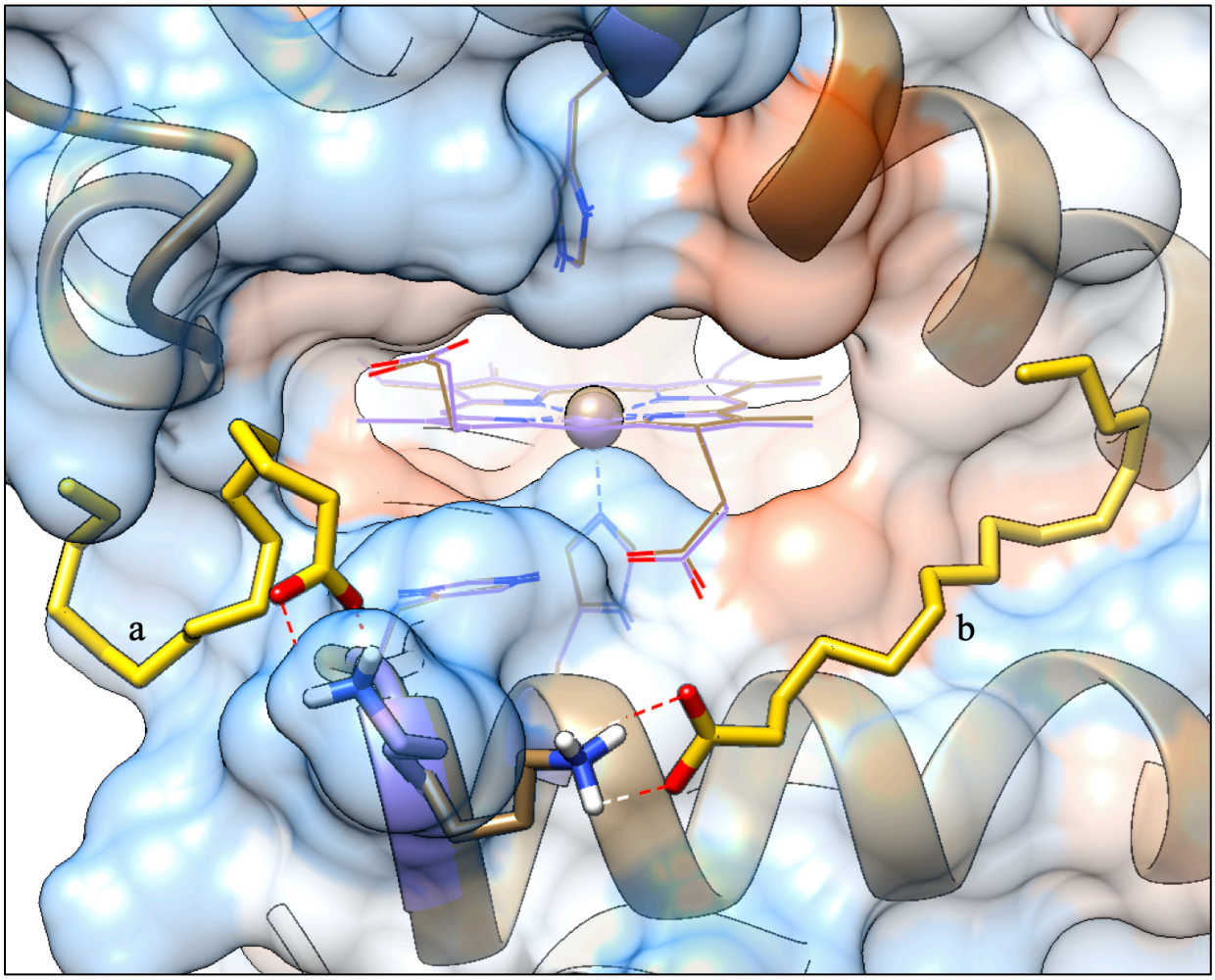

Figure 24: Close up of PAM docked to oxy- and deoxy-Mb

a) *deoxy-Mb (PDB ID: 5D5R, purple) with sheer hydrophobic surface and showing PAM docked to K96 in the hydrophilic groove and*

b) *oxy-Mb (PDB ID: 5CN5, gold) showing PAM docked to K96 in the hydrophobic groove to the left of the heme created by the F α-helix, Table 1.*

V. DISCUSSION

A. Fatty Acid Binding Sites

FA, having a negatively charged carboxyl head group, could possibly bind to any positively charged amino acid residues ie. Lysine, Arginine, or Histidine, of which Mb has thirty-two, when you also include the N-terminus we have a total of thirty-three potential positive charges. Now taking into consideration the tertiary structure of Mb we can exclude the buried residues that are not available to bind FA, this leaves us with twenty-nine possible positively charged external binding sites.

In this study AutoDock allows us to further narrow down this list to only those external positive binding sites that can support the entire FA including the hydrophobic carbon chain tail, of which AutoDock found thirteen sites, Table 1. We are also able to compare the estimated free energy of binding for the different potential binding sites and draw conclusions about selectivity.

B. Contrasting Differences for Oxy v Deoxy Mb

When oxygen (or in the case of our surrogate, carbon monoxide) associates with deoxy-Mb a tug of war (between the proximal histidine and the oxygen) ensues over the heme iron. The deoxy state shows the "puckered" out of plane position of the iron pulled close to H93. When oxygen binds it tugs the iron into the heme-plane, the proximal histidine and its secondary structural F α-helix are also pulled downwards towards the heme group, as seen in Figure 23 (Barends, Foucar et al. 2015). This shift strengthens the hydrogen bond between the 7 heme-propionate and Histidine-97 by changing the bond angles and length (Table 2). This change causes the side chain of Lysine-96 to swing away from the hydrophobic groove on the F α-helix preventing PAM from binding its carbon chain tail efficiently. The differential interaction of ligated and un-ligated Mb seen in previous experiments (Shih, Chung et al. 2014) is reinforced

through these docking models; suggesting conformational change due to ligation is a very convenient mechanism for fatty acid binding and dissociation.

Not all binding sites are effected by the oxy ↔ deoxy transition, for example the lowest energy largest clustered (LELC) binding site G1, is the N-terminus and is on the opposite side of the protein from the heme pocket, it also shows no sensitivity to oxygenation. FABP has one unique binding site for FA whereas this study suggests Mb has several specific and non-specific binding sites, some of which are dependent on oxygenation state.

VI. Conclusion

The analysis of AutoDock simulated docking experiments supports potential specific and non-specific PA—oxy-Mb binding interactions as described in previous NMR experiments (Shih, Chung et al. 2014). Lysine-96 appears to be the most frequent hydrogen donor for the PA's carboxyl head-group, however it seems that the fatty acid tail has the larger effect on the overall binding energy. When the side chain of Lysine-96 is pointed towards (i.e. oxy-Mb) the large hydrophobic groove created by the F α-helix on the 8 heme-methyl side of the heme-pocket, the tail has plenty of room to bind and take advantage of water exclusions of the hydrophobic effect. However, if the side chain of Lysine-96 is pointed away (i.e. deoxy-Mb) from the hydrophobic groove made by the F-helix the tail must coil itself into the small hydrophilic cleft on the 5 heme-methyl side of the heme-pocket (Figure 24).

Table 3
Palmitate Binding to Proteins

		Palmitate		Reference
		K_d *(M, x10^{-9})*	*ΔG (kcal/mol)*	
FABP	rH-FABP	14.0	-10.68	(Richieri, Ogata et al. 1994)
	bH-FABP	4.0	-11.42	
Albumin	Human Plasma	66.7	-8.40 to -10.6	(Spector)
	Human Serum	333	-8.80 to -11.1	(Richieri, Anel et al. 1993)
		206	-3.46 to -9.09	(Spector, John et al. 1969)
	Bovine Serum	100	-9.52 to -11.0	(Richieri, Anel et al. 1993)
		147	-4.05 to -9.29	(Spector, John et al. 1969)
		1,010	-8.15	Glatz 1983
		K_d *(M, x10^{-5})*	*ΔG (kcal/mol)*	**Reference**
Myoglobin	Oxy-Mb	400±5.1	-3 to 4	This Work
		50.9	-4.48	(Chintapalli, Bhardwaj et al. 2015)
	Deoxy-Mb		-4.81	
	MbCO	4.8	-5.87 to -5.99	(Shih, Chung et al.)
	MbCN	4.3±1.2	-5.94 to -6.69	(Sriram, Kreutzer et al. 2008)
		4.8	-5.87	Jue 2017

Chintapalli, S. V., G. Bhardwaj, R. Patel, N. Shah, R. L. Patterson, D. B. van Rossum, A. Anishkin and S. H. Adams (2015). "Molecular Dynamic Simulations Reveal the Structural Determinants of Fatty Acid Binding to Oxy-Myoglobin." PLOS ONE **10**(6): e0128496.

Richieri, G. V., A. Anel and A. M. Kleinfeld (1993). "Interactions of long-chain fatty acids and albumin: determination of free fatty acid levels using the fluorescent probe ADIFAB." Biochemistry **32**(29): 7574-7580.

Richieri, G. V., R. T. Ogata and A. M. Kleinfeld (1994). "Equilibrium constants for the binding of fatty acids with fatty acid-binding proteins from adipocyte, intestine, heart, and liver measured with the fluorescent probe ADIFAB." J Biol Chem **269**(39): 23918-23930.

Shih, L., Y. Chung, R. Sriram and T. Jue (2014). "Palmitate interaction with physiological states of myoglobin." Biochim Biophys Acta **1840**(1): 656-666.

Spector, A. A. (1975). "Fatty acid binding to plasma albumin." Journal of Lipid Research **16**(3): 165-179.

Spector, A. A., K. John and J. E. Fletcher (1969). "Binding of long-chain fatty acids to bovine serum albumin." J Lipid Res **10**(1): 56-67.

Sriram, R., U. Kreutzer, L. Shih and T. Jue (2008). "Interaction of fatty acid with myoglobin." FEBS Lett **582**(25-26): 3643-3649.

VII. REFERENCES

Barends, T. R., L. Foucar, A. Ardevol, K. Nass, A. Aquila, S. Botha, R. B. Doak, K. Falahati, E. Hartmann, M. Hilpert, M. Heinz, M. C. Hoffmann, J. Köfinger, J. E. Koglin, G. Kovacsova, M. Liang, D. Milathianaki, H. T. Lemke, J. Reinstein, C. M. Roome, R. L. Shoeman, G. J. Williams, I. Burghardt, G. Hummer, S. Boutet and I. Schlichting (2015). "Direct observation of ultrafast collective motions in CO myoglobin upon ligand dissociation." Science 350(6259): 445-450.

Berman, H. M., J. Westbrook, Z. Feng, G. Gilliland, T. N. Bhat, H. Weissig, I. N. Shindyalov and P. E. Bourne (2000). "The Protein Data Bank." Nucleic Acids Res **28**(1): 235-242.

Busse, S. C. and T. Jue (1994). "Two-dimensional NMR characterization of the deoxymyoglobin heme pocket." Biochemistry **33**(36): 10934-10943.

Carver, T. E., J. S. Olson, S. J. Smerdon, S. Krzywda, A. J. Wilkinson, Q. H. Gibson, R. S. Blackmore, J. D. Ropp and S. G. Sligar (1991). "Contributions of residue 45(CD3) and heme-6-propionate to the biomolecular and geminate recombination reactions of myoglobin." Biochemistry **30**(19): 4697-4705.

Chintapalli, S. V., G. Bhardwaj, R. Patel, N. Shah, R. L. Patterson, D. B. van Rossum, A. Anishkin and S. H. Adams (2015). "Molecular Dynamic Simulations Reveal the Structural Determinants of Fatty Acid Binding to Oxy-Myoglobin." PLOS ONE **10**(6): e0128496.

Chung, Y., S. J. Huang, A. Glabe and T. Jue (2006). "Implication of CO inactivation on myoglobin function." Am J Physiol Cell Physiol **290**(6): C1616-1624.

Chung, Y. and T. Jue (1996). "Cellular response to reperfused oxygen in the postischemic myocardium." Am J Physiol **271**(2 Pt 2): H687-695.

Chung, Y., P. A. Molé, N. Sailasuta, T. K. Tran, R. Hurd and T. Jue (2005). "Control of respiration and bioenergetics during muscle contraction." Am J Physiol Cell Physiol **288**(3): C730-738.

Elber, R. and M. Karplus (1987). "Multiple conformational states of proteins: a molecular dynamics analysis of myoglobin." Science **235**(4786): 318-321.

Flögel, U., T. Laussmann, A. Gödecke, N. Abanador, M. Schäfers, C. D. Fingas, S. Metzger, B. Levkau, C. Jacoby and J. Schrader (2005). "Lack of myoglobin causes a switch in cardiac substrate selection." Circ Res **96**(8): e68-75.

Flögel, U., M. W. Merx, A. Gödecke, U. K. M. Decking and J. Schrader (2001). "Myoglobin: A scavenger of bioactive NO." Proceedings of the National Academy of Sciences **98**(2): 735-740.

Forli, S. and A. J. Olson (2012). "A Force Field with Discrete Displaceable Waters and Desolvation Entropy for Hydrated Ligand Docking." Journal of Medicinal Chemistry **55**(2): 623-638.

Glabe, A., Y. Chung, D. Xu and T. Jue (1998). "Carbon monoxide inhibition of regulatory pathways in myocardium." American Journal of Physiology-Heart and Circulatory Physiology **274**(6): H2143-H2151.

Gloster, J. (1977). "Studies on fatty acid binding characteristics of myoglobin and Z protein." Journal of Molecular and Cellular Cardiology **9**(9, Supplement): 15.

Gloster, J. and P. Harris (1977). "Fatty acid binding to cytoplasmic proteins of myocardium and red and white skeletal muscle in the rat. A possible new role for myoglobin." Biochem Biophys Res Commun **74**(2): 506-513.

Götz, F. M., M. Hertel and U. Gröschel-Stewart (1994). "Fatty acid binding of myoglobin depends on its oxygenation." Biol Chem Hoppe Seyler **375**(6): 387-392.

Gros, G., B. A. Wittenberg and T. Jue (2010). "Myoglobin's old and new clothes: from molecular structure to function in living cells." The Journal of Experimental Biology **213**(16): 2713-2725.

Halgren, T. A. (1996). "Merck molecular force field. I. Basis, form, scope, parameterization, and performance of MMFF94." Journal of Computational Chemistry **17**(5-6): 490-519.

Hanwell, M. D., D. E. Curtis, D. C. Lonie, T. Vandermeersch, E. Zurek and G. R. Hutchison (2012). "Avogadro: an advanced semantic chemical editor, visualization, and analysis platform." Journal of Cheminformatics **4**(1): 17.

Kreutzer, U. and T. Jue (2004). "Role of myoglobin as a scavenger of cellular NO in myocardium." American Journal of Physiology-Heart and Circulatory Physiology **286**(3): H985-H991.

Kreutzer, U. and T. Jue (2006). "Investigation of bioactive NO-scavenging role of myoglobin in myocardium." Pflügers Archiv **452**(1): 36-42.

Kyte, J. and R. F. Doolittle (1982). "A simple method for displaying the hydropathic character of a protein." J Mol Biol **157**(1): 105-132.

La Mar, G. N., D. B. Viscio, K. Gersonde and H. Sick (1978). "Proton nuclear magnetic resonance study of the rotational position and oscillatory mobility of vinyl groups in allosteric monomeric insect hemoglobins." Biochemistry **17**(2): 361-367.

Lecomte, J. T. and G. N. La Mar (1985). "1H NMR study of labile proton exchange in the heme cavity as a probe for the potential ligand entry channel in myoglobin." Biochemistry **24**(25): 7388-7395.

Li, W., T. Jue, J. Edwards, X. Wang and T. H. Hintze (2004). "Changes in NO bioavailability regulate cardiac O2 consumption: control by intramitochondrial SOD2 and intracellular myoglobin." Am J Physiol Heart Circ Physiol **286**(1): H47-54.

Lin, P. C., U. Kreutzer and T. Jue (2007). "Anisotropy and temperature dependence of myoglobin translational diffusion in myocardium: implication for oxygen transport and cellular architecture." Biophys J **92**(7): 2608-2620.

Lin, P. C., U. Kreutzer and T. Jue (2007). "Myoglobin translational diffusion in rat myocardium and its implication on intracellular oxygen transport." J Physiol **578**(Pt 2): 595-603.

Lommerse, J. P. M., S. L. Price and R. Taylor (1997). "Hydrogen bonding of carbonyl, ether, and ester oxygen atoms with alkanol hydroxyl groups." Journal of Computational Chemistry **18**(6): 757-774.

Mehler, E. L. and T. Solmajer (1991). "Electrostatic effects in proteins: comparison of dielectric and charge models." Protein Engineering, Design and Selection **4**(8): 903-910.

Morris, G. M., D. S. Goodsell, R. Huey and A. J. Olson (1996). "Distributed automated docking of flexible ligands to proteins: Parallel applications of AutoDock 2.4." Journal of Computer-Aided Molecular Design **10**(4): 293-304.

Morris, G. M., R. Huey, W. Lindstrom, M. F. Sanner, R. K. Belew, D. S. Goodsell and A. J. Olson (2009). "AutoDock4 and AutoDockTools4: Automated docking with selective receptor flexibility." J Comput Chem **30**(16): 2785-2791.

Morris, G. M. G., D. S.; Pique, M. E.; Lindstrom, W.; Huey, R.; Forli, S.; Hart, W. E.; Hallyday, S.; Belew, R.; Olson, A. J. (2012). AutoDock 4.2 User Guide. T. S. R. Institute.

Nobeli, I., S. L. Price, J. P. M. Lommerse and R. Taylor (1997). "Hydrogen bonding properties of oxygen and nitrogen acceptors in aromatic heterocycles." Journal of Computational Chemistry **18**(16): 2060-2074.

O'Boyle, N. M., M. Banck, C. A. James, C. Morley, T. Vandermeersch and G. R. Hutchison (2011). "Open Babel: An open chemical toolbox." Journal of Cheminformatics **3**(1): 33.

Papadopoulos, S., V. Endeward, B. Revesz-Walker, K. D. Jurgens and G. Gros (2001). "Radial and longitudinal diffusion of myoglobin in single living heart and skeletal muscle cells." Proc Natl Acad Sci U S A **98**(10): 5904-5909.

Papadopoulos, S., K. D. Jürgens and G. Gros (1995). "Diffusion of myoglobin in skeletal muscle cells--dependence on fibre type, contraction and temperature." Pflugers Arch **430**(4): 519-525.

Ponganis, P. J., U. Kreutzer, N. Sailasuta, T. Knower, R. Hurd and T. Jue (2002). "Detection of myoglobin desaturation in Mirounga angustirostris during apnea." Am J Physiol Regul Integr Comp Physiol **282**(1): R267-272.

Ramaprasad, S., R. D. Johnson and G. N. La Mar (1984). "Vinyl mobility in myoglobin as studied by time-dependent nuclear Overhauser effect measurements." Journal of the American Chemical Society **106**(12): 3632-3635.

Rassaf, T., U. Flögel, C. Drexhage, U. Hendgen-Cotta, M. Kelm and J. Schrader (2007). "Nitrite reductase function of deoxymyoglobin: oxygen sensor and regulator of cardiac energetics and function." Circ Res **100**(12): 1749-1754.

Richieri, G. V., A. Anel and A. M. Kleinfeld (1993). "Interactions of long-chain fatty acids and albumin: determination of free fatty acid levels using the fluorescent probe ADIFAB." Biochemistry **32**(29): 7574-7580.

Shih, L., Y. Chung, R. Sriram and T. Jue (2014). "Palmitate interaction with physiological states of myoglobin." Biochim Biophys Acta **1840**(1): 656-666.

Spector, A. A., K. John and J. E. Fletcher (1969). "Binding of long-chain fatty acids to bovine serum albumin." J Lipid Res **10**(1): 56-67.

Sriram, R., U. Kreutzer, L. Shih and T. Jue (2008). "Interaction of fatty acid with myoglobin." FEBS Lett **582**(25-26): 3643-3649.

Taylor, R., O. Kennard and W. Versichel (1983). "Geometry of the imino-carbonyl (N-H...O:C) hydrogen bond. 1. Lone-pair directionality." Journal of the American Chemical Society **105**(18): 5761-5766.

Thorpe, M. F., M. Lei, A. J. Rader, D. J. Jacobs and L. A. Kuhn (2001). "Protein flexibility and dynamics using constraint theory." J Mol Graph Model **19**(1): 60-69.

Wiberg, K. B., M. Marquez and H. Castejon (1994). "Lone Pairs in Carbonyl Compounds and Ethers." The Journal of Organic Chemistry **59**(22): 6817-6822.

Wittenberg, B. A. and J. B. Wittenberg (1989). "Transport of oxygen in muscle." Annu Rev Physiol **51**: 857-878.

Wittenberg, J. B. and B. A. Wittenberg (2003). "Myoglobin function reassessed." J Exp Biol **206**(Pt 12): 2011-2020.

CHAPTER 3. OTHER WORK

I. ABSTRACT 81
II. UNPUBLISHED WORK 81
A. FA Chain Length Dependence 81
i. Previous Published NMR Studies 81
ii. AutoDock Implementation 85
a. Macromolecule Preparation 85
b. Ligand Preparation 86
iii. AutoDock Results 86
iv. Possible Conclusions 89
v. Future Studies 89
B. Whale vs Horse Mb Studies 89
i. Physiological Differences in Organisms 89
ii. Sequence Comparison 91
iii. AutoDock Implementation 91
a. Macromolecule Preparation 92
b. Ligand Preparation 92
iv. AutoDock Results 92
v. Possible Conclusions 94
III. COLLABORATIVE EFFORTS 95
A. Nonenal—Mb Studies 95
i. Previously Published Data on autoxidation and electron transfer 95
ii. AutoDock Implementation 96
a. Macromolecule Preparation 97
b. Ligand Preparation 97
iii. AutoDock Results 98
iv. Conclusions 98
B. Cytochrome C—Mb Studies 98
i. Structural Comparison 99
ii. Physiological Feasibility 100
a. $Cyt^{3+}C$ and Mb oxidation by electron transfer 100
b. Electron Transport Chain 100
c. Previous Data 101
iii. AutoDock Implementation 105
a. Macromolecule Preparation 105
b. Ligand Preparation 105
iv. Preliminary AutoDock Results 106
C. Future: Ethanol—Mb Studies 107
i. Previously Published NMR Studies 107
ii. Proposed AutoDock Implementation 108
a. Macromolecule Preparation 109
b. Ligand Preparation 109
c. Expected Results 109
IV. REFERENCES 110

LIST OF FIGURES

Figure 25: ^{1}H-NMR Spectra of MbCN with varying chain lengths FA 82
Figure 26: ^{1}H-NMR spectra of MbCN with varying concentrations of FA 84
Figure 27: Oxy- and deoxy-Mb binding various chain lengths of FA from 8-18 87
Figure 28: Model of FA flux at high palmitate concentration 90
Figure 29: Amino Acid Sequence Comparison of Horse and Whale oxy-Mb 91
Figure 30: AutoDock 100 conformers of PAM with oxy-Mb 93
Figure 31: ^{1}H NMR spectra of MbCN with and without HNE 96
Figure 32: Hydrated Nonenal 97
Figure 33: AutoDock 100 conformers of nonenal with Mb 98
Figure 34: MbCO vs Cytochrome C ribbon drawings 99
Figure 35: Electron Transport Chain 101
Figure 36: Select spectra of the MbO_2 autoxidation and electron transfer to $Cyt^{3+}C$ 103
Figure 37: Plot of MbO_2 vs. time for autoxidation and electron transfer. 104
Figure 38: Hydrated $Cyt^{3+}C$ 106
Figure 39: Preliminary docking Mb—$Cyt^{3+}C$ results 107
Figure 40: ^{1}H NMR spectra of MbCN with and without EtOH 108
Figure 41: Stick drawing of Hydrated EtOH 109

LIST OF EQUATIONS

Equation 5: Standard Reduction Potentials and The Nernst Equation 100

LIST OF TABLES

Table 3: AutoDock Binding Energy of oxy- and deoxy-Mb with FA C8-18 at K96 88
Table 4: AutoDock Binding Energy for PAM with Horse, Whale oxy-Mb 94

CHAPTER 3. OTHER WORK

I. ABSTRACT

As with most scientific research, the studies outlined here are part of larger, collaborative efforts that are dependent on the expertise of many scholars. The AutoDock framework and assumptions outlined in Chapter 1 were used to validate Nuclear Magnetic Resonance (NMR) data collected by researchers in the laboratory of Thomas Jue, Ph.D. at the University of California Davis. The combination of molecular modeling and NMR data allow for a robust investigation into the functional role of myoglobin, a prevalent protein found across the Tree of Life.

Studies of fatty acid (FA) chain length dependence, species dependence, nonenal and Cytochrome C electron transfer, and other unpublished research are explored in this chapter.

II. UNPUBLISHED WORK

A. Fatty Acid Chain Length Dependence

As described in Chapter 1.II.B.iii.b. Nuclear Magnetic Resonance (NMR) data suggests a chain length dependent interaction of fatty acid (FA) with myoglobin (Mb).

i. Previous Published NMR Studies

Previous studies using NMR methods found that FA-Mb interaction is dependent on the FA carbon chain length (Jue, Shih et al. 2017). Short-chain FAs (octanoic, OCT C8:0 and decanoic, DEC C10:0) do not appear to interact with Mb. Whereas medium and long-chain FAs (lauric acid, LAU C12:0; myristic acid, MYR C14:0; and palmitic acid, PAM C16:0) do show an interaction with Mb. A pronounced effect can be seen in LAU and its relative lauric sulfate, LAU 1-SO_4, commonly known as sodium dodecyl sulfate, or SDS, at even lower ratios than previously reported (Tofani, Feis et al. 2004). One interpretation for this would be that the detergent (DET) property of FA would explain the interaction with myoglobin, but we can refute this hypothesis

since cationic, anionic, and neutral DETs at a DET:Mb ratio of 1:1 do not perturb any Mb signal. They show no binding to Mb, neither specifically nor non-specifically.

Adding PAM (C16:0) or OLE (C18:1) to Fe (III) MbCN perturbs the hyperfine shifted 8-heme-methyl signal selectively and increases the apparent solubility of the FA, shown in Figure 25 ((Shih, Chung et al. 2015), Shih et al 2014, Sriram et al 2008). Neither PAM nor OLE appear to interact specifically or non-specifically with the unligated form, deoxy-Mb. This again supports the convenient mechanism in loading and unloading FA described in I.B.ii.b.(iii).

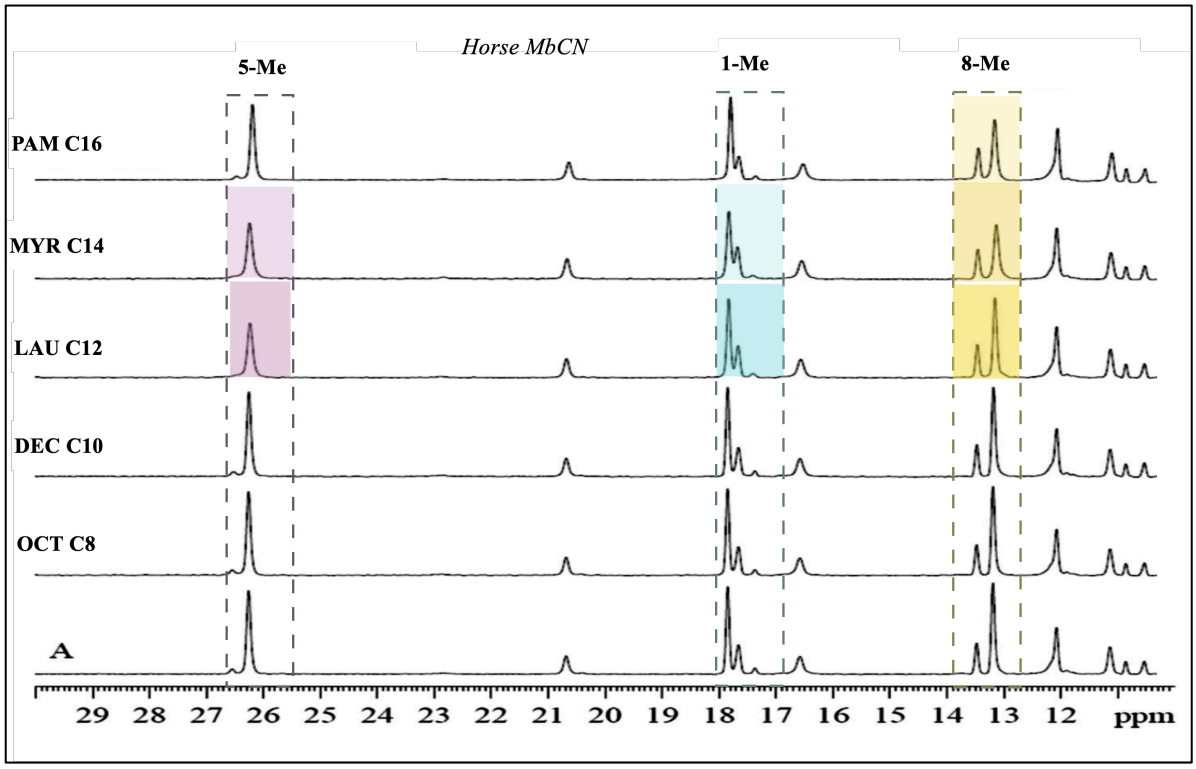

Figure 25: ^{1}H-NMR Spectra of MbCN with varying chain lengths FA
*^{1}H-NMR spectra (30– 10 ppm) of 0.8 mM MbCN in 30 mM Tris at 35°C with FA of different chain lengths at added FA to reach FA:Mb of 1:1 ratio **A** control, **B** octanoic acid (C8:0, OCT). **C** decanoic (C10:0, DEC), **D** lauric acid (C12:0, LAU), **E** myristic acid (C14:0, MYR), **F** palmitic acid (C16:0, PAM). C8:0 and C10:0 FA do not significantly perturb the spectra. C12:0 and C14:0 FA perturb both the 5- and 8-heme methyl groups. C16:0 perturbs only the 8-heme methyl group. Adapted from Jue, Shih et al. 2017.*

Further studies varying the concentration of FA:Mb at ratios: 0:1, 0.2:1, 0.5:1, 1:1, 2:1, and 4:1 show not only peak intensity decreasing, but also peak shifting at higher FA concentrations (Figure 26). LAU shows the most shifting at all 3 methyl sites, whereas LAU 1-SO_4 produces the most pronounced perturbation at all heme-methyl sites.

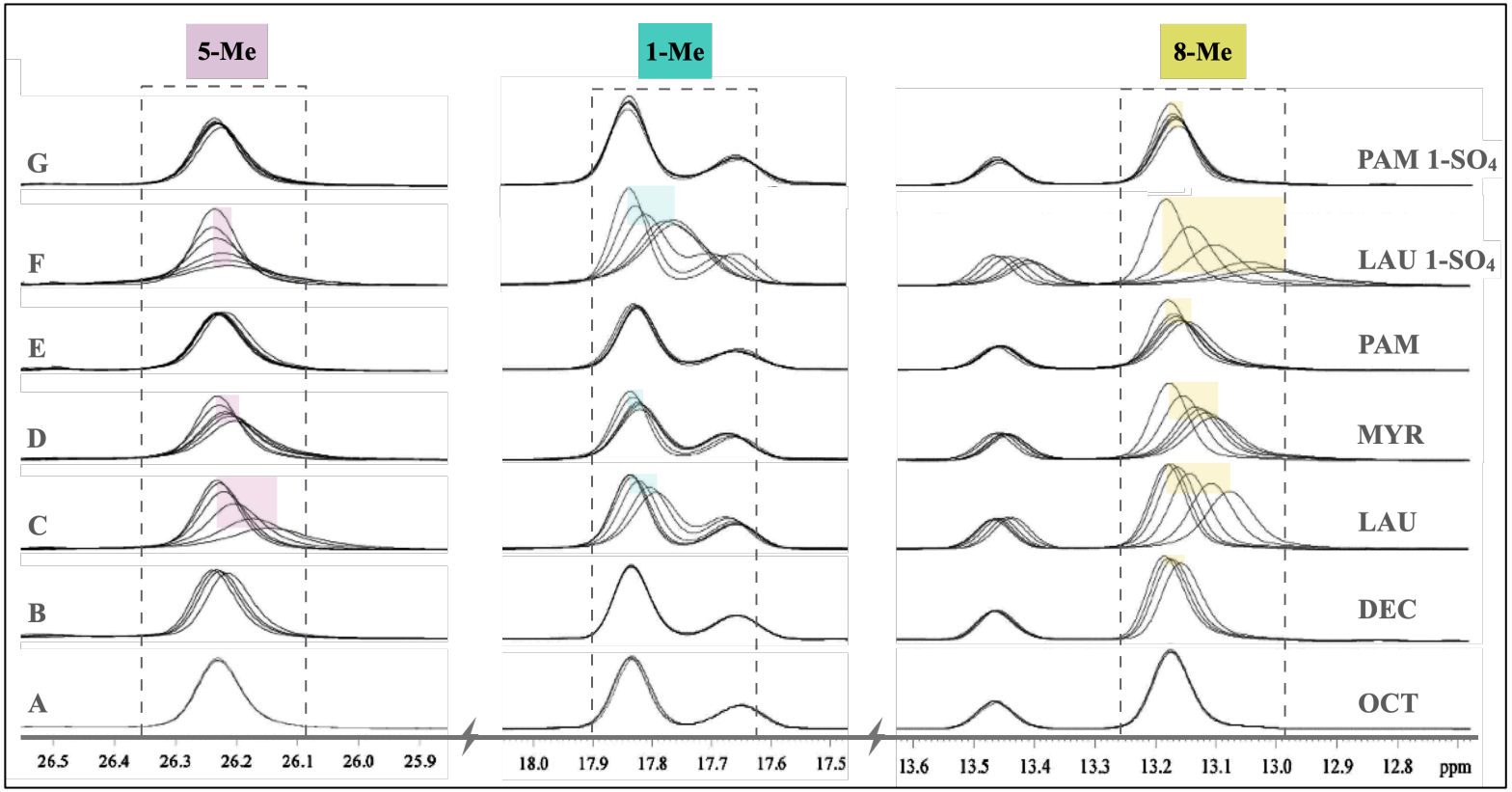

Figure 26: ^{1}H-NMR spectra of MbCN with varying concentrations of FA

0.8 mM MbCN in 30 mM Tris and 3.2 mM TSP at pH 7.4 and 35°C in the following FA:Mb ratios: 0:1, 0.2:1, 0.5:1, 1:1, 2:1, and 4:1.
***A** OCT, **B** DEC, **C** LAU, **D** MYR, **E** PAM, **F** LAU 1-SO$_4$, **G** PAM 1-SO$_4$.*

5-heme methyl signal at 26.2 ppm. OCT, DEC, PAM, and PAM 1-SO$_4$ produce insignificant changes in intensity and chemical shift. LAU and MYR produce significant changes. LAU 1-SO$_4$ produces the most pronounced perturbation.

1-heme methyl signal at 17.8 ppm. OCT, DEC, PAM, and PAM 1-SO$_4$ produce insignificant changes in intensity and chemical shift. LAU and MYR affect significant changes. LAU 1-SO$_4$ produces the most pronounced perturbation.

8-heme methyl signal at 13.2 ppm. OCT does not induce any change. DEC shifts slightly upfield. PAM and PAM 1-SO$_4$ induce both intensity loss and an upfield shift in the Mb signals. LAU and MYR affect significant changes. LAU 1-SO$_4$ produces the most pronounced perturbation. *Adapted from Jue, Shih et al. 2017.*

ii. AutoDock Implementation

To further support the NMR data on chain length dependence, the same Mb grid files used in Chapter 2 for oxy- and deoxy-Mb were used for an AutoDock investigation of all chain lengths C8-18.

a. Macromolecule Preparation

The experiments used the x-ray diffraction crystallographic coordinates from the *Research Collaboratory for Structural Bioinformatics* (RCSB) Protein DataBank (PDB) (Berman, Westbrook et al. 2000). More specifcially, an ultrafast dynamics study was performed on different states of horse (*Equus caballus*) heart myoglobin MbCO (PDB ID: 5CN5) at 1.8 Å resolution and deoxy-Mb (PDB ID: 5D5R) at 1.6 Å resolution (Barends, Foucar et al. 2015). *Equus caballus* myoglobin is more economical and more readily available than human (*Homo sapien*) myoglobin. MbCO was used as an approximation of oxygenated myoglobin, and is referred to as oxy-Mb, which is not readily available from horse heart. Sulphate ions used in the crystallization process were removed from both PDB files before any calculations in AutoDock, in accordance with the AutoDock 4 User Guide (Morris 2012).

b. Ligand Preparation

No PDB files of unbound FA is currently available. Instead, the drawing tool from the *University of Pittsburgh's* free software, Avogadro, was used to sketch the line schematic for the various chain length FAs (Hanwell, Curtis et al. 2012). The Open Babel-based built-in geometry optimization tool combined with the Merck Molecular Force-Field (MMFF94) energy minimization tool were used to refine the drawn FAs (Halgren 1996, O'Boyle, Banck et al. 2011). The refined FA models were saved in the lowest energy state and exported into PDB format, as an optimized approximation of FAs structure given the current limitations, such as a lack of x-ray crystallography data on this small molecule.

To include potentially relevant explicit waters in docking, the AutoDock method for Hydrated Docking was used. As previously discussed in Chapter 2, all of the ligand's hydrogen bond donors and acceptor groups were saturated with special W (water pseudo-atom) atoms (Forli and Olson 2012). A total of 4 W pseudo atoms were added to each FA PDB file. All other available ligand torsions were set to rotatable resulting in a total of 6-15 torsional degrees of freedom based on FA chain length.

iii. AutoDock Results

Figure 27 shows AutoDock results of OCT, DEC, LAU, MYR, PAM (also reported in Chapter 2), and OLE. Each docking experiment yielded 100 conformers that were clustered at 5 Å RMS and ranked by lowest binding energy.

The oxy- vs deoxy-Mb binding to K96 either goes into the hydrophilic patch (deoxy-Mb) or the hydrophobic patch (oxy-Mb) holds for C12-18. This supports the NMR data on chain length, further validating the findings that C12 is the shortest chain length with Mb interaction, as neither deoxy- not oxy-Mb show interaction with C8 or C10 in the hydrophobic patch.

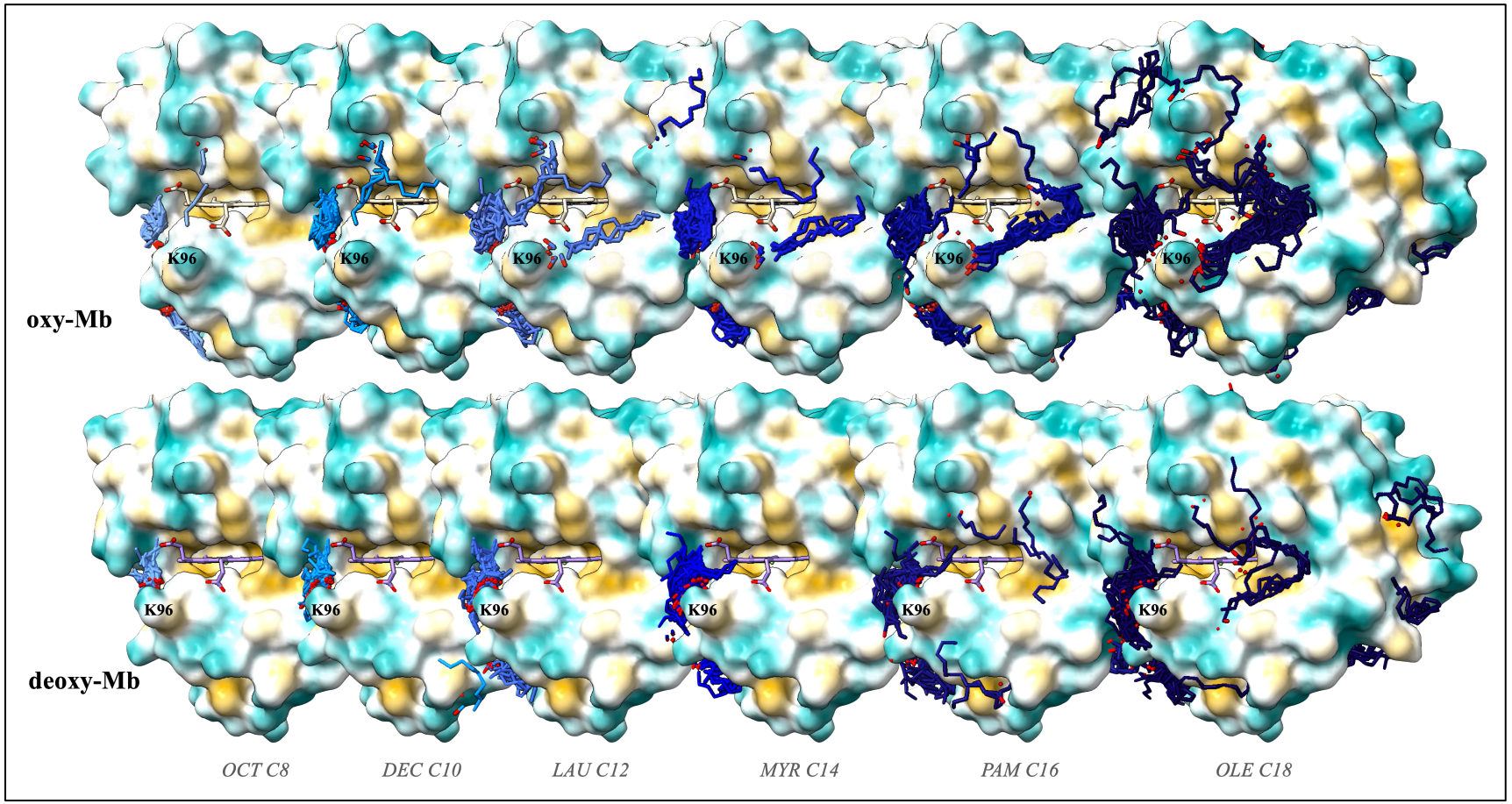

Figure 27: Oxy- and deoxy-Mb binding various chain lengths of FA from 8-18
In agreement with the NMR data, we don't see FA binding in the hydrophobic pocket of oxy-Mb until we reach a carbon chain length of 12, LAU. As for deoxy-Mb we see no binding in the hydrophobic patch at any chain length with only minimal conformers in the region starting with PAM binding to K45, not K96.

K96 – FA	oxy-Mb (5CN5)				deoxy-Mb (5D5R)			
	Final Intermolecular Energy		Torsional Energy	Total Binding Energy	Final Intermolecular Energy		Torsional Energy	Total Binding Energy
kcal/mol	IE_1	ΔH_{elec}	ΔS_{tor}	ΔG_{total}	IE_1	ΔH_{elec}	ΔS_{tor}	ΔG_{total}
OLE 18	-7.69	-1.35	4.12	-4.92	-8.83	-1.42	4.12	-4.71
PAM 16	-7.62	-1.52	3.84	-5.3	-8.69	-1.77	3.84	-4.84
MYR 14	-6.41	-1.44	3.29	-4.56	-8.22	-1.61	3.29	-4.93
LAU 12	-5.93	-1.31	2.74	-4.5	-7.69	-1.61	2.74	-4.94
DEC 10			2.2	ND	-7.1	-1.56	2.2	-4.9
OCT 8			1.65	ND	-6.75	-1.73	1.65	-5.1

Table 3: AutoDock Binding Energy of oxy- and deoxy-Mb with FA C8-18 at K96

Estimated Free Energy of Binding from AutoDock in kcal/mol of oxy-Mb and deoxy-Mb binding FA at K96. Full Box.

Oxy-Mb: We see no binding at all at K96 for OCT and DEC then we start to see binding starting with LAU. Note: DEC had 1 out of 100 conformers bind at K96.

Deoxy-Mb: While we do see binding at K96 for all chain lengths we can see in Figure 27 these conformers are binding in the hydrophilic patch away from the 8-heme-methyl, resulting in a less energetically favorable binding. Interestingly, even OCT and DEC show conformers able to bind in the hydrophilic pocket of deoxy-Mb, whereas no none was seen in oxy-Mb.

iv. Possible Conclusions

In agreement with the NMR data, we don't see FA binding in the hydrophobic pocket until a carbon chain length of 12 is reached. There is no binding at K96 for OCT and DEC; the data illustrate that binding starts with LAU.

v. Future Studies

Further AutoDock studies are necessary for the DET FA analogs: LAU 1-SO_4 and PAM 1-SO_4 to investigate the NMR data. AutoDock simulations may be helpful for elucidating an explanation for the severe peak shift and amplitude decrease seen in Figure 26 F and G.

B. Whale vs Horse Mb Studies

Our mesmerizing mammalian cousins in the sea, sperm whales (*Physeter catodon*), can dive to depths of 2,000 meters below sea level for up to 90 minutes. You'd be forgiven for thinking that these abilities must come with larger lung capacity in order to "hold their breath" for so long. However, we humans have relatively larger lungs than these massive marine mammals. The "trick" to this has to do with—you won't believe it—Myoglobin! Indeed, evidence suggests that myoglobin plays an important role in oxygen supply during marine mammals' apnea.

i. Physiological Differences in Organisms

The oxygen supply capabilities of Mb have been shown in a variety of models, including plants, mammalian tissues, and during seal apnea (Wittenberg and Wittenberg 1989, Ponganis, Kreutzer et al. 2002, Chung, Molé et al. 2005, Gros, Wittenberg et al. 2010). The high concentration of Mb in marine mammals suggests it is associated with oxygen supply during a dive or apnea (Dolar, Suarez et al. 1999, Guyton, Stanek et al. 1995, Kooyman and Ponganis 1998, Ponganis, Kreutzer et al. 2002). Resembling that of the depths of the oceans, certain avian populations show an adaptation to high altitude (compared to those who nest at sea level), which

enhances Mb expression and increases O_2 supply (Gimenez, Sanderson et al. 1977, Terrados, Jansson et al. 1990). These observations suggest a correlation between Mb concentration (O_2 supply) and the animal's respiratory and oxidative capacity (Wittenberg and Wittenberg 2003).

In contrast, the higher concentration of Mb found in marine mammal muscle (shown in Figure 28) can utilize Mb-facilitated O_2 diffusion under all physiological conditions (Lin, Kreutzer et al. 2007).

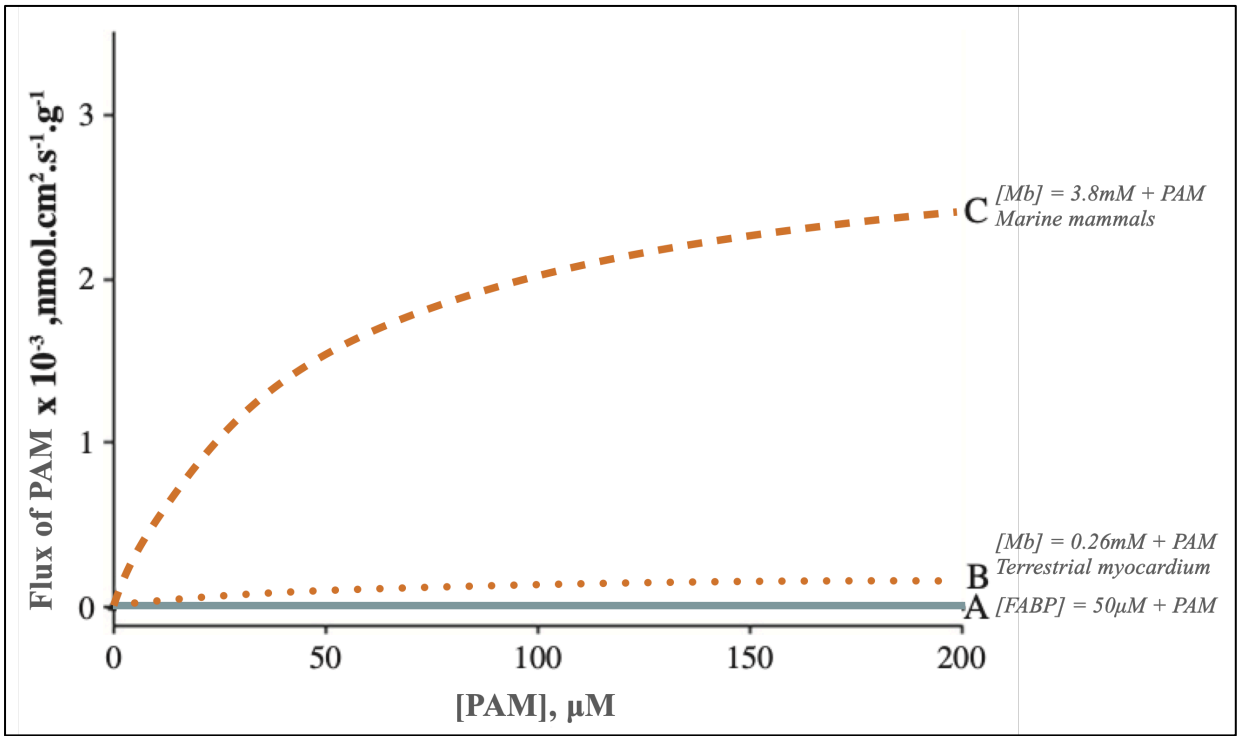

Figure 28: Model of FA flux at high palmitate concentration
A. *FABP facilitated transport of FA (50 µM FABP, K_d = 14 nM).* ***B.*** *Mb facilitated transport of PAM (Mb = 0.26 mM, K_d = 48 µM).* ***C.*** *Mb facilitated transport of PAM (Mb = 3.8 mM, K_d = 48 µM). The V_{max} values per g tissue for Mb facilitated FA transport in rat heart = 2.0×10^{-4} nmol cm^2 s^{-1} g^{-1} and in seal muscle = 30×10^{-4} nmol cm^2 s^{-1} g^{-1}. Adapted from Shih, Chung et al. 2014.*

ii. Sequence Comparison

Investigation into the differences of Mb between species should begin with the primary—of course—structure. The amino acid residue sequence comparison shown in Figure 29 shows sperm whale MbO_2 (PDB ID: 1MBO) with horse heart MbCO (PDB ID: 5CN5). Again, as in Chapter 2, carboxy-Mb is being used as a surrogate for and will be referred to as oxy-Mb as to distinguish it from MbO_2. There are a few substitutions of positively charged side chains, but since K45 is in the heme pocket where both NMR and AutoDock studies have shown interaction previously, it is of the most interest.

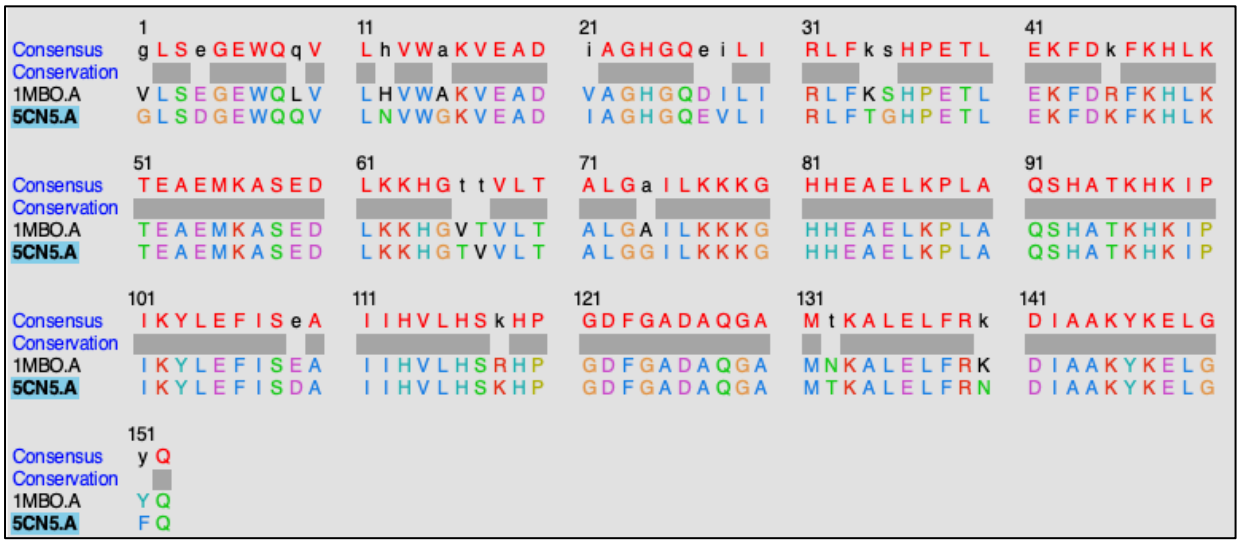

Figure 29: Amino Acid Sequence Comparison of Horse and Whale oxy-Mb
Noting the substitutions of positively charged side chains at Positions: 12, 34, 45, 118, 140. K45 being in the heme pocket and therefore of interest.

iii. AutoDock Implementation

AutoDock simulations using both whale and horse oxy- and deoxy-Mb binding with PAM were used to continue investigating if there are any detectable differences between the two.

a. Macromolecule Preparation

The docking simulations used the same x-ray diffraction crystallographic coordinates from the *RCSB* Protein DataBank: MbCO (PDB ID: 5CN5) and deoxy-Mb (PDB ID: 5D5R) that were used in Chapter 2 (Barends, Foucar et al. 2015). Again, MbCO was used as an approximation of MbO_2 oxygenated horse heart myoglobin, and will be referred to as oxy-Mb, whose PDB is not available. Sperm Whale oxy-Mb (PDB ID: 1MBO) at 1.6 Å resolution. Sperm whale deoxy-Mb (PDB ID: 1A6N) at 1.15 Å resolution (Vojtechovský, Chu et al. 1999). As always, sulphate ions used in the crystallization process were removed from all PDB files before any calculations in AutoDock in accordance with the AutoDock 4 User Guide (Morris 2012).

b. Ligand Preparation

As previously stated, no PDB file of unbound PAM is currently available. Instead, the same optimized approximation of PAM structure created previously will be used again for the ligand PDB file.

Again, to include potentially relevant explicit waters in docking, AutoDock's method for Hydrated Docking was used. A total of 4 W pseudo atoms were added to the PAM PDB. All other available ligand torsions were set to rotatable resulting in a total of 14 torsional degrees of freedom.

iv. AutoDock Results

AutoDock results of PAM with horse oxy-Mb (also reported in Chapter 2), and whale oxy-Mb are shown in Figure 30. Each docking experiment yielded 100 conformers that were clustered at 5 Å RMS and ranked by lowest binding energy.

The more positively charged R45 was expected to be a more favorable binding site from PAM in whale oxy-Mb, compared to K45 in horse oxy-Mb, simply by effecting the electrostatic energy portion of the total binding energy. Unfortunately, no change in overall binding energy nor electrostatic energy was observed in AutoDock simulations, suggesting further NMR research is necessary to determine if species dependence is more than just a matter of Mb concentration variation.

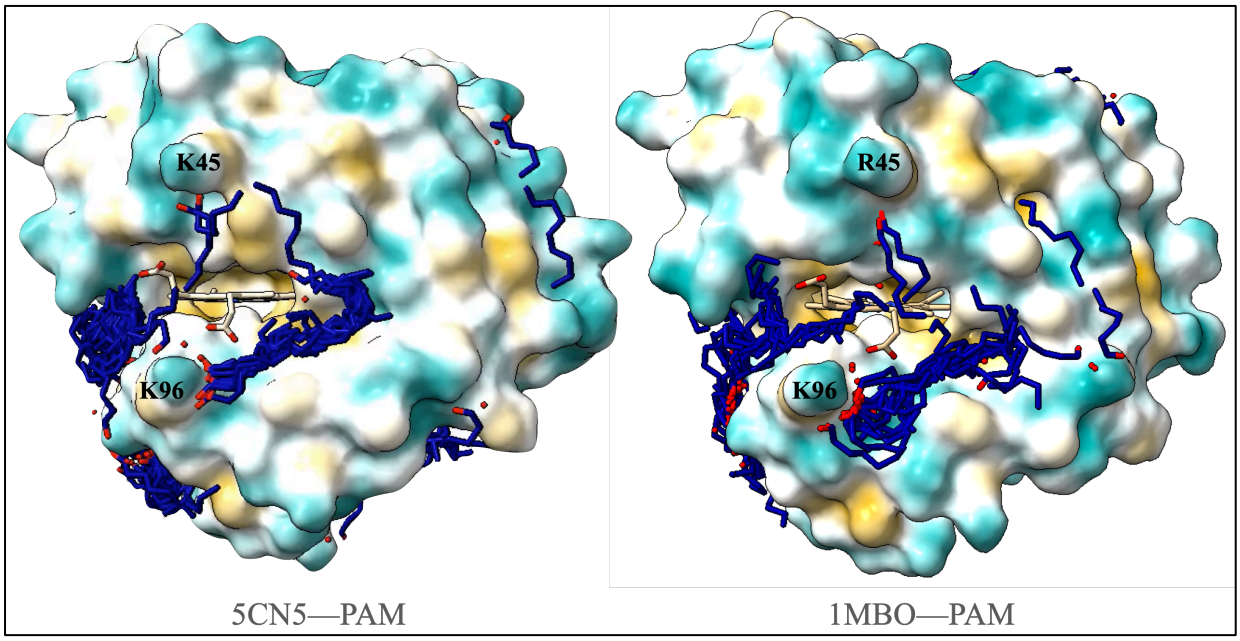

Figure 30: AutoDock 100 conformers of PAM with oxy-Mb
Left: *horse oxy-Mb (PDB ID: 5CN5) and PAM;* ***Right:*** *sperm whale oxy-Mb (PDB ID: 1MBO) and PAM. Not shown: N-terminus on rear of protein, opposite heme pocket, shown in Chapter 2.*

The box sizing protocols from Chapter 2 were used again here, data for the full-box and half-sized box are given in Table 4. Future investigation could narrow the box size to focus on AA 45, instead of K96 (this data) to better elucidate any docking there in particular. The full-box experiments showed, in agreement with Chapter 2 results, the negatively charged carboxyl head group of PAM binding non-selectively to the positively charged external AA binding sites. The most common are listed below in Table 4.

Palm16		Horse oxy-Mb (5CN5)				Whale oxy-Mb (1MBO)			
		Energy (kcal/mol)				**Energy** (kcal/mol)			
	Binding Site	Final Intermolecular Energy		Torsional Energy	Total Binding Energy	Final Intermolecular Energy		Torsional Energy	Total Binding Energy
		IE_1	ΔH_{elec}	ΔS_{tor}	ΔG_{total}	IE_1	ΔH_{elec}	ΔS_{tor}	ΔG_{total}
Half Box	K96	-7.15	-1.57	3.84	-4.87	-7.8	-1.7	3.84	-5.65
	K42	-7.27	-1.34	3.84	-4.77	-7.2	-1.94	3.84	-5.3
	45	-6.72	-1.72	3.84	-4.60	-7.79	-.97	3.84	-4.92
	K98	-6.66	-1.66	3.84	-4.47	-6.67	-1.84	3.84	-4.76
Full Box	1	-7.65	-2.03	3.84	-5.84	-7.57	-2.07	3.84	-5.8
	K96	-7.62	-1.52	3.84	-5.3	-7.57	-1.44	3.84	-5.17
	K42	-6.9	-1.59	3.84	-4.65	-7.02	-2.05	3.84	-5.23
	K98	-6.2	-1.66	3.84	-4.02	-6.53	-2.09	3.84	-4.78
	45	-6.72	-1.76	3.84	-4.45	-7.13	-1.17	3.84	-4.46

Table 4: AutoDock Binding Energy for PAM with Horse, Whale oxy-Mb
Note: the full box 45 data is <10 conformers

v. Possible Conclusions

Whale oxy-Mb in the full box has similar values for overall binding compared to horse oxy-Mb at positions 1, 96, and 45. However, the half box suggests that whale oxy-Mb has consistently tighter binding energies at positions 96, 42, 45, and 98. Further AutoDock simulations are necessary on the deoxy-Mb from whale, to determine if the oxy- vs deoxy-Mb hydrophobic vs hydrophilic patch binding seen in horse Mb (Chapter 2, and earlier in this Chapter) holds for whale Mb as well.

III. Collaborative Efforts

A. Myoglobin—Nonenal Studies

i. Previously Published Data on Autoxidation and Electron Transfer

Recent studies report an equine Mb autoxidation rate constant of 1.64×10^{-3} min^{-1}, which is consistent with published literature values range from 0.9 to 2.2×10^{-3} min^{-1}, depending on the Mb isozyme, temperature, buffer condition and pH (Germolus, Rehman et al. 2022).

Experiments claiming nonenal (HNE)-enhanced Mb autoxidation used an HNE:Mb ratio of 6:1 and 1.5% ethanol (EtOH) to solubilize the HNE at pH 7.2, even though 1 mg of HNE will dissolve in 1 mL of phosphate buffer saline (PBS) solution to reach a concentration of 6.4 mM. In order to reduce non-specific interactions that can lead to hemichrome formation, and thus impacting the NMR interpretation, recent studies have used lower ratios of HNE:Mb up to 4:1, and ratios comparable to the FA:Mb ratios used in other NMR studies to contextualize analysis (Akhrem, Andreyuk et al. 1989, Shih, Chung et al. 2014, Shih, Chung et al. 2015, Germolus, Rehman et al. 2022). Mb autoxidation remains constant even up to HNE:Mb of 4:1. In short, these studies concluded HNE does not impact Mb autoxidation.

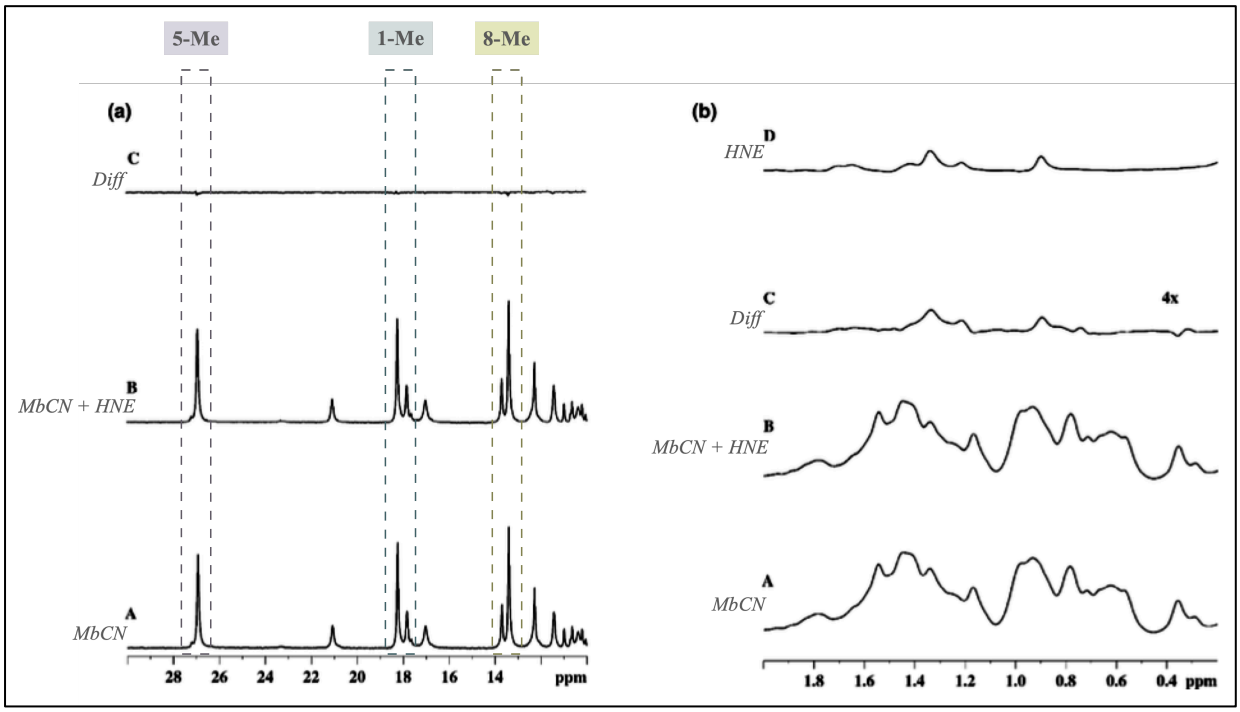

Figure 31: ^{1}H NMR spectra of MbCN with and without HNE

0.4 mM MbCN (12–30 ppm) with and without 0.4 mM HNE in 30 mM Tris and 1 mM EDTA at pH 7.40 and at 35°C.

*(a) Left panel: Spectra (30–10 ppm) of **A** MbCN with no HNE, **B** with HNE and **C** difference spectra (bottom to top). The hyperfine shifted signals in the region show no interaction with HNE, as reflected in the prominent 5-CH_3 (26.9 ppm), 1-CH_3 (18.3 ppm) and 8-CH_3 (13.4 ppm) signals.*

*(b) Right panel: ^{1}H NMR spectra (0.2–2 ppm) of 0.4 mM MbCN with and without 0.4 mM HNE in 30 mM Tris and 1 mM EDTA at pH 7.40 and at 35°C. Spectra (2.0–0.2 ppm) of **A** MbCN with no HNE, **B** with HNE at HNE:Mb 4:1 ratio, **C** difference spectrum with vertical scaling increased by four times and **D** solution spectra of 1.6 mM HNE (bottom to top).*

Adapted from Germolus, Rehman et al. 2022.

ii. AutoDock Implementation

The NMR data described in Figure 31 is from MbCN, which was used as another surrogate for oxy-Mb. Because map files for oxy-Mb (surrogate: MbCO, PDB ID:5CN5) had already been generated, the AutoDock simulations of HNE with oxy-Mb was expected to be straightforward.

a. Macromolecule Preparation

The docking simulations used the same x-ray diffraction crystallographic coordinates from the *RCSB* Protein DataBank: MbCO (PDB ID: 5CN5) and deoxy-Mb (PDB ID: 5D5R) that were used in Chapter 2 (Berman, Westbrook et al. 2000, Barends, Foucar et al. 2015). As always, sulphate ions used in the crystallization process were removed from both PDB files before any calculations in AutoDock in accordance with the AutoDock 4 User Guide (Morris 2012).

b. Ligand Preparation

HNE structure was available through the Protein DataBank as a ligand, (PDB ID: HNE) originally downloaded as an ideal Structure Data File (SDF), opened in Chimera, and saved in PDB file format so that it could be hydrated (Pettersen, Goddard et al. 2004). As previously described, the Hydrated Docking method was used. This technique added 5 W pseudo atoms to the nonenal PDB as seen in Figure 32. All other available ligand torsions were set as "rotatable" resulting in a total of 7 torsional degrees of freedom.

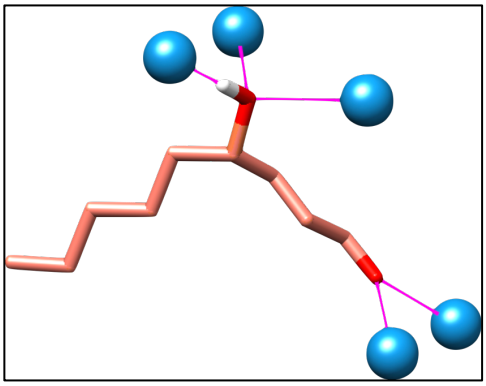

Figure 32: Hydrated Nonenal
HNE in salmon with W pseudo atoms in blue attached by non-rotatable (pink) bonds.

iii. AutoDock Results

AutoDock results were consistent with the NMR data, and did not show any binding to K96 inside the hydrophobic patch, as seen in Figure 33. However, some binding to K96 is seen in the hydrophilic patch for both oxy- and deoxy-Mb. It seems both oxy- and deoxy-Mb show binding at sites: I101, H97, K96, K102, K42, R31, H82, K56.

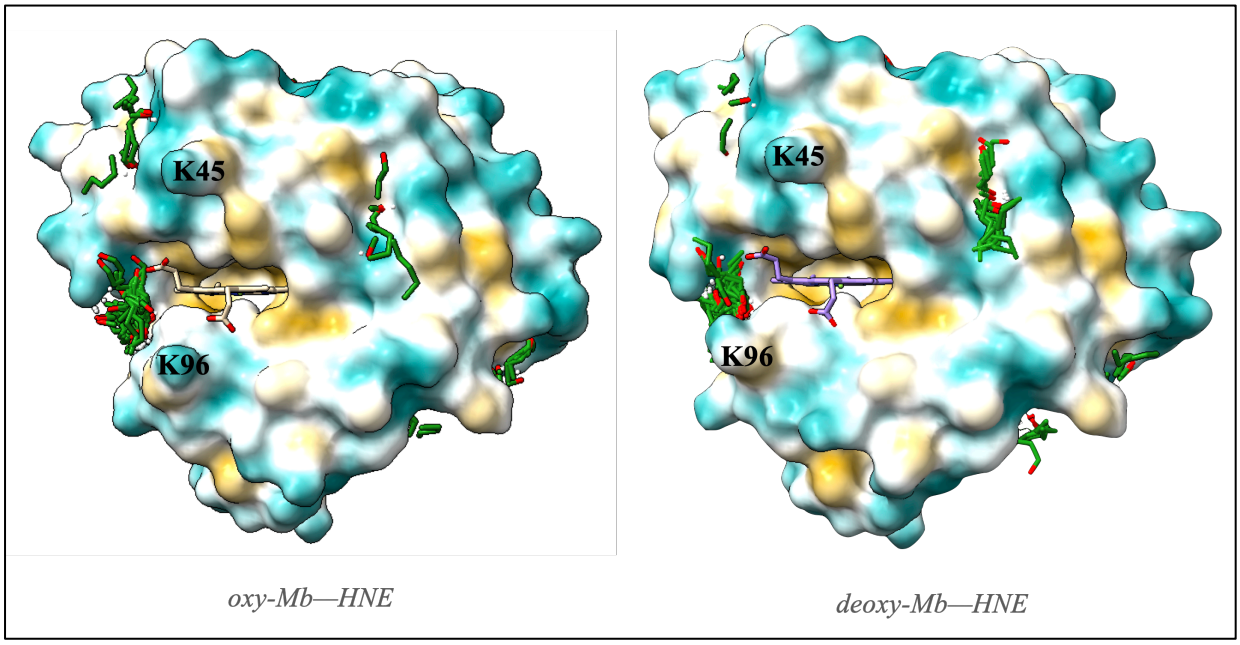

Figure 33: AutoDock 100 conformers of nonenal with Mb
Left: *oxy-Mb (PDB ID: 5CN5) and HNE in green;* ***Right:*** *deoxy-Mb (PDB ID: 5D5R) and HNE in green*

iv. Conclusions

The AutoDock results are consistent with both the UV-Vis data seen in Figure 37, and the NMR data in Figure 31. These results reinforce that HNE does not modulate the autoxidation nor the oxidation by electron transfer of Mb.

B. Cytochrome C—Mb Studies

To further investigate the mechanism(s) of Mb oxidation, given that findings do not suggest an association with HNE, an experiment was designed to test the theory that Mb is oxidized by electron transfer to Cytochrome C, as postulated by Germolus et al.

i. Structural Comparison

Mb is a monomeric protein made up of 8 α-helices that stabilize a heme group that can bind O_2 but whose function is uncertain. To investigate the potential functions of Mb, it's structure was compared to its relatives and nearest neighbors. Another heme protein cousin, called Cytochrome C Oxidase ($Cyt^{3+}C$), shown in Figure 34 is also monomeric. Its secondary structure consists of 5 α-helices and weighs 12 kDa (in comparison to Mb's 16-17 kDa mass). It also contains a Heme group, however its heme doesn't bind O_2, but its function is widely agreed upon. $Cyt^{3+}C$ is a part of the Electron Transport Chain (ETC) shown in Figure 35 (Bushnell, Louie et al. 1990).

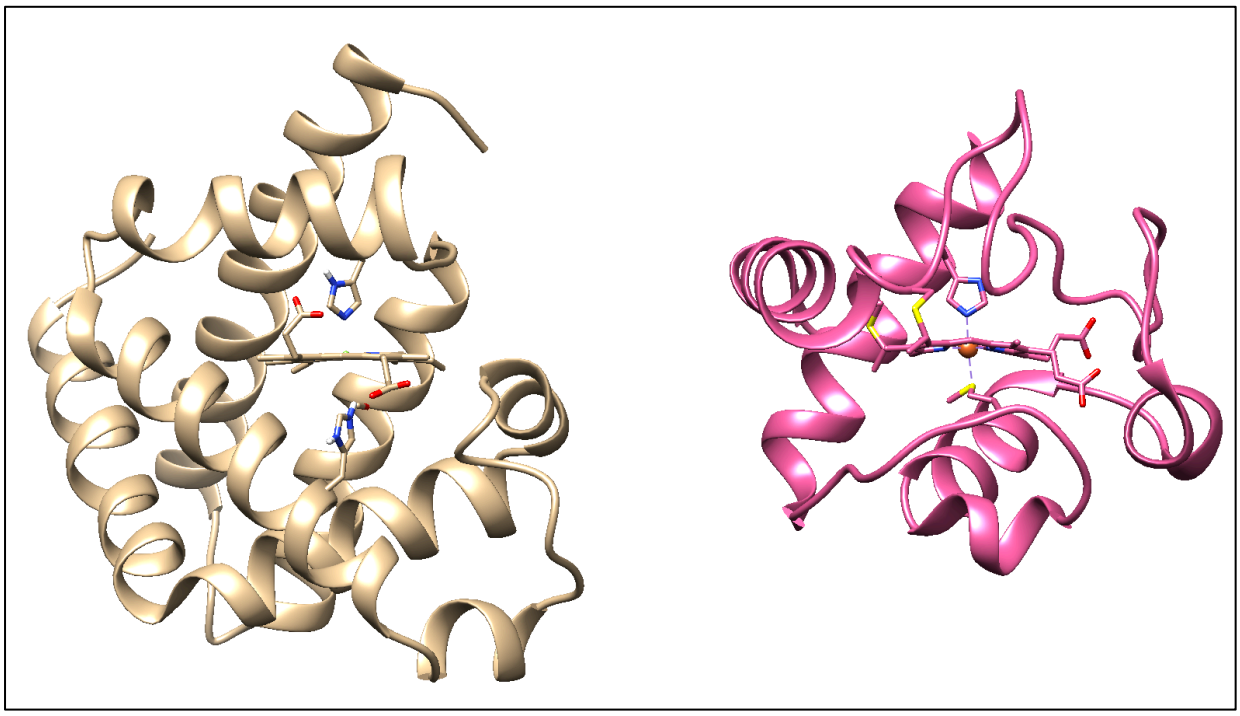

Figure 34: MbCO vs Cytochrome C ribbon drawings
Left: *MbCO (PDB ID: 5CN5) in tan compared to* ***Right:*** *Cytochrome C (PDB ID: 1HRC) in pink*

ii. Physiological Feasibility

a. $Cyt^{3+}C$ and Mb oxidation by electron transfer

As opposed to the autoxidation of Mb, an appropriate electron acceptor can also oxidize Mb. Not only do standard reduction potentials (shown in Equation 5) suggest Mb will transfer an electron to $Cyt^{3+}C$, qualitative spectrophotometric data also shows this electron transfer from MbO_2 to $Cyt^{3+}C$ (Taylor and Morgan 1942, Rodkey and Ball 1947).

Equation 5: Standard Reduction Potentials and The Nernst Equation

Eqn. 5

$$Mb^{3+} + e^- \longrightarrow Mb^{2+} \quad 0.046\ V$$
$$Cyt^{3+}C + e^- \longrightarrow Cyt^{2+}C \quad 0.255\ V$$
$$Mb^{2+} + Cyt^{3+}C \longrightarrow Mb^{3+} + Cyt^{2+}C \quad 0.209\ V$$

$$\frac{[Mb^{3+}][Cyt^{2+}C]}{[Mb^{2+}][Cyt^{3+}C]} = 10^{\left(\frac{0.209}{0.0592}\right)} \simeq 3392$$

b. Electron Transport Chain

Cytochrome C, seen in dark orange in Figure 35, comes into play between complex 3 and 4 of the ETC. Complex 3 reduces Cytochrome C so it can then go to Complex 4 to be oxidized. If Mb oxidization by electron transfer could be used as a short cut to produce the reduced form of Cytochrome C without Complex 3, then the ETC could continue to Complex 4. Also considering EtOH has been found to increase Mb electron transport (see Ch.3.III.A.), this interaction could be a way to potentially 'super charge' the ETC.

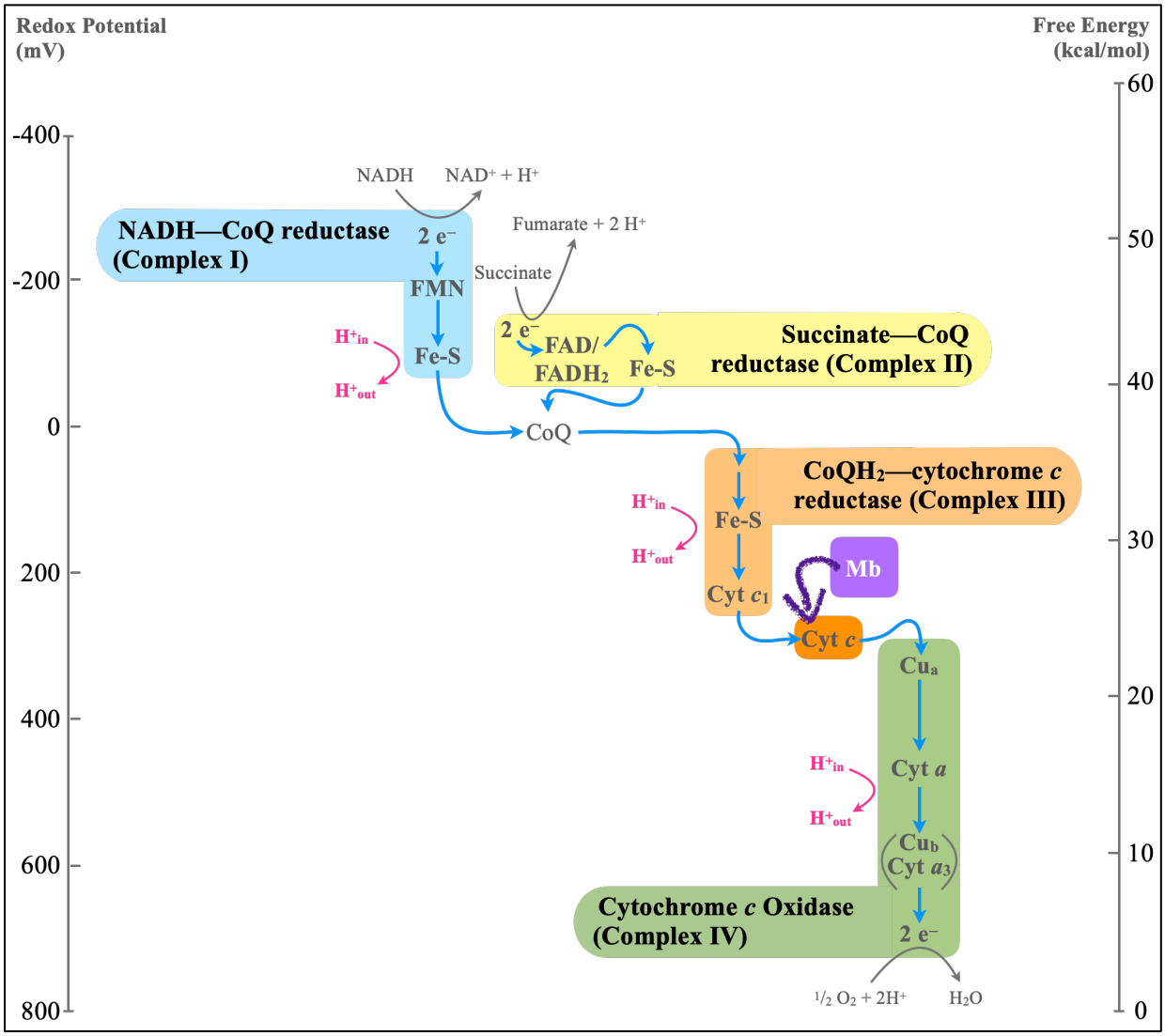

Figure 35: Electron Transport Chain
With Proposed Mb position in Purple. Figure adapted from Molecular Cell Biology Sixth Edition (Lodish 2008)

c. Previous Data

UV-vis data shows peak lines marked in red for MbO_2 , brown for met-Mb, blue for $Cyt^{2+}C$, and green for $Cyt^{3+}C$ in Figure 36. In electron transfer experiments (bottom panels), MbO_2 peaks at 542 nm and 580 nm decrease and $Cyt^{3+}C$ peak at 530 nm decreases. Meanwhile, the $Cyt^{2+}C$ peaks at 520 nm and 550 nm and the met-Mb peak at 630 nm increase, regardless of the addition of HNE, which is consistent with earlier AutoDock results and NMR

results. However, the physiological feasibility of electron transfer to CytC, is observed in the UV-Vis data.

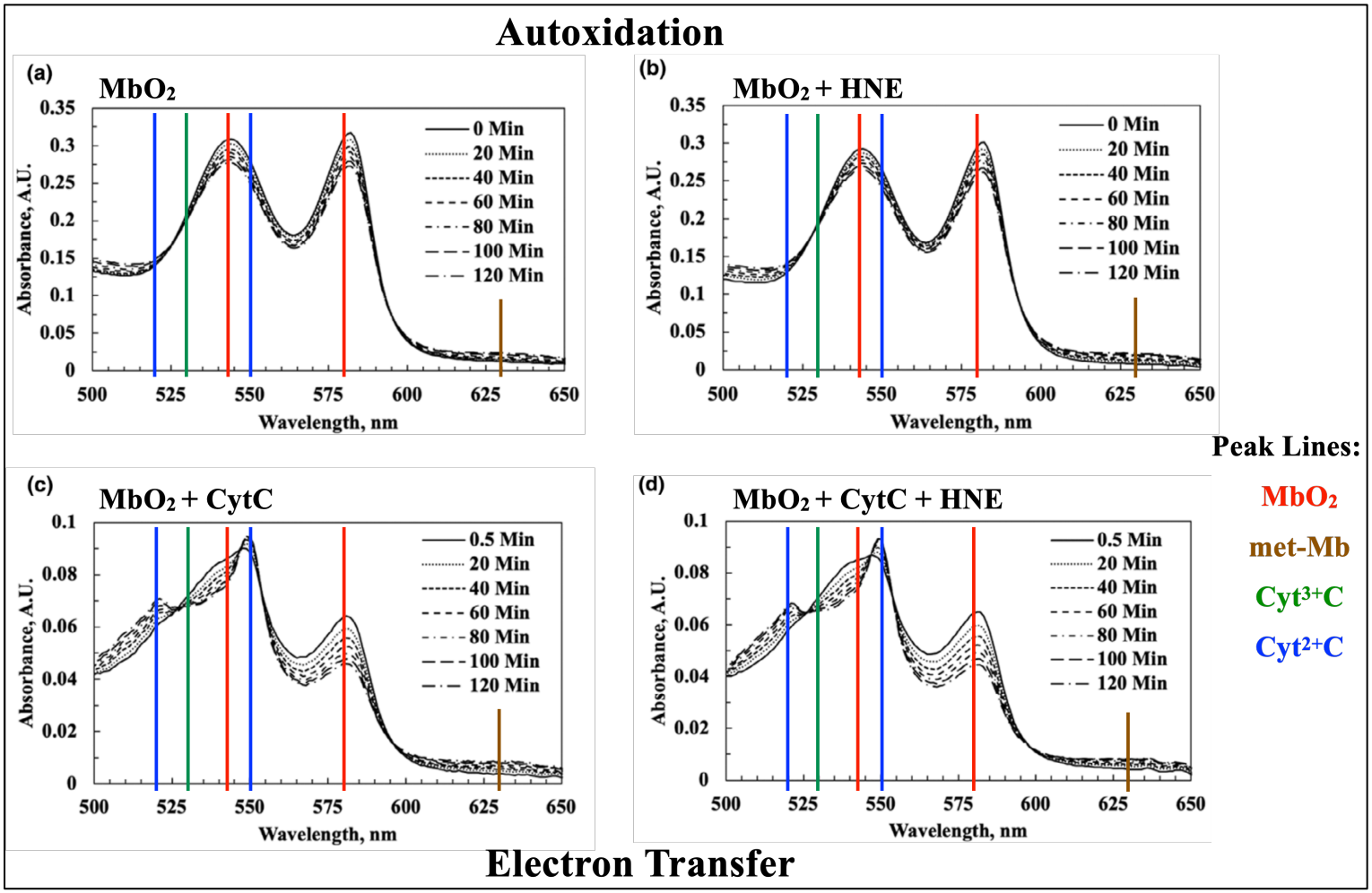

Figure 36: Select spectra of the MbO_2 autoxidation and electron transfer to $Cyt^{3+}C$
8 or 50 μM MbO_2 in 30 mM Tris and 1 mM EDTA at pH 7.40 and 35 °C.
Top: Autoxidation experiments, (a) with no HNE and (b) with HNE in HNE:Mb ratio of 1:1.
Bottom: Electron transfer experiment, (c) with no HNE and (d) with HNE in HNE:Mb ratio of 1:1.
The spectrophotometer acquired a spectrum every 5 min over the 120 min time course.

Adapted from Germolus, Rehman et al. 2022.

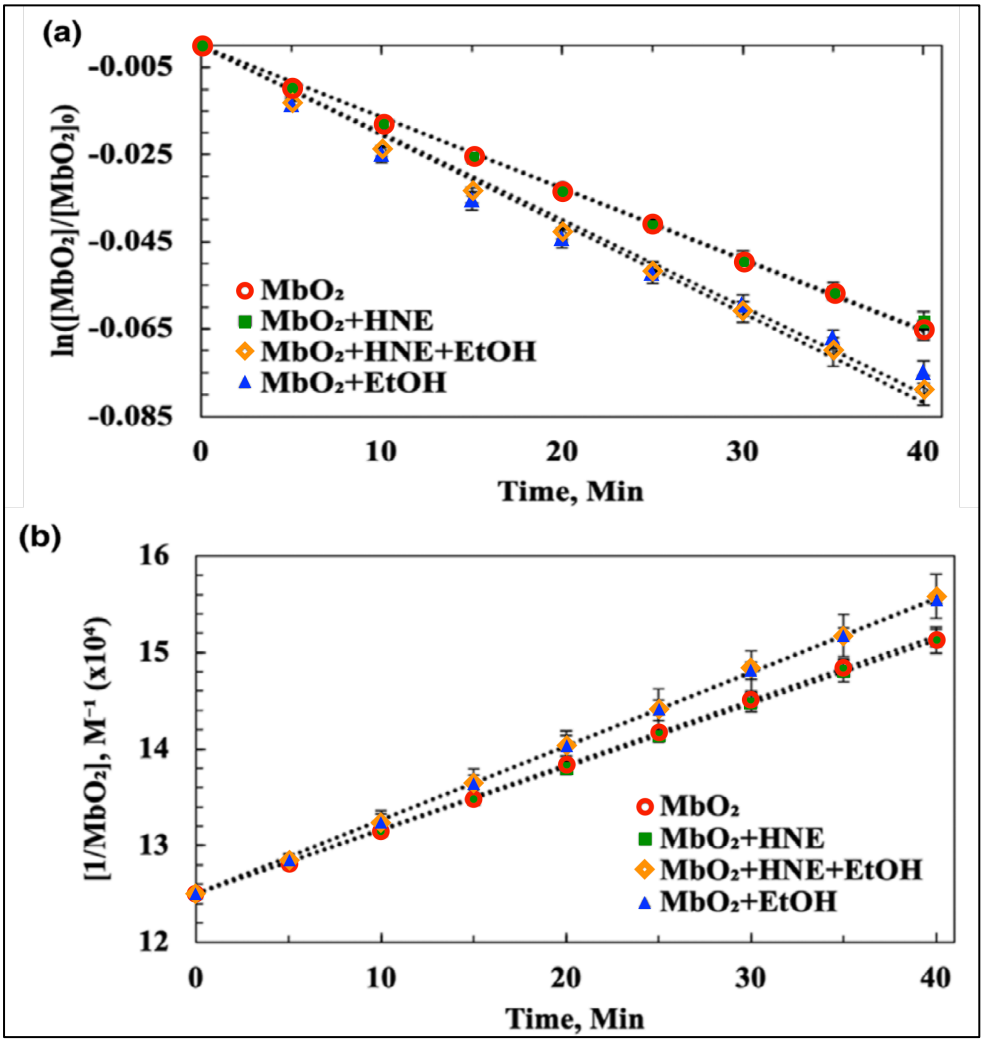

Figure 37: Plot of MbO_2 vs. time for autoxidation and electron transfer.

(a) For autoxidation of MbO_2 with no HNE, with 1:1 MbO_2: HNE, with 1:1 MbO_2:HNE + 1.5% ethanol (EtOH) and with only 1.5% EtOH, the plots of $\ln\left(\frac{[MbO_2]}{[MbO_2]_0}\right)$ *vs. time lead to the following linear regressions:*

without HNE: $Y = -1.64 \times 10^{-3}\, X \quad (R^2 = 1.000)$,

with HNE: $Y = -1.63 \times 10^{-3}\, X \quad (R^2 = 0.999)$,

with HNE and 1.5% EtOH: $Y = -2.05 \times 10^{-3}\, X \quad (R^2 = 0.998)$,

with 1.5% EtOH: $Y = -2.00 \times 10^{-3}\, X \quad (R^2 = 0.994)$.

(b) For electron transfer from MbO_2 to $Cyt^{3+}C$, the plots of $\frac{1}{[MbO_2]}$ *vs. time at Mb:$Cyt^{3+}C$ ratio = 1 lead to following linear regressions:*

without HNE: $Y = 0.067\, X + 12.5 \times 10^4 \quad (R^2 = 0.999)$,

with HNE at HNE: MbO_2 ratio of 1: $Y = 0.066\, X + 12.5 \times 10^4 \quad (R^2 = 0.999)$,

with HNE and 1.5% EtOH: $Y = 0.077\, X + 12.5 \times 10^4 \quad (R^2 = 0.999)$,

with 1.5% EtOH: $Y = 0.076\, X + 12.5 \times 10^4 \quad (R^2 = 0.999)$.

Adapted from Germolus, Rehman et al. 2022.

iii. AutoDock Implementation

AutoDock simulated docking studies were performed on horse oxy-Mb, as the macromolecule, and horse $Cyt^{3+}C$, as the ligand, in order to investigate possible electron transfer between the two proteins.

a. Macromolecule Preparation

The docking simulations used the same horse heart myoglobin MbCO (PDB ID: 5CN5) and deoxy-Mb (PDB ID: 5D5R) as previous experiments (Barends, Foucar et al. 2015). Again, MbCO was used as an approximation of MbO_2, oxygenated horse heart Mb, and will be referred to as oxy-Mb, whose PDB is not available. As always, sulphate ions used in the crystallization process were removed from all PDB files before any calculations in AutoDock in accordance with the AutoDock 4 User Guide (Morris 2012).

b. Ligand Preparation

Horse heart $Cytochrome^{3+}C$ (PDB ID: 1HRC) at 1.9 Å resolution was used as the 'ligand' for this docking simulation experiment (Bushnell, Louie et al. 1990).

The previously described hydrated docking method was used; 433 W pseudo-atoms were added to the $Cyt^{3+}C$ PDB, as seen in Figure 38. In the case of horse $Cyt^{3+}C$, the selected side chain torsions were on residues: C14, C17, H18, T28, K79, M80, I81, and F82. All side chain torsions were set to rotatable resulting in a total of 20 torsional degrees of freedom.

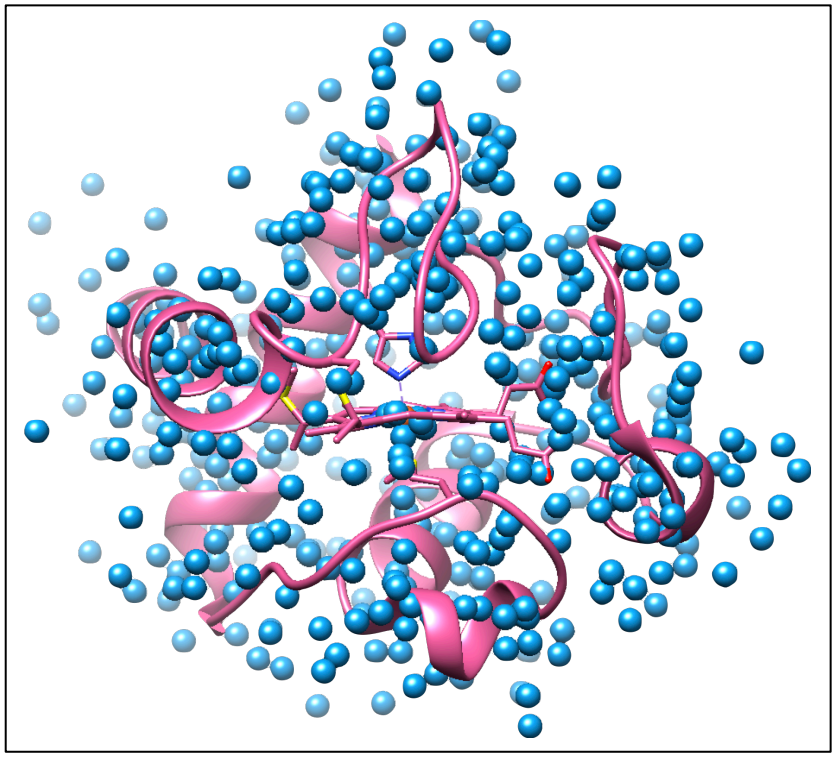

Figure 38: Hydrated $Cyt^{3+}C$
$Cyt^{3+}C$ ribbon in pink, W pseudo atoms in blue

iv. Preliminary AutoDock Results

A preliminary docking conformation from AutoDock, shown in Figure 39, shows $Cyt^{3+}C$ M80 perpendicularly aligned with the 8-heme-methyl. This could be a potential path for the electron transfer hypothesized by Germolus et al as part of the ETC as shown in Figure 35.

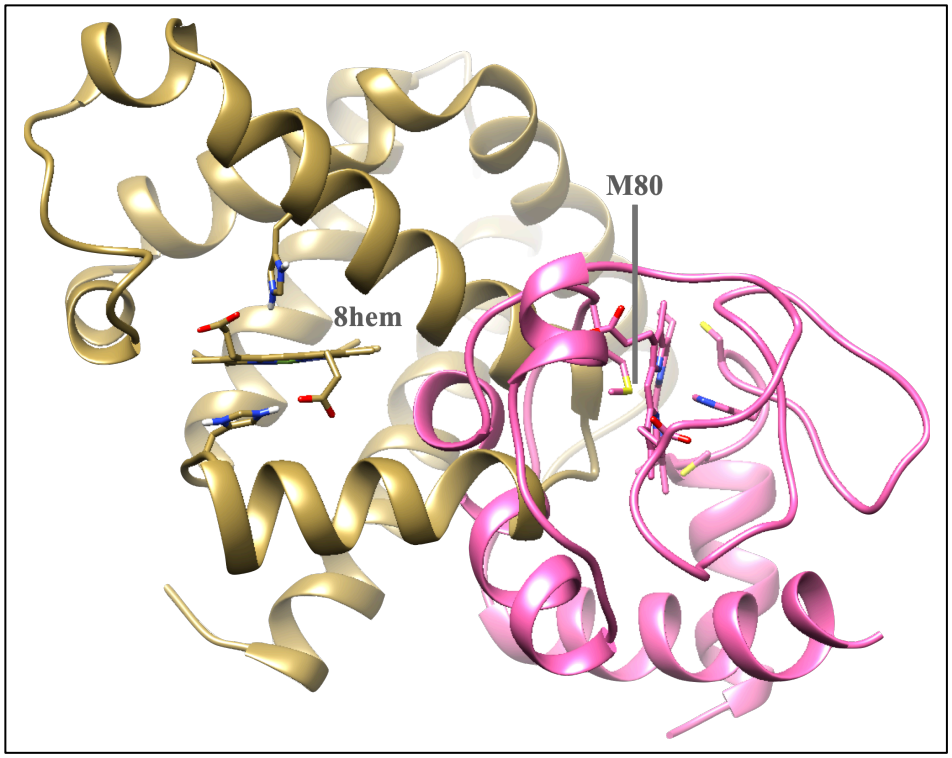

Figure 39: Preliminary docking Mb—Cyt^{3+}C results
Preliminary data Cyt^{3+}C (pink) M80, 8-heme-methyl of oxy-Mb (tan).

C. Future: Mb—Ethanol Studies

Since previous NMR studies have shown EtOH, not HNE, interacting with Mb, AutoDock simulations could be considered to investigate potential binding sites.

i. Previously Published NMR Studies

EtOH's hydrophobicity properties are known to disrupt protein structure, therefore its use in solubilizing the HNE draws questions about methodology (Yoshikawa, Hirano et al. 2012, Kundu, Aswal et al. 2017). Considering a HNE solution with the addition of 1.5% EtOH perturbs Mb structure (seen in Figure 40) and increases MbO_2 autoxidation, it is more likely that the EtOH is doing the heavy lifting in increasing Mb autoxidation. HNE has no observed effect.

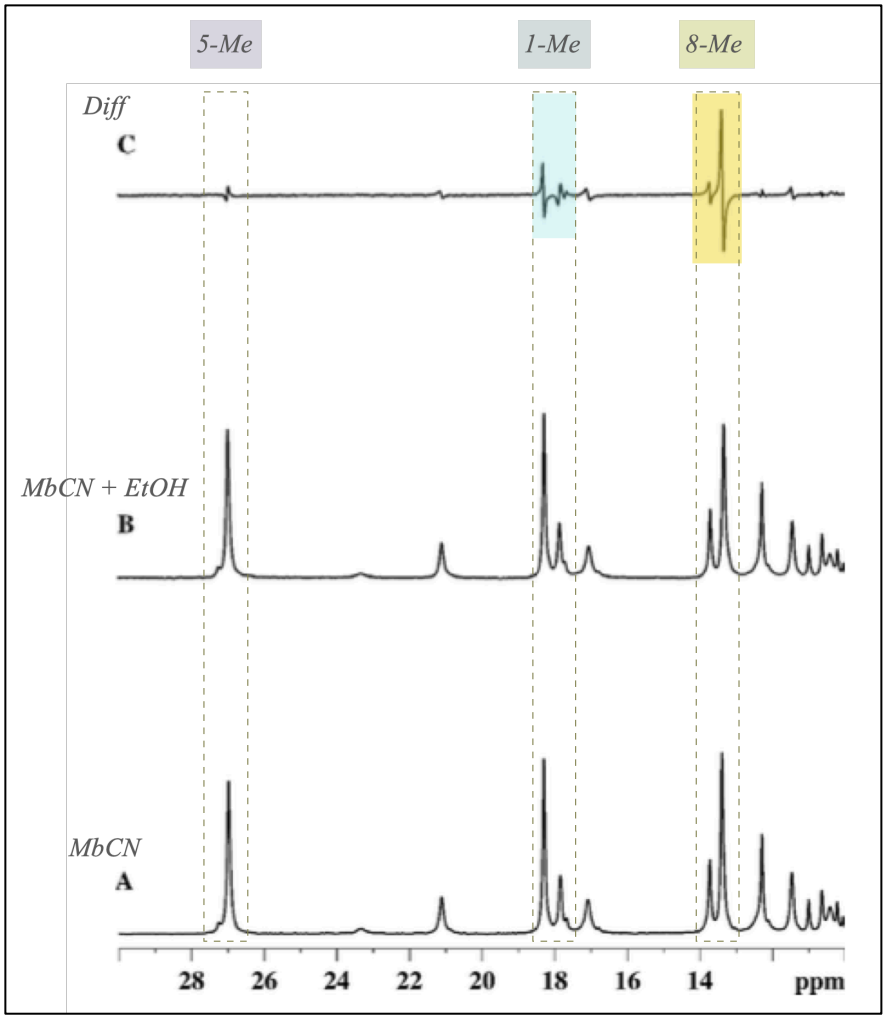

Figure 40: ^{1}H NMR spectra of MbCN with and without EtOH
0.4 mM MbCN (12–30 ppm) with and without 1.5% ethanol. Top spectrum shows the difference (bottom to top). The heme 8-CH_3 (13.4 ppm) and 1-CH_3 (18.3 ppm) signals shift upfield with the addition of EtOH. Adapted from Germolus, Rehman et al. 2022.

We can also see evidence of EtOH impact on Mb in the UV-Vis data from Figure 37, also confirming it is EtOH not HNE that influences both the autoxidation and oxidation by electron transfer of Mb.

ii. Proposed AutoDock Implementation

Since the AutoDock map files already exist for Mb, using MbCO (PDB ID: 5CN5) as surrogate, implementation of EtOH studies should be fairly straight forward.

a. Macromolecule Preparation

The same Mb model described before using MbCO (PDB ID: 5CN5), as a surrogate for MbO_2, and deoxy-Mb (PDB ID: 5D5R) should be suitable for these future experiments as well.

b. Ligand Preparation

The structure of EtOH was available through the Protein DataBank as a ligand (PDB ID: EOH) downloaded as an ideal Structure Data File (SDF), opened in Chimera and saved in PDB file format so that it could be hydrated (Pettersen, Goddard et al. 2004). This technique added 3 W pseudo atoms to the EtOH PDB as seen in Figure 41. All other available ligand torsions were set to rotatable resulting in a total of 1 torsional degree of freedom.

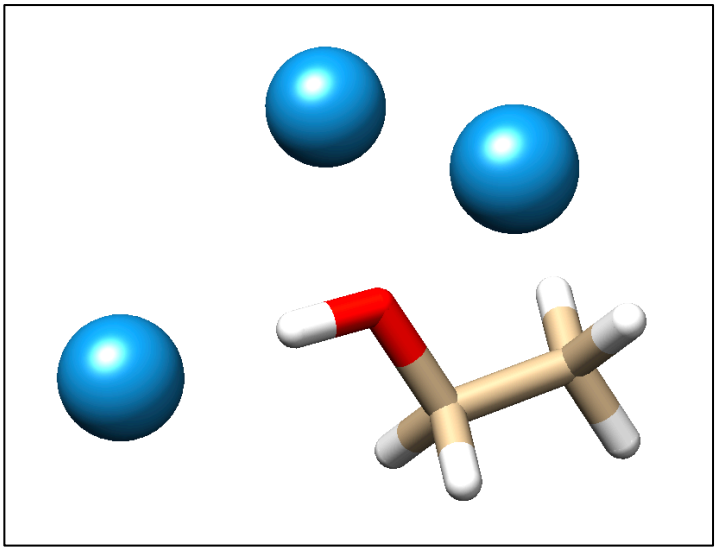

Figure 41: Stick drawing of Hydrated EtOH
EtOH in tan with W pseudo atoms in blue.

c. Expected Results

While an interaction between Mb and EtOH is expected, the exact binding sites are unknown beyond the NMR data suggesting interaction at 1- and 8-heme-methyls. This makes it a prime candidate for AutoDock simulations.

IV. REFERENCES

Akhrem, A. A., G. M. Andreyuk, M. A. Kisel and P. A. Kiselev (1989). "Hemoglobin conversion to hemichrome under the influence of fatty acids." Biochimica et Biophysica Acta (BBA) - General Subjects 992(2): 191-194.

Barends, T. R., L. Foucar, A. Ardevol, K. Nass, A. Aquila, S. Botha, R. B. Doak, K. Falahati, E. Hartmann, M. Hilpert, M. Heinz, M. C. Hoffmann, J. Köfinger, J. E. Koglin, G. Kovacsova, M. Liang, D. Milathianaki, H. T. Lemke, J. Reinstein, C. M. Roome, R. L. Shoeman, G. J. Williams, I. Burghardt, G. Hummer, S. Boutet and I. Schlichting (2015). "Direct observation of ultrafast collective motions in CO myoglobin upon ligand dissociation." Science **350**(6259): 445-450.

Berman, H. M., J. Westbrook, Z. Feng, G. Gilliland, T. N. Bhat, H. Weissig, I. N. Shindyalov and P. E. Bourne (2000). "The Protein Data Bank." Nucleic Acids Res **28**(1): 235-242.

Bushnell, G. W., G. V. Louie and G. D. Brayer (1990). "High-resolution three-dimensional structure of horse heart cytochrome c." J Mol Biol **214**(2): 585-595.

Chung, Y., P. A. Molé, N. Sailasuta, T. K. Tran, R. Hurd and T. Jue (2005). "Control of respiration and bioenergetics during muscle contraction." Am J Physiol Cell Physiol **288**(3): C730-738.

Dolar, M. L., P. Suarez, P. J. Ponganis and G. L. Kooyman (1999). "Myoglobin in pelagic small cetaceans." J Exp Biol **202**(Pt 3): 227-236.

Forli, S. and A. J. Olson (2012). "A Force Field with Discrete Displaceable Waters and Desolvation Entropy for Hydrated Ligand Docking." Journal of Medicinal Chemistry **55**(2): 623-638.

Germolus, C. B., U. N. Rehman, A. A. Ramahi and T. Jue (2022). "Lipid oxidation product nonenal and myoglobin oxidation." International Journal of Food Science & Technology **57**(10): 6602-6612.

Gimenez, M., R. J. Sanderson, O. K. Reiss and N. Banchero (1977). "Effects of altitude on myoglobin and mitochondrial protein in canine skeletal muscle." Respiration **34**(3): 171-176.

Gros, G., B. A. Wittenberg and T. Jue (2010). "Myoglobin's old and new clothes: from molecular structure to function in living cells." The Journal of Experimental Biology **213**(16): 2713-2725.

Guyton, G. P., K. S. Stanek, R. C. Schneider, P. W. Hochachka, W. E. Hurford, D. G. Zapol, G. C. Liggins and W. M. Zapol (1995). "Myoglobin saturation in free-diving Weddell seals." J Appl Physiol (1985) **79**(4): 1148-1155.

Halgren, T. A. (1996). "Merck molecular force field. I. Basis, form, scope, parameterization, and performance of MMFF94." Journal of Computational Chemistry **17**(5-6): 490-519.

Hanwell, M. D., D. E. Curtis, D. C. Lonie, T. Vandermeersch, E. Zurek and G. R. Hutchison (2012). "Avogadro: an advanced semantic chemical editor, visualization, and analysis platform." Journal of Cheminformatics **4**(1): 17.

Jue, T., L. Shih and Y. Chung (2017). "Differential Interaction of Myoglobin with Select Fatty Acids of Carbon Chain Lengths C8 to C16." Lipids **52**(8): 711-727.

Kooyman, G. L. and P. J. Ponganis (1998). "The physiological basis of diving to depth: birds and mammals." Annu Rev Physiol **60**: 19-32.

Kundu, S., V. K. Aswal and J. Kohlbrecher (2017). "Effect of ethanol on structures and interactions among globular proteins." Chemical Physics Letters **670**: 71-76.

Lin, P. C., U. Kreutzer and T. Jue (2007). "Myoglobin translational diffusion in rat myocardium and its implication on intracellular oxygen transport." J Physiol **578**(Pt 2): 595-603.

Lodish, H. F. (2008). Molecular Cell Biology 6th Edition, W. H. Freeman and Company.

Morris, G. M. G., D. S.; Pique, M. E.; Lindstrom, W.; Huey, R.; Forli, S.; Hart, W. E.; Hallyday, S.; Belew, R.; Olson, A. J. (2012). AutoDock 4.2 User Guide. T. S. R. Institute.

O'Boyle, N. M., M. Banck, C. A. James, C. Morley, T. Vandermeersch and G. R. Hutchison (2011). "Open Babel: An open chemical toolbox." Journal of Cheminformatics **3**(1): 33.

Pettersen, E. F., T. D. Goddard, C. C. Huang, G. S. Couch, D. M. Greenblatt, E. C. Meng and T. E. Ferrin (2004). "UCSF Chimera--a visualization system for exploratory research and analysis." J Comput Chem **25**(13): 1605-1612.

Phillips, S. E. (1980). "Structure and refinement of oxymyoglobin at 1.6 A resolution." J Mol Biol **142**(4): 531-554.

Ponganis, P. J., U. Kreutzer, N. Sailasuta, T. Knower, R. Hurd and T. Jue (2002). "Detection of myoglobin desaturation in Mirounga angustirostris during apnea." Am J Physiol Regul Integr Comp Physiol **282**(1): R267-272.

Rodkey, F. L. and E. G. Ball (1947). "Oxidation-reduction potentials of cytochrome c." Fed Proc **6**(1 Pt 2): 286.

Shih, L., Y. Chung, R. Sriram and T. Jue (2014). "Palmitate interaction with physiological states of myoglobin." Biochim Biophys Acta **1840**(1): 656-666.

Shih, L., Y. Chung, R. Sriram and T. Jue (2015). "Interaction of myoglobin with oleic acid." Chem Phys Lipids **191**: 115-122.

Taylor, J. F. and V. E. Morgan (1942). "OXIDATION-REDUCTION POTENTIALS OF THE METMYOGLOBIN-MYOGLOBIN SYSTEM." Journal of Biological Chemistry **144**(1): 15-20.

Terrados, N., E. Jansson, C. Sylvén and L. Kaijser (1990). "Is hypoxia a stimulus for synthesis of oxidative enzymes and myoglobin?" J Appl Physiol (1985) **68**(6): 2369-2372.

Tofani, L., A. Feis, R. E. Snoke, D. Berti, P. Baglioni and G. Smulevich (2004). "Spectroscopic and interfacial properties of myoglobin/surfactant complexes." Biophys J **87**(2): 1186-1195.

Vojtechovský, J., K. Chu, J. Berendzen, R. M. Sweet and I. Schlichting (1999). "Crystal structures of myoglobin-ligand complexes at near-atomic resolution." Biophys J **77**(4): 2153-2174.

Wittenberg, B. A. and J. B. Wittenberg (1989). "Transport of oxygen in muscle." Annu Rev Physiol **51**: 857-878.

Wittenberg, J. B. and B. A. Wittenberg (2003). "Myoglobin function reassessed." J Exp Biol **206**(Pt 12): 2011-2020.

Yoshikawa, H., A. Hirano, T. Arakawa and K. Shiraki (2012). "Effects of alcohol on the solubility and structure of native and disulfide-modified bovine serum albumin." Int J Biol Macromol **50**(5): 1286-1291.